Doctoral Thesis

Research of ceramicines from *Chisocheton ceramicus* on anti-lipid droplets accumulation activity

平成２４年度

星薬科大学大学院　生薬学教室

Wong Chin Piow

Table of Contents

Abbreviations

AMPK	5' Adenosine Monophosphate-Activated Protein Kinase
CD	Circular Dichroism
C/EBP	CCAAT/Enhancer-Binding-Protein
CHOP	C/EBP-Homologous Protein
COSY	Correlated Spectroscopy
DEC2	Class E Basic Helix-Loop-Helix Protein 41
DEX	Dexamethasone
ESI-MS	Electron Spray Ionization Mass Spectrometry
GLUT4	Glucose Transporter Type 4
HMBC	Heteronuclear Multiple Bond Correlation
HR-ESI-TOF-MS	High Resolution-Electron Spray Ionization-Time of Flight-Mass Spectrometry
HSD11β1	11-Beta Hydroxysteroid Dehydrogenase
HSQC	Heteronuclear Single Quantum Coherence
HPLC	High Performance Liquid Chromatography
IBMX	3-Isobutyl-1-Methylxanthine
iNOS	Inducible Nitric Oxide Synthase
IR	Infrared
KLF	Krüppel Like Factor
LDA	Lipid Droplets Accumulation
LPL	Lipoprotein Lipase
LPS	Lipopolysaccharide
MDI	Mixture of 0.5 mM IBMX, 25 nM DEX and 5 μg/ml insulin
NMR	Nuclear Magnetic Resonance
NOESY	Nuclear Overhauser Effect Spectroscopy
PPAR	Peroxisome Proliferator-Activated Receptor Protein
ROESY	Rotating-frame nuclear Overhauser Effect Spectroscopy
SREBP1c	Sterol Regulatory Element-Binding Protein-1c
TLC	Thin Layer Chromatography
TGR5	G Protein-Coupled Bile Acid Receptor 1
UV	Ultraviolet

Chapter I - Introduction

Plants have been co-evolved with pathogens and pests from the time where plants first appeared on earth. Under this pressure of evolution, plants have developed numerous defenses to counter attacks from pathogens and pests. One of such employed mechanisms is the development of a vast array of metabolites that confers them selective survival advantages against this natural pressure [1,2]. It is for the reason that plants holds an abundance of unique and diverse metabolites found nowhere else. Having this knowledge, human has been taking advantage of plant ability to solve our problems with pathogens. As a consequence, plants have been herald as a mainstay agent for medicinal purpose from ancient to modern times [3]. Usage of plants as a healing agent can be traced back to period of ancient humans. Clay tablet from Mesopotamia period were the first ever record on usage of plants to treat human disease, where licorice (*Glycyrrhiza glabra*), myrrh (*Commiphora* species), and poppy (*Papaver somniferum*) were documented and are still in use presently. Compounds isolated from *Papaver somniferum* that were still in use presently include morphine, codeine, narcotine, and papaverine (Figure I-1) [4].

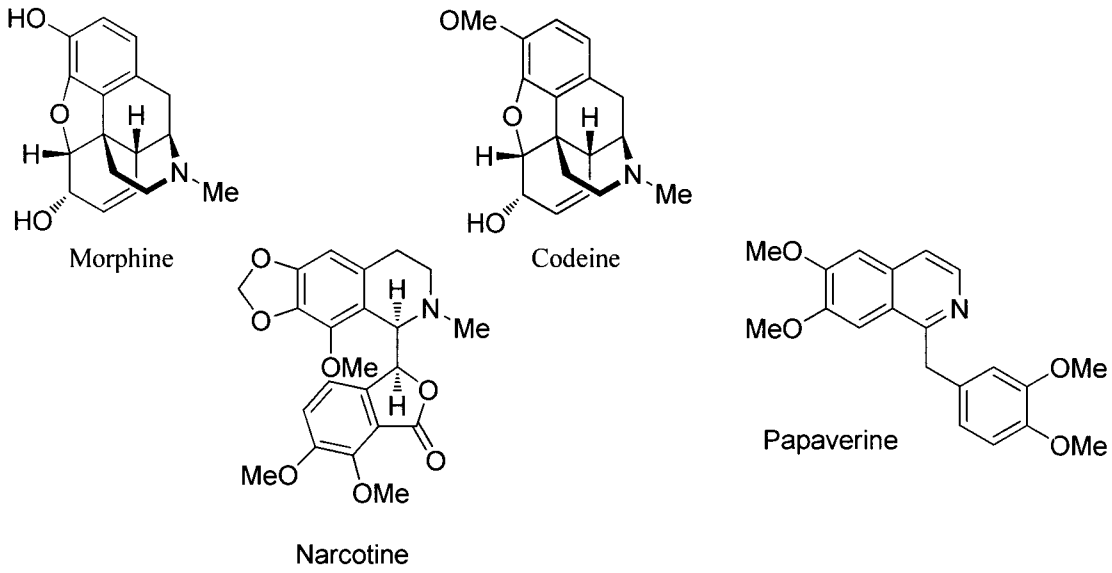

Figure I-1. Known compounds from *Papaver somniferum*

The invaluable terrestrial plants as a source of drug candidates initiate us to delve deeper in the research plant natural products. Countless species from the Meliaceae family have generated much interest due to their various significant biological activities. Activities such as insecticidal, insect anti-feedant, anti-bacterial, anti-fungal, anti-malarial, anti-cancer,

and anti-viral have so far been reported [4-9]. Possibly the most recognizable species from Meliaceae is *Azadirachta indica* (*A. indica*) or commonly known as neem. Traditionally use in Ayurvedic treatment in India and its neighboring country for various ailments, neem has been considered as one of the alternative treatment in modern time. Virtually, all part of this part from leaf to root can be use medicinally, leading to the isolation of over 135 compounds [10,11]. Some of the famous limonoids include nimbin and azadirachtin (Figure I-2) [12].

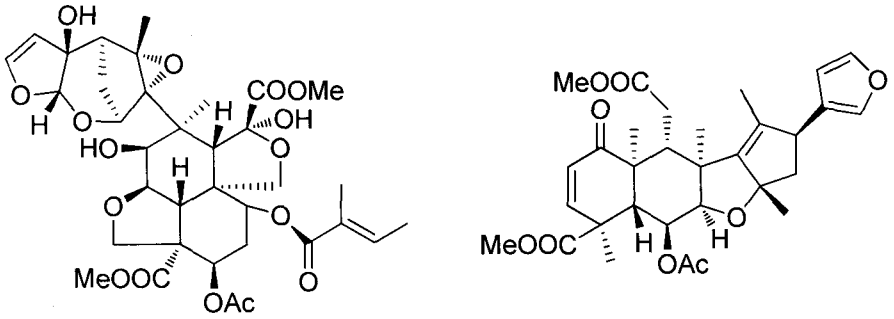

Azadirachtin Nimbin

Figure I-2. Compounds isolated from *Azadirachta indica*

This study focused on another plant from Meliaceae family, *Chisocheton ceramicus* Miq (*C. ceramicus*). A large canopy tree reaching 30 meter in height and bearing 40 centimeter in diameter when fully grown and were distributed in the tropic region encompassing Malaysia, Indonesia, Brunei, Papua New Guinea, Philippines and Vietnam [13]. *C. ceramicus* have not been known to be used for any medicinal purposes but is largely known as a source of hardwood timber in its native region.

Several researches have been done on *C. ceramicus*, as a result two series of bioactive limonoids have so far been isolated, ceramicines series and chisomicines series, respectively (Figure I-3). Studies have showed that ceramicine B isolated from *C. ceramicus* possess potent anti-malarial activity in *Plasmodium falciparum* strain 3D7. Additionally, ceramicine A showed moderate cytotoxic activity on murine leukemia cell line (P388), while chisomicine A showed weak inducible nitric oxide synthase (iNOS) inhibitory activity on LPS-stimulated murine macrophage cell line (J774.1) [14-17].

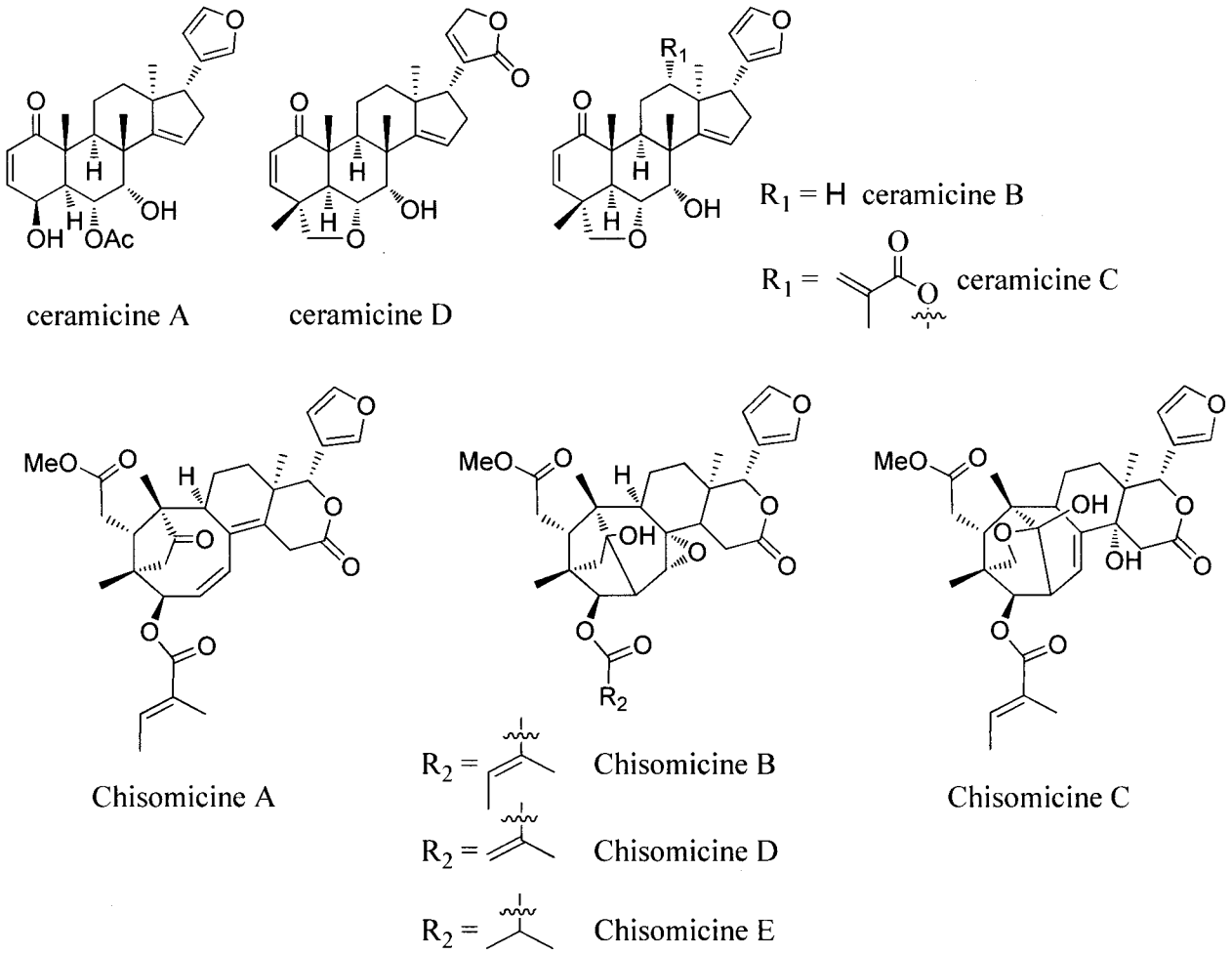

Figure I-3. Known compounds from *Chisocheton ceramicus*

The biological activities shown by plant natural products made it an interesting source for various medical conditions including obesity. Obesity is a medical condition, in which a person overall health is affected by excessive body weight due to unhealthy diet and lifestyle. Cardiovascular disease, diabetes mellitus type 2, obstructive sleep apnea, osteoarthritis, asthma, hypertension, and certain type of cancer are among some of the disease associated with obesity, which are the leading preventable cause of death, particularly in developed and developing country [18]. The risks of obesity can be reduced through healthy diet and lifestyle, and more recently by consumption of anti-obesity drugs [19]. The cause of obesity morbidity is divided into two attributes, increase of lipid mass and increase of lipid cells numbers [18]. Both of these attributes could be decreased by reducing lipid-droplets accumulation (LDA) and adipocyte differentiation. Apart from reducing LDA, obesity morbidity could be treated by preventing absorption of fats from diet. This is practiced by drug called Orlistat, a lipstatin derivative first isolated from *Streptomyces toxytricini* (Figure I-4) [20,21]. Orlistat also

moderately reduces blood pressure and have been suggested to prevent onset of type 2 diabetes, which both conditions are related with obesity [22]. A more controversial method, an anorexic inducing drug, promoting weight loss through induction of satiety. This method is utilized by a drug named Lorcaserin (Figure I-4). A 5-HT_{2C} receptor agonist, Lorcaserin stimulates the activation of proopiomelanocortin production and consequently suppressing appetite [23].

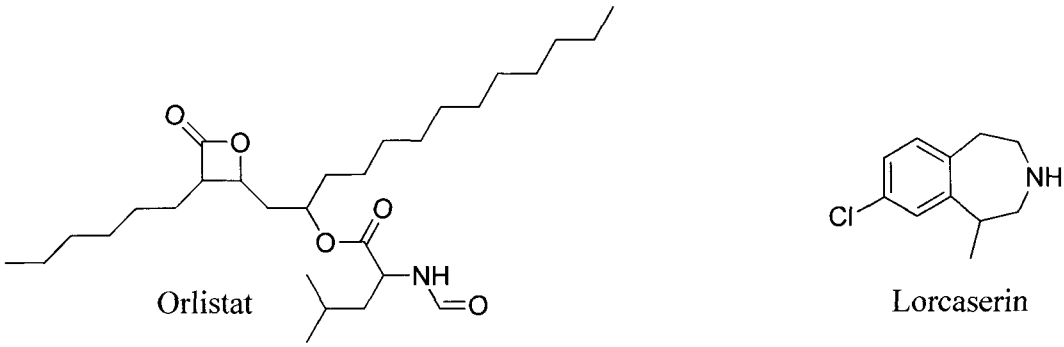

Figure I-4. Drugs for obesity, Orlistat and Lorcaserin

Apart from the approved anti-obesity drugs, Orlistat and Lorcaserin, several other botanical examples that are currently being studied for development as weight loss product include *Alpinia officinarum* from Zingiberaceae family. As a result, a potent inhibitor of pancreatic lipase, 3-methylethergalangin (Figure I-5) was identified. Ethanol extract from *Alpinia officinarum* administered to Sprague-Dawley rats for a 6-week period showed promising anti-obesity effect [24,25]. *Dioscorea nipponica* or wild yam yielded a steroidal saponin, pseudoprotodioscin (Figure I-5) that inhibit adipogenesis both *in vitro* and *in vivo*. Regulation was found to be *via* inhibition of p38 mitogen-activated protein kinase. While several key adipogenic genes were also repressed, including CCAAT/enhancer-binding-protein-α (C/EBPα), lipoprotein lipase (LPL), peroxisome proliferator-activated receptor protein-γ (PPARγ) and leptin [26]. Another example is the bitter melon or scientifically known as *Momordica charantia*. Rats feed with freeze-dried juice of this plant unripe fruits shown observable reduction in visceral fat mass and hepatic triacylglycerol [27,28]. From the fruits of *Momordica charantia*, momordicoside S was isolated and exhibited potent activation of 5' adenosine monophosphate-activated protein kinase (AMPK) pathway and reduction in adipocyte transcription factor PPARγ and sterol regulatory element-binding protein-1c (SREBP1c) [29]. Berberine which was used as a positive control in this study can be isolated from the berberis genus plants [30] (Figure I-5). It has been suggested that, berberine induced

weight lost by upregulating C/EBPs inhibitor, C/EBP-Homologous Protein (CHOP) and Class E basic helix-loop-helix protein 41 (DEC2) [31].

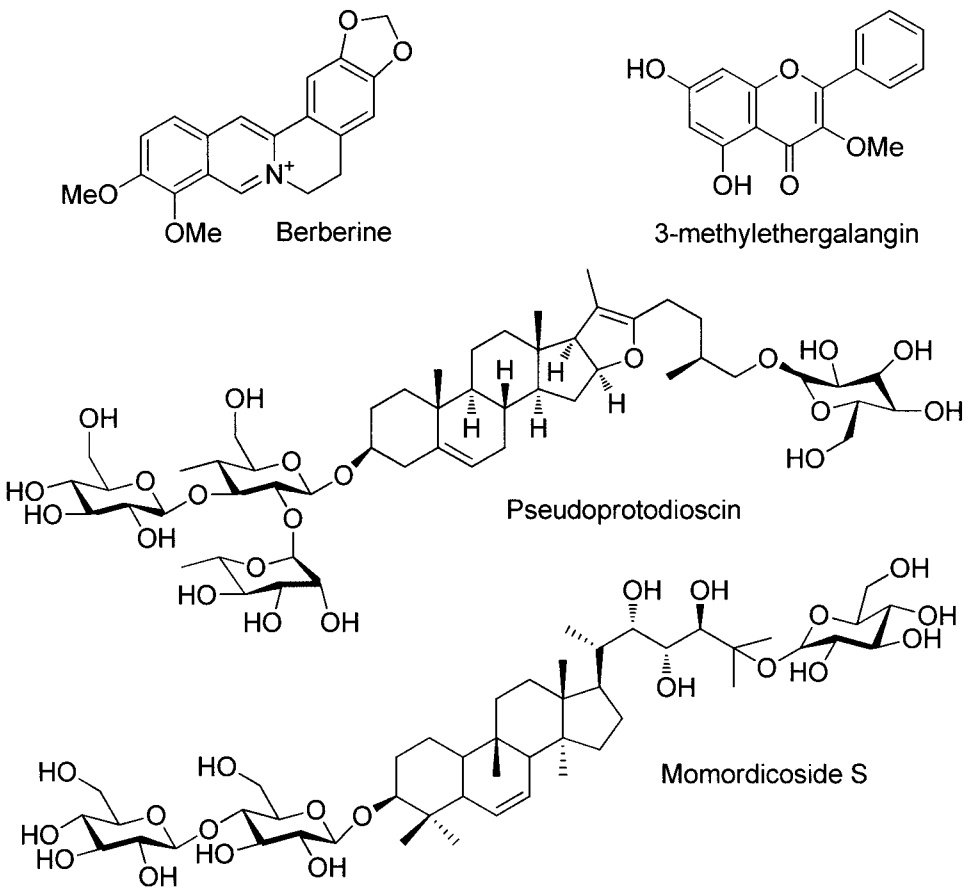

Figure I-5. Anti-obesity compounds from natural sources

Research for anti-obesity drugs is ongoing but only a few make it pass clinical trials. This currently generates a void in the discovery phase for new anti-obesity drug candidates. To offset this matter, efforts on the discovery of new possible lead have to be intensified. On an interesting note, only a few researches were done on limonoids with anti-obesity properties. A limonoid isolated from grape fruits juice, nomilin have been suggested to activate G protein-coupled bile acid receptor 1 (TGR5) to prevent obesity [32,33]. While, meliacinolin isolated from *A. indica* were shown to possess in vivo anti-diabetic property in streptozotocin-nicotinamide-induced type 2 diabetic mice [34].

Through our continuous screening effort to identify compounds as an anti-obesity drug lead, we have identified that previously isolated limonoid, ceramicines A and B from *C. ceramicus* bark extract [14,15] to possess potent anti-LDA activity. Thus further studies were carried out on constituents of *C. ceramicus* bark extract. As a result, eight new limonoids,

ceramicines E-L were isolated. Their relative structures were elucidated using 1D and 2D NMR data. These eight new limonoids potential as anti-obesity drug lead, were measure *via* their ability to inhibit LDA activity on mouse pre-adipocyte cell line, MC3T3-G2/PA6. Data showed that, ceramicine I possess moderate anti-LDA activity while others showed weak or inactive. While previously isolated ceramicine B was found to be most potent compound with anti-LDA activity and its mechanism of action is reported in this study.

Chapter II - Constituents of *Chisocheton ceramicus*

II.1 Separation and Purification

The dried ground bark of *C. ceramicus* (500 g) was extracted with methanol, yielding 56 g of extract. A small portion of the extract (7 g) was further partitioned with hexane, ethyl acetate, *n*-butanol, and water, successively for small scale constituents' studies. The hexane-soluble materials were further partitioned with a silica gel column (hexane/EtOAc, 10:0 → 1:1, and then $CHCl_3$/MeOH, 10:0 → 0:10). Fraction eluted from the silica gel column with $CHCl_3$/MeOH (7:2) was identified as previously isolated ceramicine B [15]. While, fraction eluted from the silica gel column with $CHCl_3$/MeOH (7:3) was further purified using C_{18} HPLC under gradient elution (50%-100% MeOH) to yield ceramicine E (**1**, 2.0 mg, 0.029% yield), and ceramicine F (**2**, 9.5 mg, 0.14% yield), both as colorless solid. Fraction eluted with $CHCl_3$/MeOH (1:1) was purified also on C_{18} HPLC under gradient elution (70%-100% MeOH) to obtain ceramicine G (**3**, 5.6 mg, 0.08% yield) as colorless solid. Whereas, fraction eluted with $CHCl_3$/MeOH (4:6) was purified on C_{18} HPLC under gradient elution (50%-100% MeOH) to afford previously identified ceramicine C [15], and two new limonoids, ceramicine H (**4**, 0.3 mg, 0.004% yield) and ceramicine I (**5**, 4.3 mg, 0.06% yield).

Further isolation on minor compounds was performed on the remaining 46 g of extract. Similarly the extract was further partitioned with hexane, ethyl acetate, *n*-butanol, and water, successively. The hexane-soluble materials were partitioned with a silica gel column (hexane/EtOAc, 10:0 → 1:1, and then $CHCl_3$/MeOH, 10:0 → 0:10). Fraction eluted from the silica gel column with hexane/EtOAc (3:7) was idenfied as ceramicine B [15]. Fraction eluted from the silica gel column with hexane/EtOAc (1:9) was purified a silica gel column (toluene/EtOAc, 6:1 → 4:1). Fraction eluted from the silica gel column with toluene/EtOAc (4:1) and 100% EtOAc were finally purified using HPLC chiral column under isocratic elution (78%/22% MeOH/H_2O) to yield ceramicine J (**6**, 1.0 mg, 0.0002%), ceramicine K (**7**, 0.6 mg, 0.00012% yield) and ceramicine L (**8**, 0.8 mg, 0.00016% yield) together with previously identified ceramicines A and C [14,15], all as colorless amorphous solid.

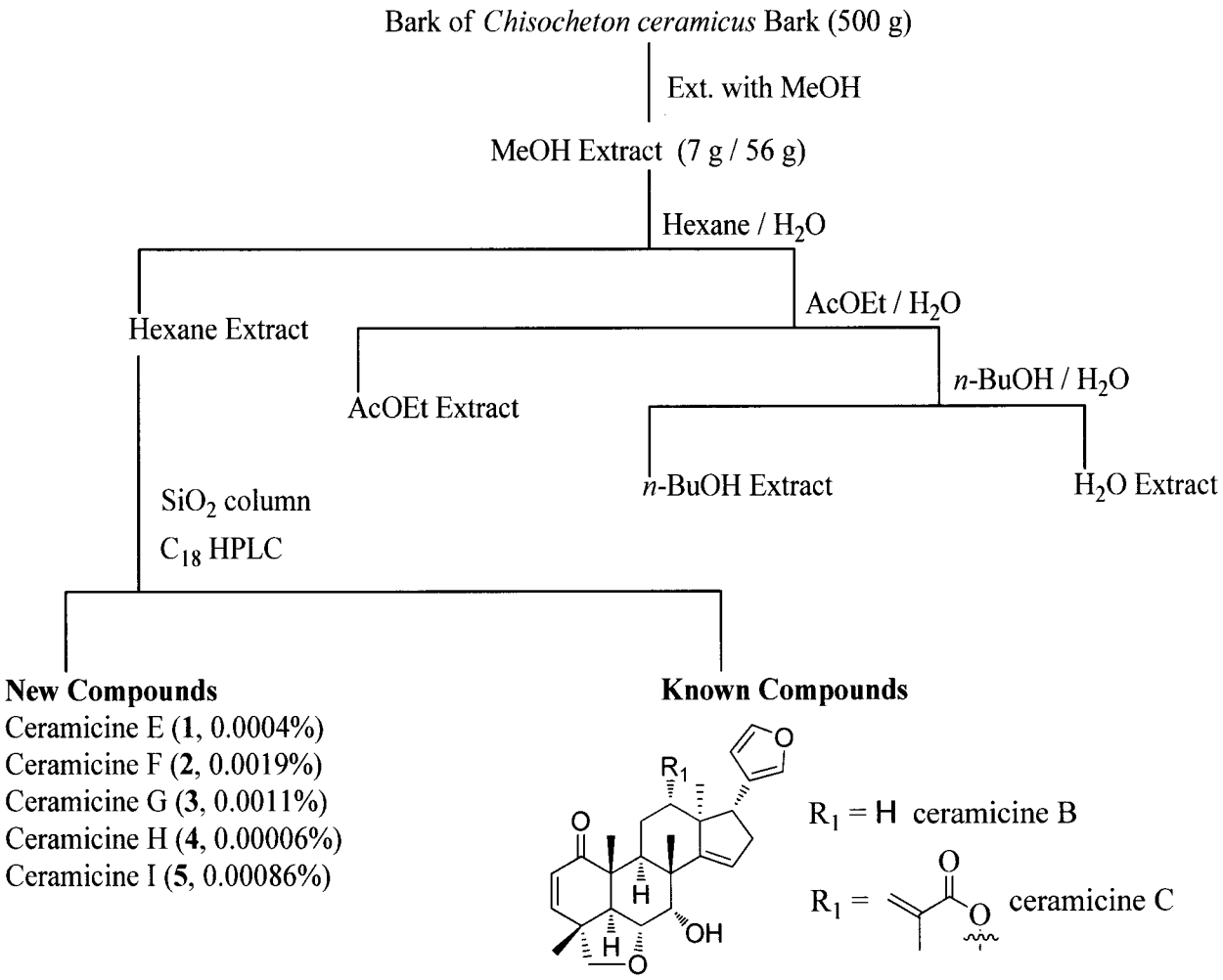

Figure II-1. Small scale isolation scheme of **1-5** from *C. ceramicus* bark

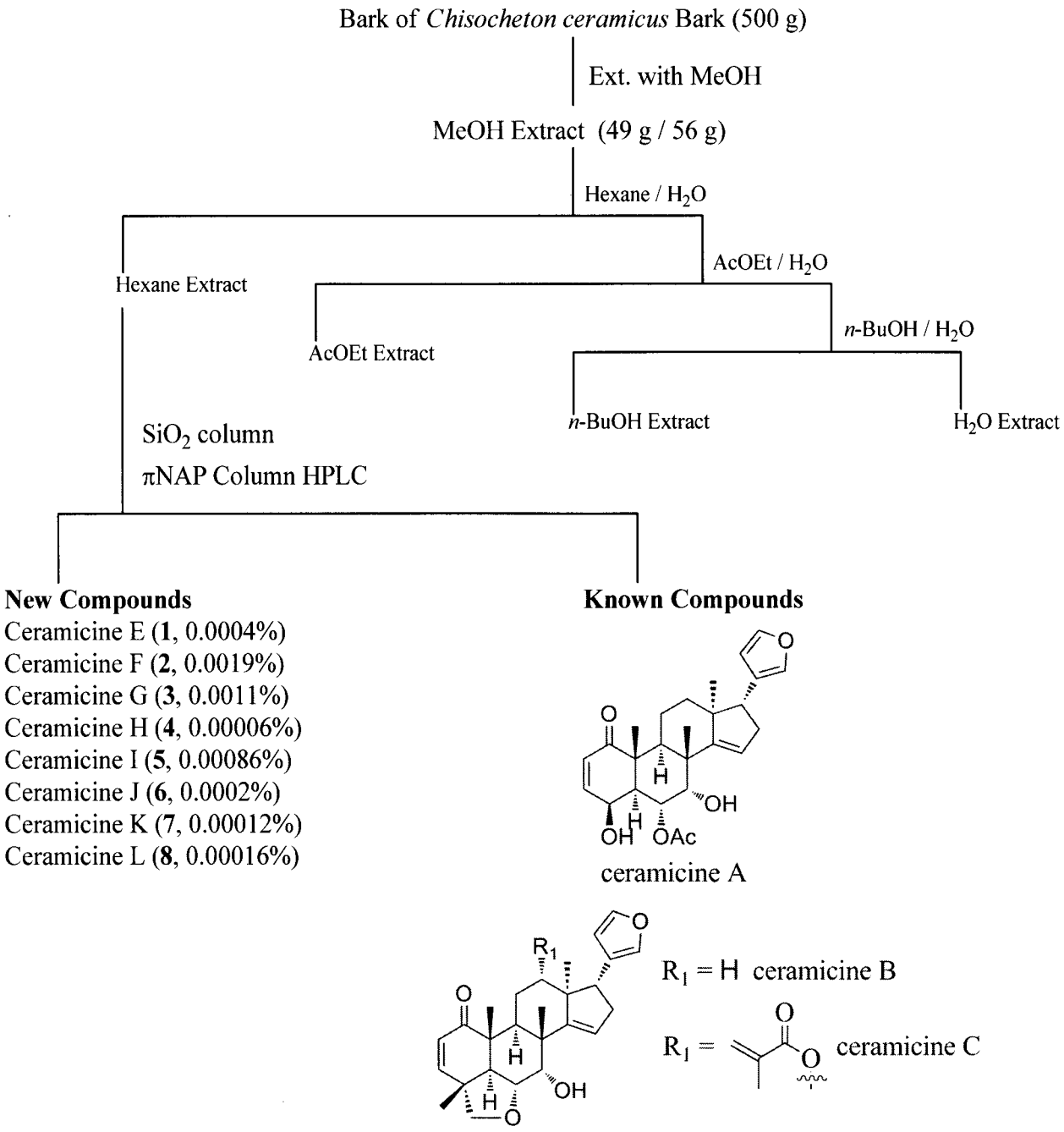

Figure II-2. Full scale isolation scheme of **6-8** from *C. ceramicus* bark

II.2 Structure Elucidation

II.2.1 Ceramicine E (1)

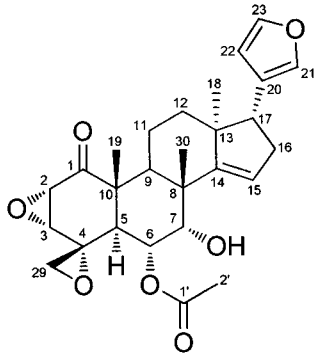

Ceramicine E (**1**)

Ceramicine E {**1**, $[\alpha]_D^{28}$ +20 (c 0.5, $CHCl_3$)} was isolated as a colorless amorphous solid and had molecular formula, $C_{27}H_{32}O_7$ as determined by high resolution-electrospray ionization-time of flight-mass spectra (HR-ESI-TOF-MS) [m/z 469.2206 $(M + H)^+$, Δ -2.0 mmu]. IR absorptions suggested the presence of a carbonyl (1718 cm^{-1}) and a hydroxyl (3437 cm^{-1}) groups. ^1H and ^{13}C NMR data (Tables II-1) revealed 27 carbon resonances due to two carbonyls, two sp^2 quaternary carbons, four sp^3 quaternary carbons, four sp^2 methines, seven sp^3 methines, four sp^3 methylenes, and four methyls. Among them, two sp^2 methines (δ_C 139.7 and 142.6), four sp^3 methines (δ_C 52.9, 57.5, 65.3, and 74.2), one sp^3 quaternary carbon (δ_C 57.1), and one sp^3 methylene (δ_C 47.7) are connected to an oxygen atom.

Five partial structures **a** (from C-2 to C-3), **b** (from C-5 to C-7), **c** (from C-9 to C-12), d (from C-15 to C-17), and **e** (from C-22 to C-23) were deduced from ^1H-^1H correlation spectroscopy (COSY) analysis of **1** in $CDCl_3$ (Figure II-3). The existence of two epoxides at C-2 and C-3, and C-4 and C-29 was deduced by the ^1H and ^{13}C chemical shifts (H-2: δ_H 3.35, C-2: δ_C 52.9; H-3: δ_H 3.01, C-3: δ_C 57.5; C-4: δ_C 57.1; H-29: δ_H 2.84 and 3.24, C-29: δ_C 47.7), which was confirmed by heteronuclear multiple bond connectivity (HMBC) analysis for H-3 of C-4, for H-5 of C-4 and C-29, and for H2-29 to C-3 as shown in (Figure II-3). The HMBC correlations for H-2 and H_3-19 of C-1 (δ_C 202.3), for H_3-19 of C-5 (δ_C 31.8), C-9 (δ_C 32.0), and C-10 (δ_C 51.6), and for H_3-30 of C-7 (δ_C 74.2), C-8 (δ_C 43.9), and C-9 bridged the partial structures of **a**, **b**, and **c** through C-1, C-8, and C-10. The HMBC correlations for H_3-18 of C-12 (δ_C 33.2), C-13 (δ_C 46.9), C-14 (δ_C 159.1), and C-17 (δ_C 51.9), for H-15 of C-13, and for H_3-30 of C-14 indicated the connectivity between structures **b**, **c**, and **d**. The connectivity of

partial structure **e** (β-furyl ring) to **d** was shown by HMBC correlations for H-21 of C-17, C-20 (δ_C 124.4), and C-23 (δ_C 142.6), and for H-22 to C-20. Further analysis of HMBC correlations for H-6 and H-2' to C-1' (δ_C 170.6) indicated the presence of an acetate at C-6. Therefore, **1** was established as a new limonoid with a cyclopenta[α]phenanthren ring system with a β-furyl ring at C-17, an acetate at C-6, and two epoxide rings.

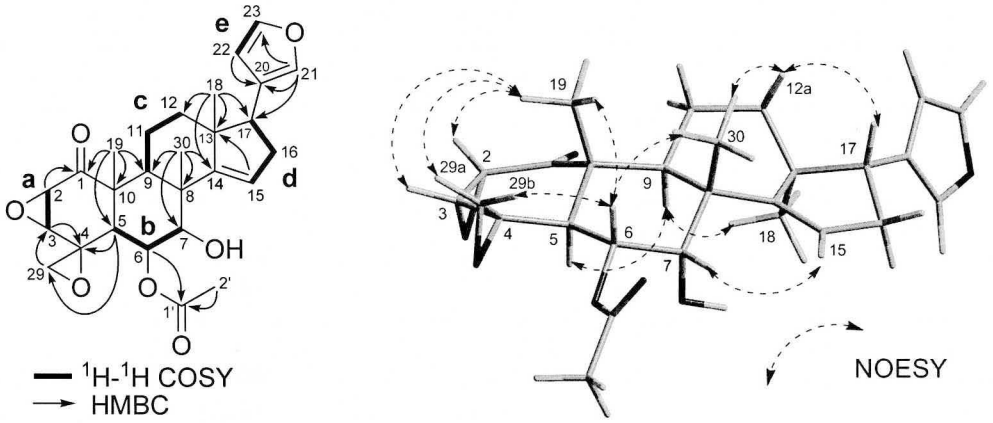

Figure II-3. Selected 2D-NMR correlations for ceramicine E (**1**)

The relative stereochemistry of **1** was elucidated by nuclear overhauser effect spectroscopy (NOESY) correlations as shown in computer-generated 3D rendering (Figure II-3). NOESY correlations of H_3-19/H-2, H-3, H-29a, and H-6, and H-6/H-29b and H_3-30 suggested stereochemistry of two epoxides, H-6, H_3-19, and H_3-30 to take as shown in Fig. 2. The ^3J proton coupling constants ($^3J_{H\text{-}5/H\text{-}6}$ = 11.7 Hz and $^3J_{H\text{-}6/H\text{-}7}$ = 2.6 Hz) as well as NOESY correlations of H-9/H-5 and H_3-18, H-7/H-15, and H-12a/H-17 and H_3-30 indicated that H-6, H-7, and H-17 adopted a β-configurations, and H-5, H-9, and C-18 adopted an α-configurations as shown in Figure II-3.

Table II-1. ^{1}H and ^{13}C-NMR data of **1** in $CDCl_3$ at 300 K

	[δ_H (J, Hz)]	[δ_C]
1		202.3
2	3.35 (d, 3.6)	52.9
3	3.01 (d, 3.6)	57.5
4		57.1
5	3.18 (d, 11.7)	31.8
6	5.32 (dd, 11.7, 2.6)	65.3
7	3.78 (brd, 2.6)	74.2
8		43.9
9	2.68 m	32.0
10		51.6
11a	1.60 m	18.2
11b	2.35 m	
12a	1.60 m	33.2
12b	1.91 m	
13		46.9
14		159.1
15	5.52 (dd, 1.4, 3.4)	120.5
16a	2.40 (ddd, 15.5, 7.5, 3.4)	34.3
16b	2.51 (ddd, 15.5, 10.9, 1.4)	
17	2.85 (dd, 7.5, 10.9)	51.9
18	0.88 s	21.6
19	1.24 s	14.3
20		124.4
21	7.25 m	139.7
22	6.29 (dd, 1.6, 0.6)	111.0
23	7.38 (dd, 1.6, 1.6)	142.6
29a	2.84 (dd, 3.7, 0.8)	47.7
29b	3.24 (d, 3.7)	
30	1.18 s	25.6
1'		170.6
2'	2.13 s	21.4

II.2.2 Ceramicine F & G (2 & 3)

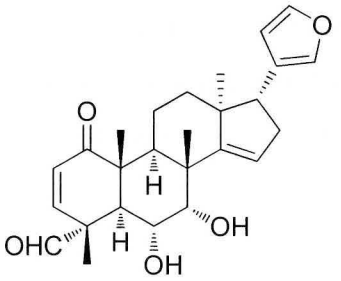

Ceramicine F (**2**)

Ceramicine F {**2**, $[\alpha]_D^{28}$ +101 (*c* 0.5, $CHCl_3$)} was isolated as a colorless amorphous solid and had molecular formula of $C_{26}H_{32}O_5$ as determined by HR-ESI-TOF-MS [*m/z* 447.2120 $(M + Na)^+$, Δ -2.7 mmu]. IR absorptions showed the presence of carbonyl (1724 and 1679 cm^{-1}) and hydroxyl groups (3437 cm^{-1}). ^1H and ^{13}C NMR data (Tables II-2) revealed 26 carbon resonance due to two carbonyls, two sp^2 quaternary carbons, four sp^3 quaternary carbons, six sp^2 methines, five sp^3 methines, three sp^3 methylenes and four methyls. In which, two sp^2 methines (δ_C 139.6 and 142.6), and two sp^3 methines (δ_C 66.3, and 74.6) are attached to an oxygen atom. The existence of an aldehyde group attached to the C-4 (δ_C 51.8) was indicated by HMBC correlations for H_3-29 of C-3 (δ_C 143.9), C-4, C-5 (δ_C 44.1), and C-28 (δ_C 200.9). Based on the HR-ESI-TOF-MS and 2D NMR data, the structure of **2** was assigned as in Figure II-4.

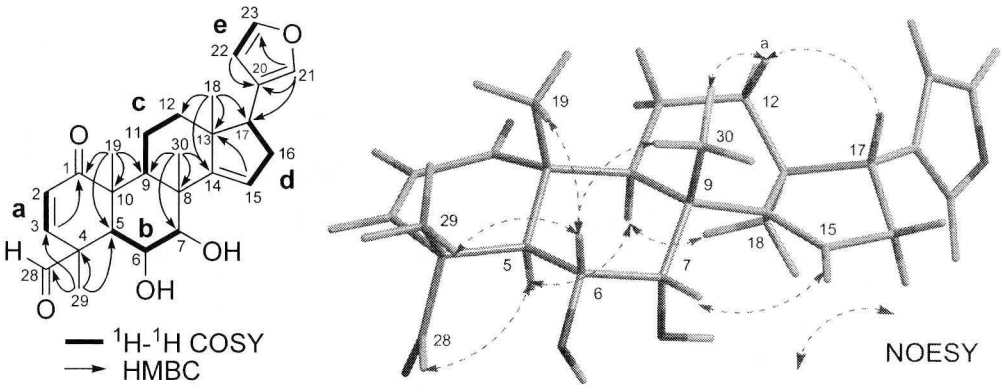

Figure II-4. Selected 2D-NMR correlations for ceramicine F (**2**)

The relative stereochemistry of **2** was elucidated by NOESY correlations as shown in computer-generated 3D drawing (Figure II-4). As shown by Figure 3, the relative stereochemistry was shown to be similar to **1**. NOESY correlations of H-6/H_3-29, H_3-19, and H_3-30, and H-5/H-28, suggested the presence of the hydroxyl attached to C-6 and the aldehyde attached to C-4 to adopt the α-configuration.

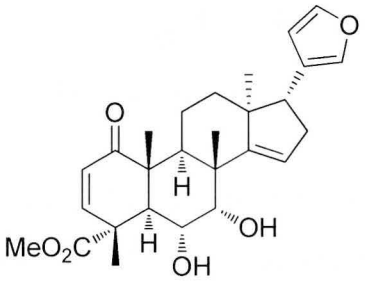

Ceramicine G (**3**)

Ceramicine G {**3**, $[\alpha]_D^{28}$ -39 (*c* 0.5, $CHCl_3$)} was isolated as a white powder and had molecular formula of $C_{27}H_{34}O_6$ as determined by HR-ESI-TOF-MS [*m/z* 447.2244 $(M + Na)^+$, Δ -0.9 mmu], which was a CH_2O unit larger than ceramicine F (**2**). ^1H and ^{13}C NMR data (Table II-2) of **3** were analogous to those of **2**, but instead of an aldehyde at C-4, the presence of a methoxycarbonyl group at C-4 (δ_C 47.9) was indicated by the HMBC correlations for H_3-1', H_3-29, H-3, and H-5 of C-28 (δ_C 175.9) and H_3-29 of C-3 (δ_C 146.4), C-4, and C-5 (δ_C 43.3). The NOESY correlations between H-6/H_3-29, H_3-19, and H_3-30 suggested that methoxycarbonyl group to adopt the α-configuration (Figure II-5).

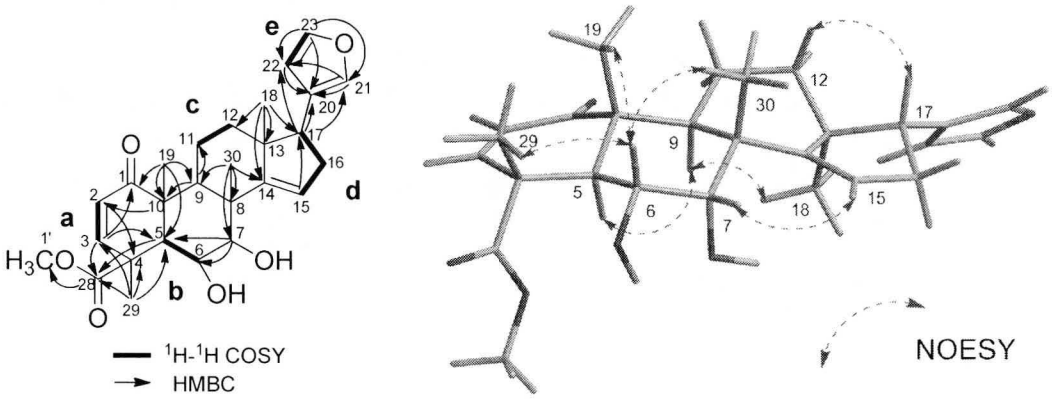

Figure II-5. Selected 2D-NMR correlations for ceramicine G (**3**)

Table II-2. ^{1}H and ^{13}C-NMR data of **2** and **3** in $CDCl_3$ at 300 K

	2		**3**	
	[δ_H (*J*, Hz)]	[δ_C]	[δ_H (*J*, Hz)]	[δ_C]
1		202.8		203.3
2	5.95 (d, 10.1)	128.8	5.83 (d, 10.1)	127.0
3	6.06 (d, 10.1)	143.9	6.32 (d, 10.1)	146.4
4		51.8		47.9
5	2.82 (d, 11.4)	44.1	3.35 (d, 11.6)	43.3
6	4.09 (ddd, 12.1, 10.9, 3.1)	66.3	4.05 (brd, 11.9)	66.6
7	4.02 (dd, 3.1, 1.6)	74.6	3.99 (d, 2.4)	75.0
8		44.0		44.2
9	2.52 m	33.2	2.52 m	33.6
10		47.9		48.6
11a	1.63 m	17.9	1.58 m	17.9
11b	2.56 m		2.54 m	
12a	1.59 m	32.8	1.58 m	32.9
12b	1.92 m		1.93 m	
13		47.0		47.1
14		160.4		160.7
15	5.57 (dd, 3.6, 1.6)	120.2	5.57 (dd, 1.1, 3.4)	120.0
16a	2.41 (ddd, 15.6, 7.4, 3.6)	34.2	2.42 (ddd, 15.4, 7.3, 3.4)	34.3
16b	2.51 m		2.52 m	
17	2.86 (dd, 10.9, 7.4)	51.8	2.86 (dd, 11.1, 7.3)	51.9
18	0.90 s	21.3	0.90 s	21.4
19	1.29 s	16.4	1.28 s	16.2
20		124.3		124.4
21	7.26 s	139.6	7.26 brs	139.6
22	6.29 (dd, 1.8, 1.0)	110.9	6.30 m	111.0
23	7.39 (dd, 1.8, 1.6)	142.6	7.38 (dd, 1.7, 1.7)	142.6
28a	9.28 s	15.5		175.9
28b				
29a	1.54 s	26.1	1.61 s	17.0
29b				
30	1.18 s		1.18 s	26.4
1'			3.70 s	52.8

II.2.3 Ceramicine H & I (4 & 5)

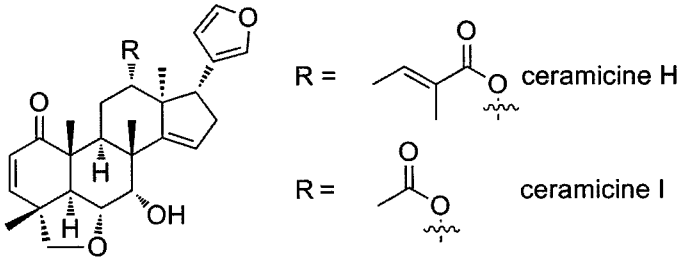

Ceramicine H (**4**) and ceramicine I (**5**)

Ceramicine H {**4**, $[\alpha]_D^{26}$ +77 (*c* 0.15, MeOH)} was isolated as a colorless amorphous solid and had molecular formula of $C_{31}H_{38}O_6$ as determined by HR-ESI-TOF-MS [*m/z* 529.2565 $(M + Na)^+$, Δ -0.1 mmu]. Whereas, ceramicine I {**5**, $[\alpha]_D^{26}$ +13 (*c* 0.3, MeOH)} possessing molecular formula of $C_{28}H_{35}O_6$ determined by HR-ESI-TOF-MS [*m/z* 489.2227 $(M + Na)^+$, Δ -2.6 mmu] was isolated as a colorless amorphous solid. ^1H and ^{13}C NMR data (Tables II-3) of **4** and **5** were found to be similar to those of the previously isolated ceramicine C [15]. Based on the 2D NMR (^1H-^1H COSY, heteronuclear single quantum coherence (HSQC), and HMBC) data, **4** was found to be an analogue of ceramicine C but with a tiglate group attached to C-12 (δ_C 77.2), whereas **5** was found with acetate group substituted to C-12 (δ_C 77.2) instead of methacrylate at C-12 of ceramicine C, which was confirmed by HMBC correlations for H_3-5' and H-12 of C-1' (δ_C 167.7) and the chemical shifts [35,36] of H-3' (δ_H 6.58) and C-5' (δ_C 11.7) in **4** and for H_3-2' and H-12 of C-1' (δ_C 171.0) in **5** (Figure II-6,7). The side chain attached to C-12 of ceramicine H is suggested to be a tiglate but not of an angelate based on its ^{13}C chemical shift of C-4' and C-5' (δ_C 14.3 and 11.7) [37]. The relative structures of **4** and **5** were shown to be similar to that of ceramicine B [15]. The NOESY correlations between H-12/H-17 and H_3-30 for **4** and **5** indicated that both the tiglate at C-12 and acetate at C-12 were to adopt the β-configurations (Figure II-6 and 7).

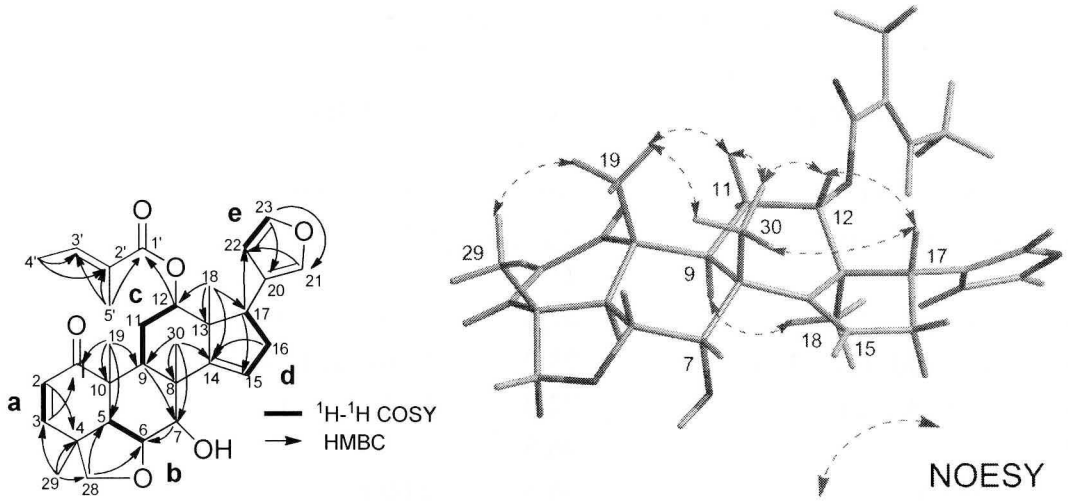

Figure II-6. Selected 2D-NMR correlations for ceramicine H (**4**)

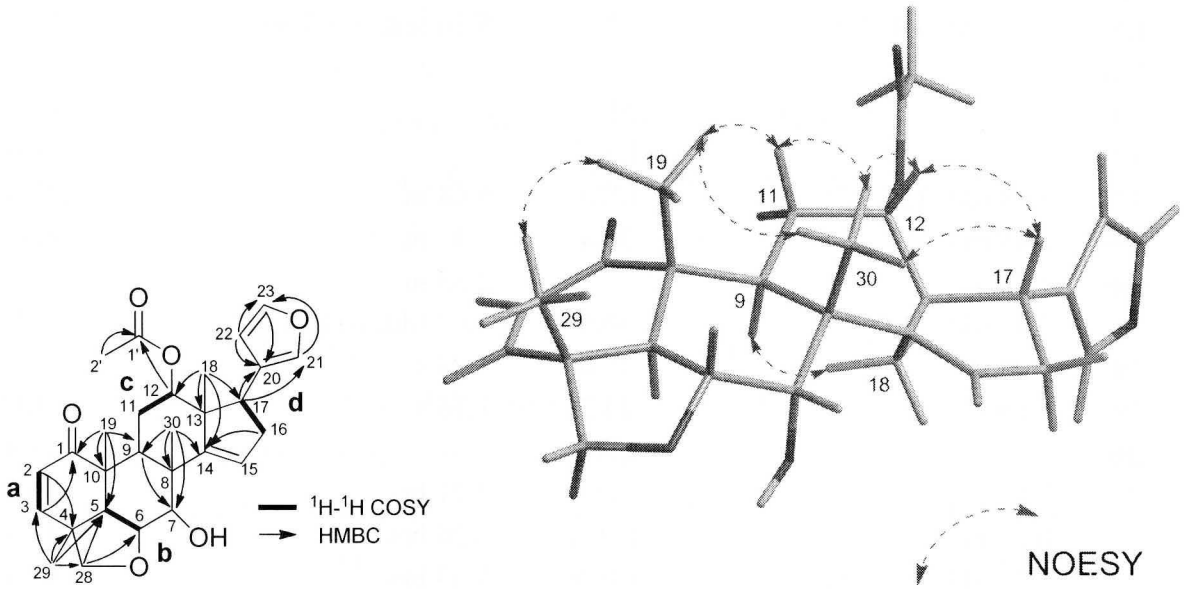

Figure II-7. Selected 2D-NMR correlations for ceramicine I (**5**)

Table II-3. ^{1}H and ^{13}C-NMR data of **4** and **5** in $CDCl_3$ at 300 K

	4		**5**	
	[δ_H (J, Hz)]	[δ_C]	[δ_H (J, Hz)]	[δ_C]
1		202.4		202.4
2	5.82 (d, 9.6)	130.0	5.83 (d, 9.6)	130.0
3	6.95 (d, 9.6)	151.0	6.96 (d, 9.6)	151.1
4		41.8		41.8
5	2.69 (d, 12.4)	47.6	2.69 (d, 12.4)	47.6
6	4.29 (dd, 12.4, 3.2)	73.7	4.26 (dd, 12.4, 3.2)	73.7
7	4.24 (d, 3.2)	72.0	4.24 (d, 3.2)	72.0
8		46.5		46.4
9	2.59 m	36.5	2.60 m	36.2
10		47.2		47.1
11a	2.27 m	26.9	2.30 m	26.8
11b	2.49 m		2.42 m	
12a	5.10 (dd, 9.0, 7.0)	77.2	5.10 (dd, 9.0, 7.0)	77.2
12b				
13		51.7		51.4
14		156.7		156.6
15	5.68 (dd, 1.2, 3.2)	122.6	5.68 m	122.6
16a	2.45 m	36.4	2.47 m	36.4
16b	2.55 m		2.53 m	
17	3.04 (dd, 11.0, 7.8)	50.6	3.04 (dd, 10.8, 8.0)	50.5
18	1.08 s	16.0	1.04 s	15.9
19	1.16 s	14.2	1.16 s	14.1
20		124.3		124.4
21	7.13 brs	140.4	7.21 brs	140.2
22	6.22 brs	111.8	6.26 brs	111.7
23	7.27 (dd, 1.6, 1.6)	141.8	7.33 brs	142.1
28a	3.63 m	79.9	3.63 m	79.9
28b	3.79 (d, 6.8)		3.79 (d, 7.2)	
29a	1.33 s	20.1	1.34 s	20.1
29b				
30	1.13 s	26.5	1.12 s	26.5
1'		167.7		171.0
2'		128.6	1.93 s	21.4
3'	6.58 (brq, 7.6)	137.8		
4'	1.72 (brd, 7.6)	14.3		
5'	1.65 brs	11.7		

II.2.4 Ceramicine J (6)

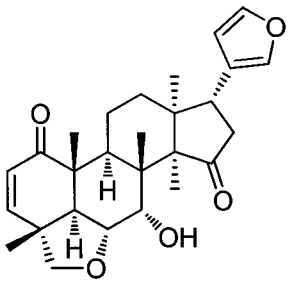

Ceramicine J (**6**)

Ceramicine J {**6**, $[\alpha]_D^{25}$ -88 (*c* 0.5, $CHCl_3$)} was isolated as a colorless amorphous solid and had molecular formula, $C_{26}H_{32}O_5$ as determined by HR-ESI-TOF-MS [*m/z* 425.2328 $(M+H)^+$, Δ -0.3 mmu]. IR absorptions suggested the presence of two carbonyls (1724 and 1675 cm^{-1}). ^1H and ^{13}C NMR data (Tables II-4) revealed 26 carbon resonances due to two carbonyls, one sp^2 quaternary carbons, four sp^3 quaternary carbons, five sp^2 methines, six sp^3 methines, four sp^3 methylenes, and four methyls. Among them, two sp^2 methines (δ_C 140.2 and 142.8), two sp^3 methines (δ_C 73.6 and 69.4), and one sp^3 methylene (δ_C 79.8) are connected to an oxygen atom.

^1H and ^{13}C NMR data (Tables II-4) of **6** were analogous to those of previously reported ceramicine B [15], but instead an olefin between C-14 and C-15, C-15 (δ_C 120.3) formed a carbonyl. Based on data from COSY analysis of **6** in $CDCl_3$ (Figure II-8), five partial structures **a** (from C-2 to C3), **b** (from C-5 to C-7), **c** (from C-9 to C-12), **d** (from C-16 to C-17), and **e** (from C-22 to C-23) were deduced. The HMBC correlations for H_3-29 of C-3 to C-5; H-2 of C-4 and C-10; H_3-19 of C-1, C-5, C-9; H_3-30 of C-7, C-9, and C-14; and H_3-18 of C-12 to C-14 bridged the partial structure of **a**, **b**, and **c** through C-1, C-8, and C-10, thus forming a phenantren ring system. The relation between partial structure **c** and **d** could be assigned by HMBC correlations for H_3-18 of C-12 to C-14, and C-17; H_2-16 and H-14 of C-15, such that a cyclopentanone was deduced to be attached to the phenantren ring system through C-13 and C-14. The connectivity of partial structure **e** (β-furyl ring) to **d** was shown by HMBC correlations for H-20 of C-17, H-21 of C-20, and C-22. Further analysis of HMBC correlations of H_3-29 of C-3 and C-5, and H_2-28 of C-6, indicated the presence of a tetrahydrofuran ring at C-4 – C6 and C-28. Therefore, ceramicine J (**6**) was established as a new limonoid with a cyclopentanone[α]phenanthren ring system with a β-furyl ring at C-17, and a tetrahydrofuran ring.

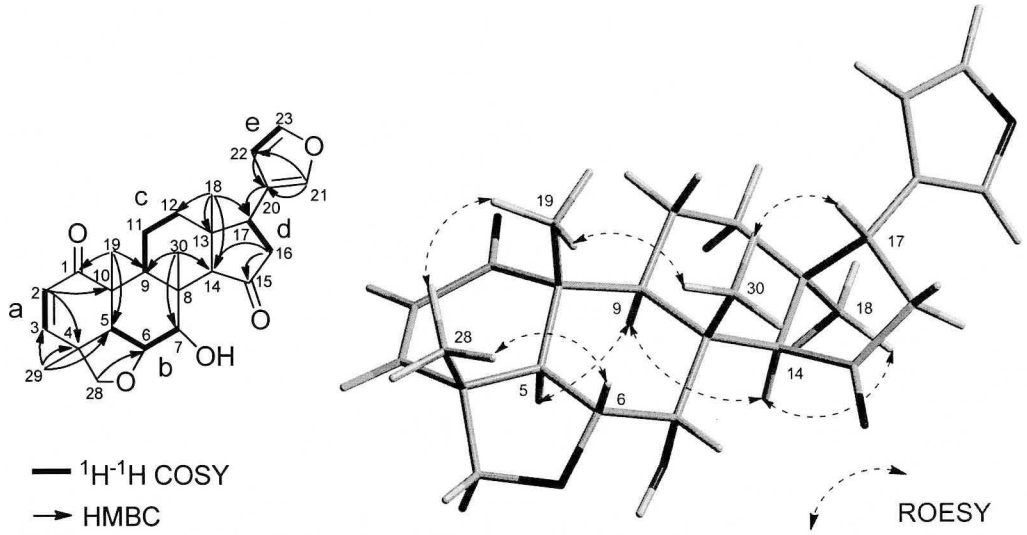

Figure II-8. Selected 2D-NMR correlation for ceramicine J (**6**)

The relative stereochemistry of **6** was elucidated by ROESY correlations as shown in computer-generated 3D rendering (Figure II-8). ROESY correlations of H_3-29/H-6, and H_3-19 suggested stereochemistry of C-29 methyl group to take as shown in figure II-8. The ^3J proton coupling constants ($^3J_{H\text{-}5/H\text{-}6}$ = 12.5 Hz and $^3J_{H\text{-}6/H\text{-}7} \approx 0$ Hz) as well as ROESY correlations of H-7/H-6 and H-14, and H_3-18/H-14 indicated that H-6, and H-7 adopted a β-configurations, and H-5, H-9, and C-18 adopted an α-configurations as shown in figure II-8.

Table II-4. ^{1}H and ^{13}C-NMR data of **6** in $CDCl_3$ at 300 K

	[δ_H (J, Hz)]	[δ_C]
1		202.5
2	5.84 (d, 9.7)	130.0
3	6.95 (d, 9.7)	151.0
4		41.8
5	2.61 (d, 12.5)	47.1
6	4.20 (dd, 12.5, 2.9)	73.6
7	4.17 brs	69.4
8		44.1
9	1.73 m	43.7
10		46.4
11a	1.71 m	19.1
11b	2.54 m	
12a	1.32 (d, 14.6)	34.2
12b	1.94 (dt, 14.6, 2.8)	
13		42.1
14	2.91 s	60.7
15		219.1
16a	2.52 (2H, m)	43.4
16b		
17	3.49 (t, 9.9)	37.7
18	0.78 s	27.6
19	1.17 s	15.0
20		123.0
21	7.27 s	140.2
22	6.30 s	110.8
23	7.40 s	142.8
28a	3.60 (d, 7.1)	79.8
28b	3.79 (d, 7.1)	
29	1.32 s	20.0
30	1.07 s	17.7

II.2.5 Ceramicine K & L (7 & 8)

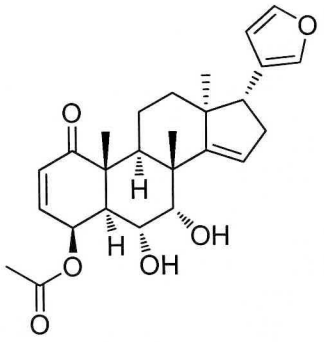

Ceramicine K (**7**)

Ceramicine K {**7**, $[\alpha]_D^{26}$ +6 (*c* 0.4, $CHCl_3$)} was isolated as a colorless amorphous solid and had molecular formula of $C_{26}H_{32}O_6$ as determined by HR-ESI-TOF-MS [*m/z* 463.2136 $(M+Na)^+$, Δ +3.9 mmu], which was an oxygen larger than ceramicine J (**6**). IR absorptions showed the presence of two carbonyls (1747 and 1691 cm^{-1}). ^1H and ^{13}C NMR data (Tables II-5) revealed 26 carbon resonance due to two carbonyls, two sp^2 quaternary carbons, three sp^3 quaternary carbons, six sp^2 methines, six sp^3 methines, three sp^3 methylenes and four methyls. In which, two sp^2 methines (δ_C 139.7 and 142.7), and three sp^3 methines (δ_C 65.2, 65.6, and 74.8) are attached to an oxygen atom. Further observation into ^{13}C NMR data, the presence of an olefin on C-14 and C-15 (δ_C 160.7 and 120.0, respectively) was observed to replace the carbonyl on C-15 (δ_C 219.1) as of seen on ceramicine J (**6**). In addition, HMBC correlations for H-4 and H_3-2' of C-1' included the presence of acetate at C-4 position (δ_C 65.2). Based on these NMR data including 2D NMR (COSY, HSQC, and HMBC) as well as HR-RES-TOF-MS, the plane structure of **7** was elucidated shown in figure II-9.

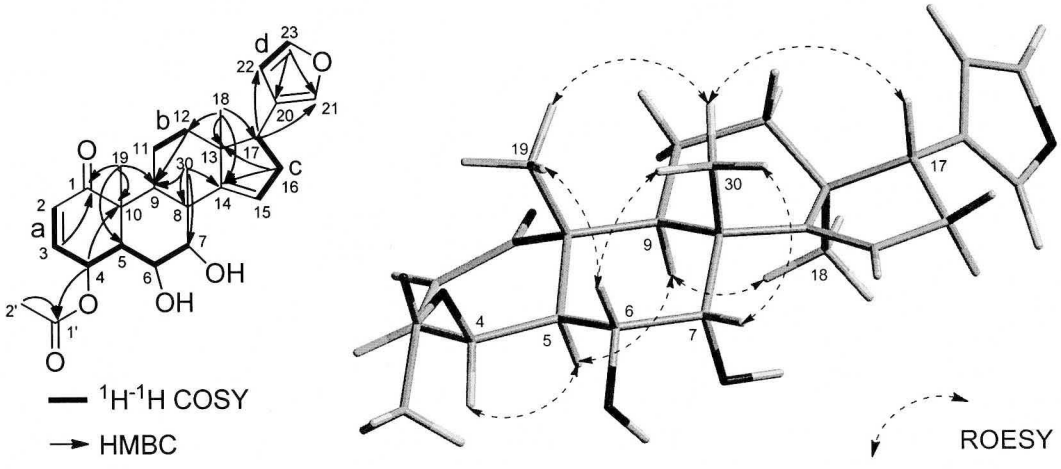

Figure II-9. Selected 2D-NMR correlations for ceramicine K (**7**)

The relative stereochemistry of **7** was elucidated by ROESY correlations as shown in computer-generated 3D drawing (Figure II-9). As shown by Figure II-9, the relative stereochemistry was shown to be similar to **6**. ROESY correlations of H-6/H_3-19, and H_3-30; H-7/H-15, and H_3-30 suggested the presence of both hydroxyls attached to C-6 and C-7 to adopt the α-configuration. In contrast, the ^3J proton coupling constants ($^3J_{H\text{-}4/H\text{-}5}$ = 4.6 Hz), along with ROESY correlation of H-4/H-5 implied the acetate attached to C-4 to adopt the β-configuration.

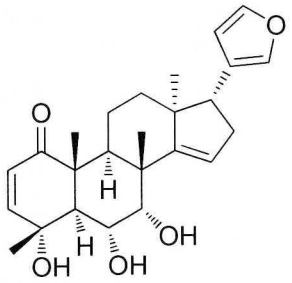

Ceramicine L (**8**)

Ceramicine L {**8**, $[\alpha]_D^{27}$ +14 (*c* 0.3, $CHCl_3$)} was isolated as a colorless amorphous with molecular formula of $C_{25}H_{32}O_6$ as established by HR-ESI-TOF-MS [*m/z* 435.2147 $(M+Na)^+$, Δ +2.6 mmu], which was smaller than that of ceramicine K (**7**) by a CO unit. ^1H and ^{13}C NMR data (Tables II-5) of **8** were analogous to those of **7**, but instead of acetate attached at C-4 in **7**, the presence of a sp^3 quaternary carbon for C-4 with a methyl and a hydroxy group was suggested by the HMBC correlations H_3-29 to C-3, C-4 (δ_C 71.5), and C-5 (Figure II-10). The ROESY correlations between H-6/H_3-29 and H_3-30, H-7/H_3-30, and H_3-29/H_3-19 suggested that all three hydroxyls adopted the α-configuration (Figure II-10).

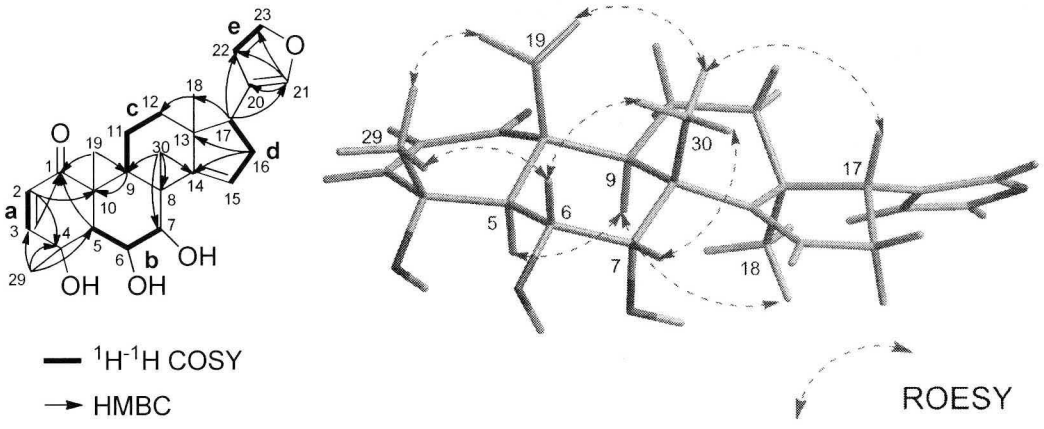

Figure II-10. Selected 2D-NMR correlations for ceramicine L (**8**)

Table II-5. ^{1}H and ^{13}C-NMR data of **7** and **8** in $CDCl_3$ at 300 K

	7		**8**	
	[δ_H (*J*, Hz)]	[δ_C]	[δ_H (*J*, Hz)]	[δ_C]
1		203.7		203.8
2	5.93 (d, 10.0)	130.1	5.75 (d, 10.3)	125.6
3	6.77 (ddd, 17.1, 10.0, 4.6)	139.2	6.41 (d, 10.3)	149.8
4	5.65 (t, 4.6)	65.2		71.5
5	2.46 (dd, 9.0, 4.6)	43.6	2.63 (d, 11.6)	50.9
6	4.12 (t, 9.0)	65.0	4.39 m	68.4
7	4.05 brs	74.8	3.98 (d, 2.4)	75.0
8		47.2		44.3
9	2.49 m	32.7	2.50 m	33.5
10		48.0		49.1
11a	1.62 m	17.9	1.55 m	17.8
11b	2.52 m		2.55 m	
12a	1.60 m	32.7	1.59 m	33.1
12b	1.93 m		1.92 (dt, 13.0, 2.9)	
13		44.2		47.1
14		160.7		160.6
15	5.58 s	120.0	5.58 s	120.3
16a	2.43m	34.3	2.42 m	34.3
16b	2.55 m		2.54 m	
17	2.87 (dd, 11.0, 7.4)	52.0	2.87 (dd, 10.9, 7.3)	51.9
18	0.88 s	21.3	0.89 s	21.5
19	1.33 s	16.0	1.25 s	15.8
20		124.4		124.4
21	7.26 s	139.7	7.26 s	139.7
22	6.30 s	111.0	6.30 s	111.0
23	7.39 s	142.7	7.39 s	142.7
28a				
28b				
29			1.62 s	23.8
30	1.22 s	26.3	1.19 s	26.4
1'		170.5		
2'	2.15 s	21.1		

Chapter III – Absolute Configuration of Ceramicine B

Absolute stereostructures of a series of ceramicines are still remained to be solved. Hence, in this report the absolute configuration of ceramicine B, a major limonoid from *C. ceramicus*, was elucidated by using the exciton chirality CD method [38]. The CD spectrum of *p*-Br-benzoyl derivative of ceramicine B was shown in Figure III-1A. At first position, [λ_{max} 246 nm ($\Delta\varepsilon$ -9.89)] was of a negative value, while at the second position [λ_{max} 225 nm ($\Delta\varepsilon$ 14.52)] was of a positive value. This indicates that the chirality of the two chromophores (benzoate chromophore and α,β-unsaturated ketone chromophore) was a left-handed screw or oriented in a counter clockwise manner, as shown in Figure III-1B. Therefore, absolute configuration at C-7 could be assigned as *S*.

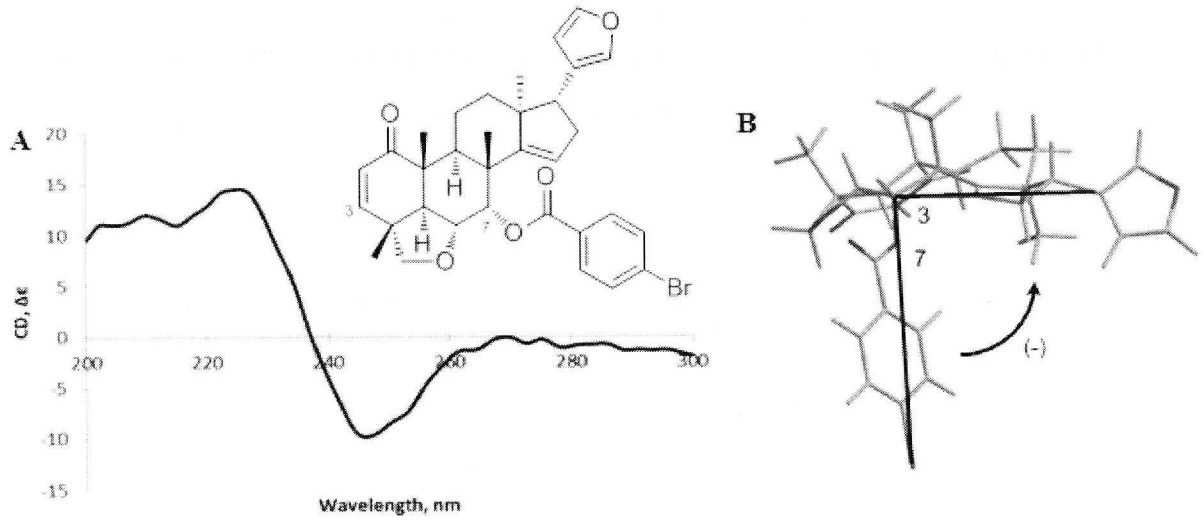

Figure III-1. A) CD spectrum. B) 3D structure of *p*-Br benzoate of ceramicine B.

Apart from using exciton chirality method, the crystal structure of ceramicine B was also determined using X-ray crystallography method. The addition X-ray crystallography results showed that, total structure of ceramicine B including its absolute structure was confirmed by the Flack parameter [39], χ = -0.0(2) of X-ray analysis for the crystal obtained from MeOH/H_2O (Figure III-2). Therefore, the absolute configuration of ceramicine B was assigned as (4*R*, 5*S*, 6*R*, 7*S*, 8*R*, 9*S*, 10*R*, 13*S*, and 17*R*).

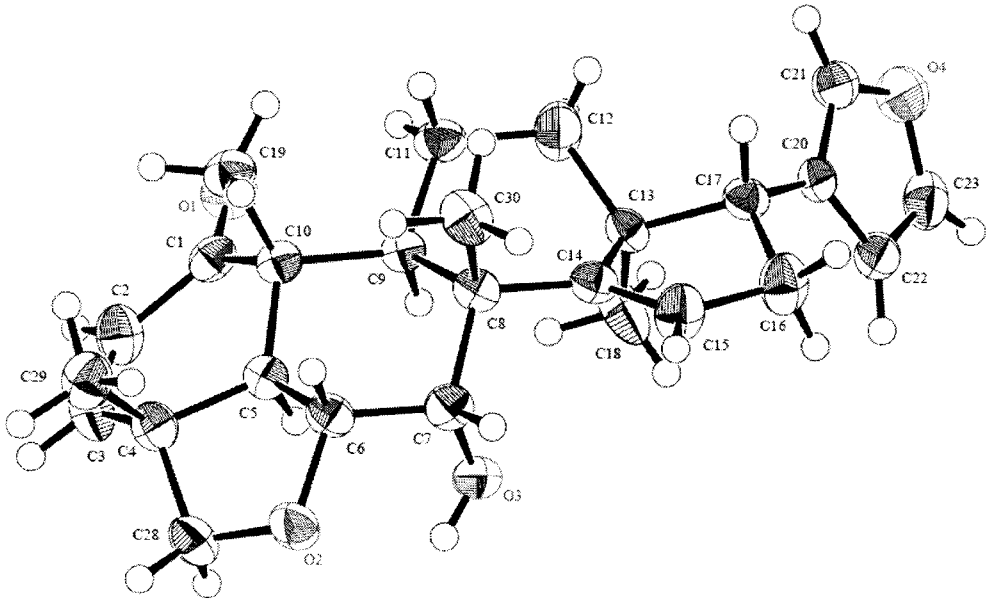

Figure III-2. Molecular structure of ceramicine B obtained by X-ray analysis [Flack parameter: χ = -0.0(2)].

Chapter IV - Anti-Lipid Droplets Accumulation Activity of Ceramicines

IV.1 Introduction

In our effort to identify compounds as an anti-obesity drug lead, the eight new limonoids, ceramicines E-L (**1-8**) isolated from *C. ceramicus* bark extract were tested for anti-LDA activity on mouse pre-adipocyte cell line, MC3T3-G2/PA6. Apart from examining their anti-LDA activity, present study also investigates their structure activity relationship.

IV.2 Results

IV.2.2 Anti-Lipid Droplets Accumulation Activity of Ceramicines

As a result from anti-LDA screening, we have identified that the methanol extracts of C. ceramicus bark to exhibit anti-LDA activity. The extract of C. ceramicus showed a dose dependent reduction of LDA from 6.25 μg/mL to 50 μg/mL. Although having weaker anti-LDA activity compared to berberine, C. ceramicus bark extract exhibited higher cell viability as showed by mitochondrial succinate dehydrogenase activity (Figure IV-1).

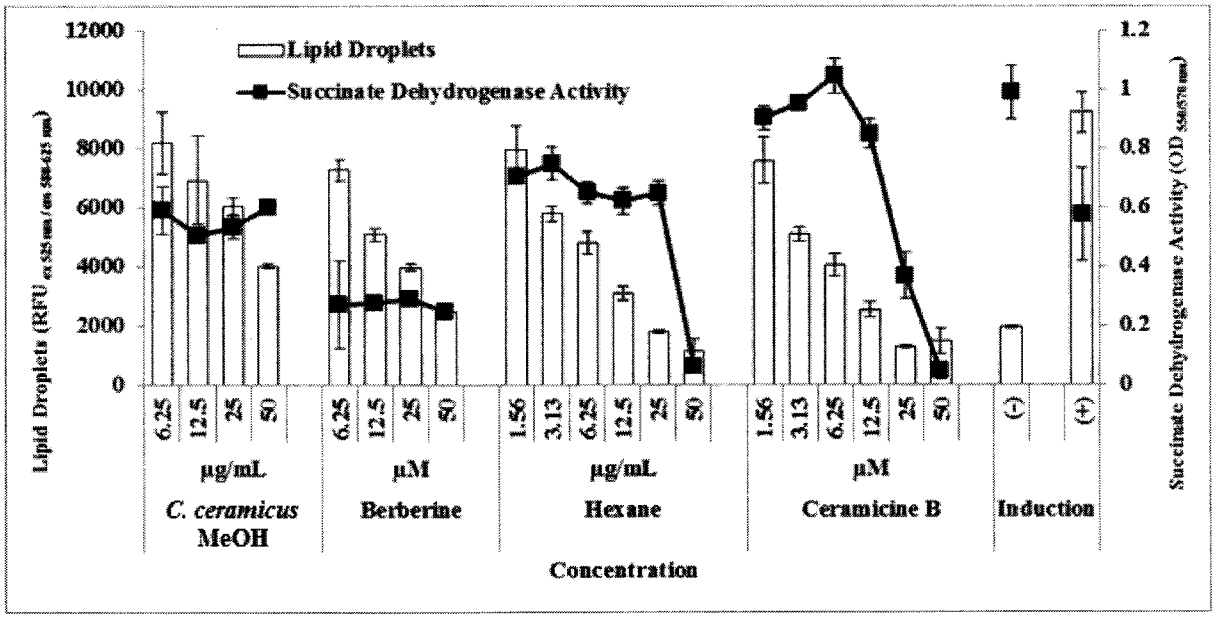

Figure IV-1. Anti-LDA activity of Chisocheton ceramicus bark methanol extract, hexane fraction, and ceramicine B on mouse pre-adipocyte cell line, MC3T3-G2/PA6 cells were compared to berberine used a control (bar). Anti-LDA activity was measured using nile red lipid droplets fluorescent staining method. Samples cytotoxicity was measured indirectly via mitochondrial succinate dehydrogenase activity (solid square) using MTT assay. Cells were pre-incubated 2 days prior to MDI induction. Analysis was carried out on day six. Each data point represents the mean ± SD of three independent experiments carried out in triplicate.

Nile red lipid droplets fluorescent staining result indicated that only hexane fraction showed promising anti-LDA activity (Figure IV-2) (results not shown for ethyl acetate, *n*-butanol and water fraction). Similar to result of prior methanol extract, hexane fraction also showed anti-LDA activity in a dose dependent manner from 1.56 µg/mL to 25 µg/mL. However, decrease in cell viability was observable in the presence of 50 µg/mL of hexane fraction under microscope.

Further purification carried out on the *C. ceramicus* bark extract yielded a series of 12 new compounds named as ceramicine A-L. Nile red lipid droplets fluorescent staining result showed ceramicine B is the most potent compound in inhibiting LDA in MC3T3-G2/PA6 cells with estimated IC_{50} at 1.8 µM. Ceramicine B however showed cytotoxicity at concentration above 25 µM as microscopic observation showed. While ceramicine A also showed potent anti-LDA activity, it is weaker compared to ceramicine B with estimated IC_{50} at 6.2 µM. Both ceramicine A and B showed dose dependent manner in their anti-LDA activity. On the other hand, ceramicine G and I exhibited a moderate anti-LDA activity with

slight cytotoxicity on higher concentration. The remaining ceramicines were inactive in inhibiting LDA activity.

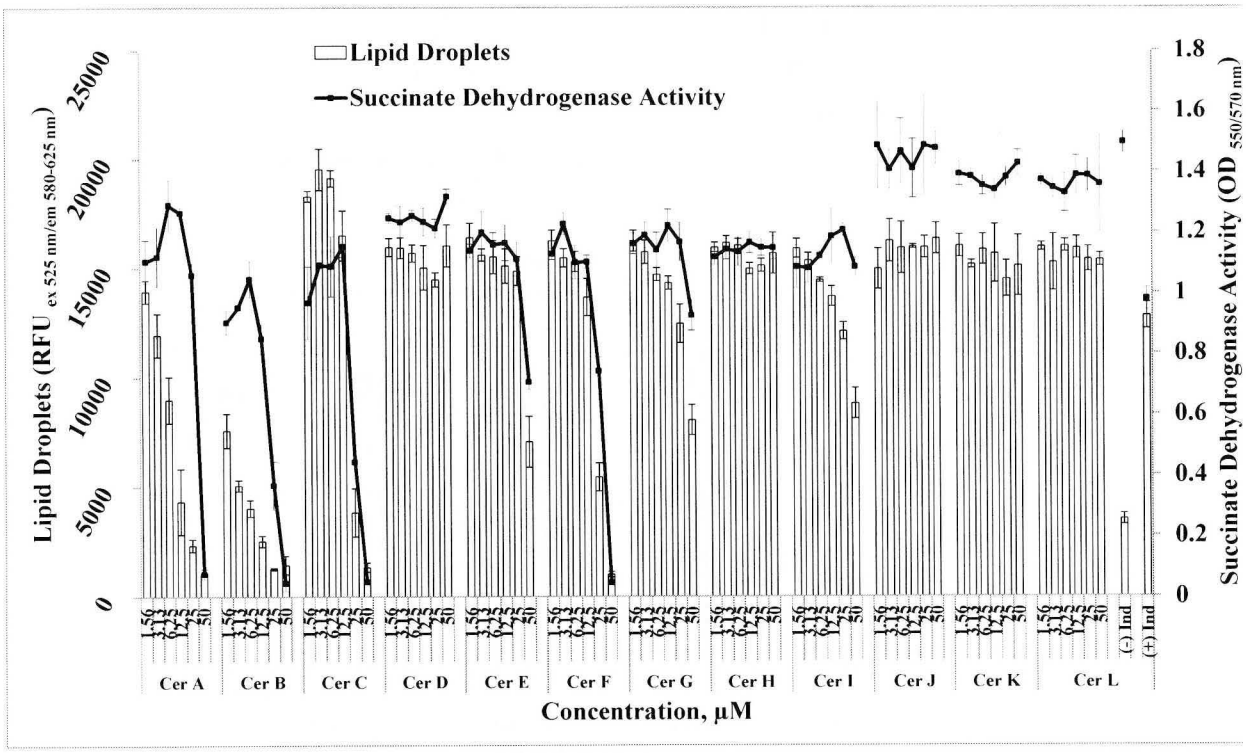

Figure IV-2. Anti-LDA activity of ceramicines A-L. Treatment conditions and measurement of anti-LDA were same as previous mention. A six point serially diluted concentrations (1.56 – 50 µM) of ceramicine were tested for both anti-LDA activity and cytotoxicity to MC3T3-G2/PA6 cells. Each data point represents the mean ± SD of three independent experiments carried out in triplicate.

IV.2.3 Structure Activity Relationship of Ceramicines

The preliminary structural activity relationship of **1-8** and the previously isolated ceramicines A-D were studied. Comparison between most potent ceramicine B with **4** and **5** showed that, substitution of C-12 proton with tiglate or acetate group showed no activity and reduced activity, respectively to MC3T3-G2/PA6 cells. While, substitution with methacrylate group as in ceramicine C were shown to cause cytotoxicity (Figure IV-3).

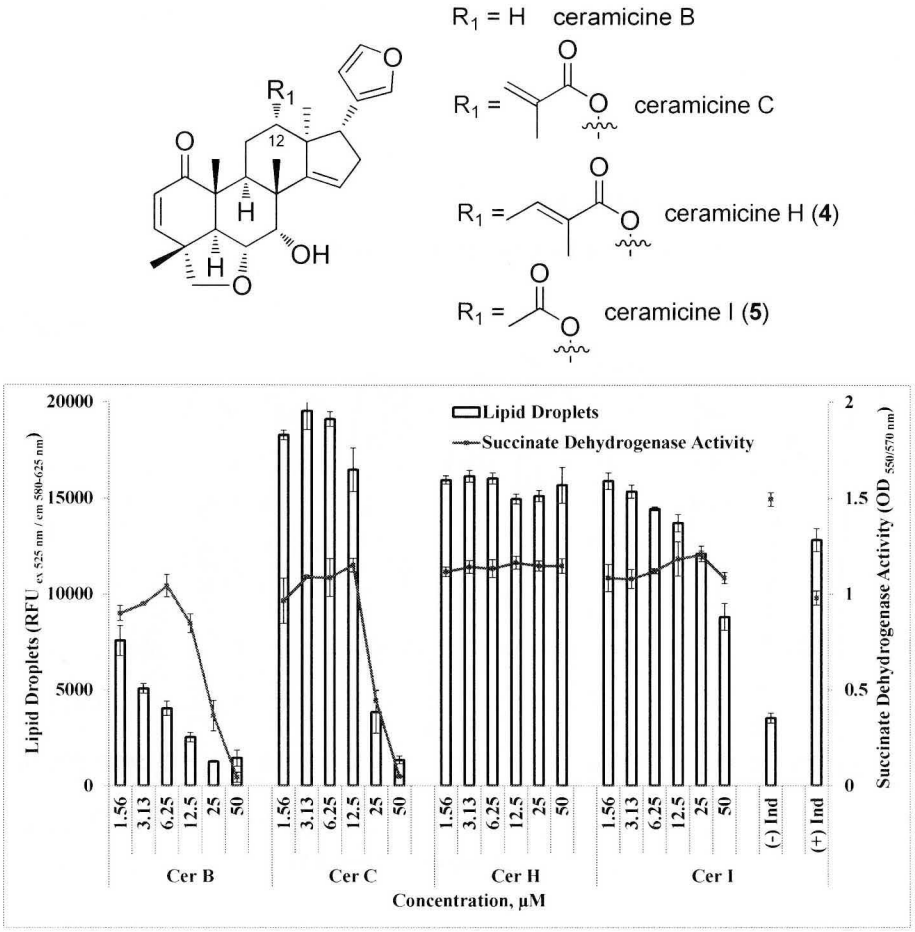

Figure IV-3. Ceramicines B, C, H (**4**), and I (**5**) (top). Comparison of ceramicines B, C, **4**, and **5** anti-lipid droplets accumulation activity (below).

By comparing ceramicine B, most potent compound with the inactive compound, ceramicine D, it is revealed that, the furan ring attached to C-17 were important for elicitation of anti-LDA activity, as substitution with a furolactone ring completely reduced the anti-LDA activity (Figure IV-4).

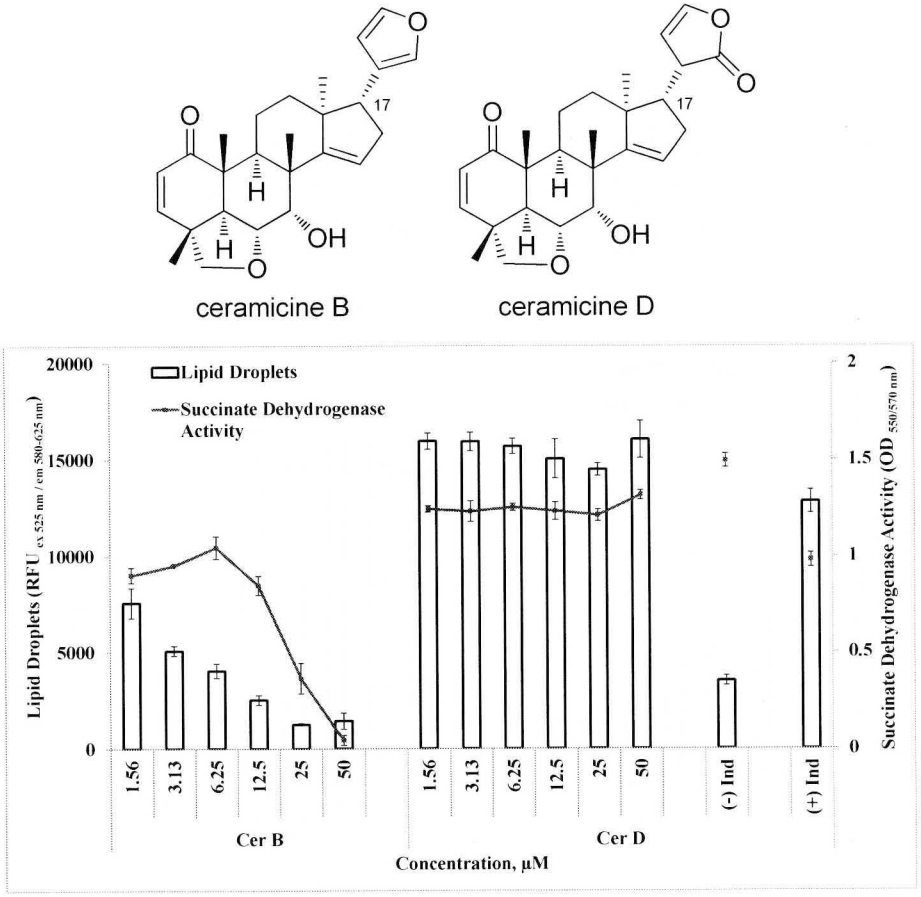

Figure IV-4. Ceramicines B and D (top). Comparison of ceramicines B and D anti-lipid droplets accumulation activity (below).

On other hand, change from C-14 and C-15 double bond in ceramicine B to C-15 carbonyl group in **6** reduced anti-LDA activity. This indicates that C-14 and C-15 double bond is important for anti-LDA activity (Figure IV-5).

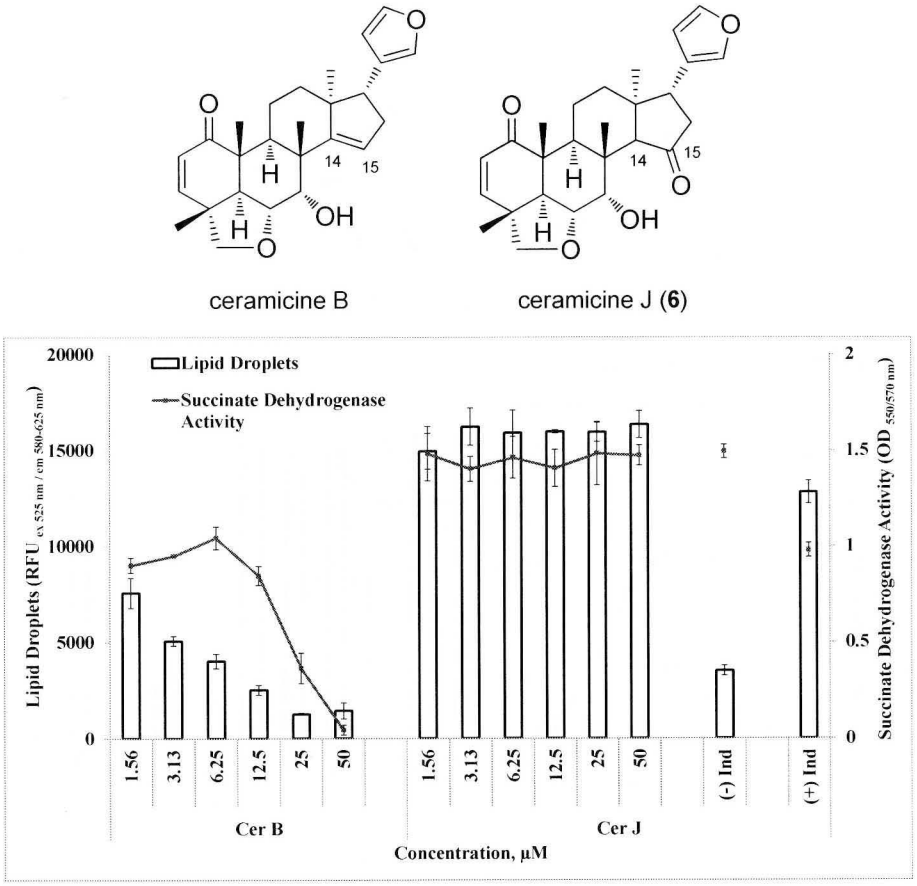

Figure IV-5. Ceramicines B and J (**6**) (top). Comparison of ceramicines B and **6** anti-lipid droplets accumulation activity (below).

Additionally, the double bond formed between C-2 and C-3 is important for anti-LDA activity. As comparison between ceramicine A and E (**1**), existence of an epoxy group at C-2 and C-3; and substitution of C-4 hydroxyl with an epoxy group showed a complete reversal of its activity (Figure IV-6).

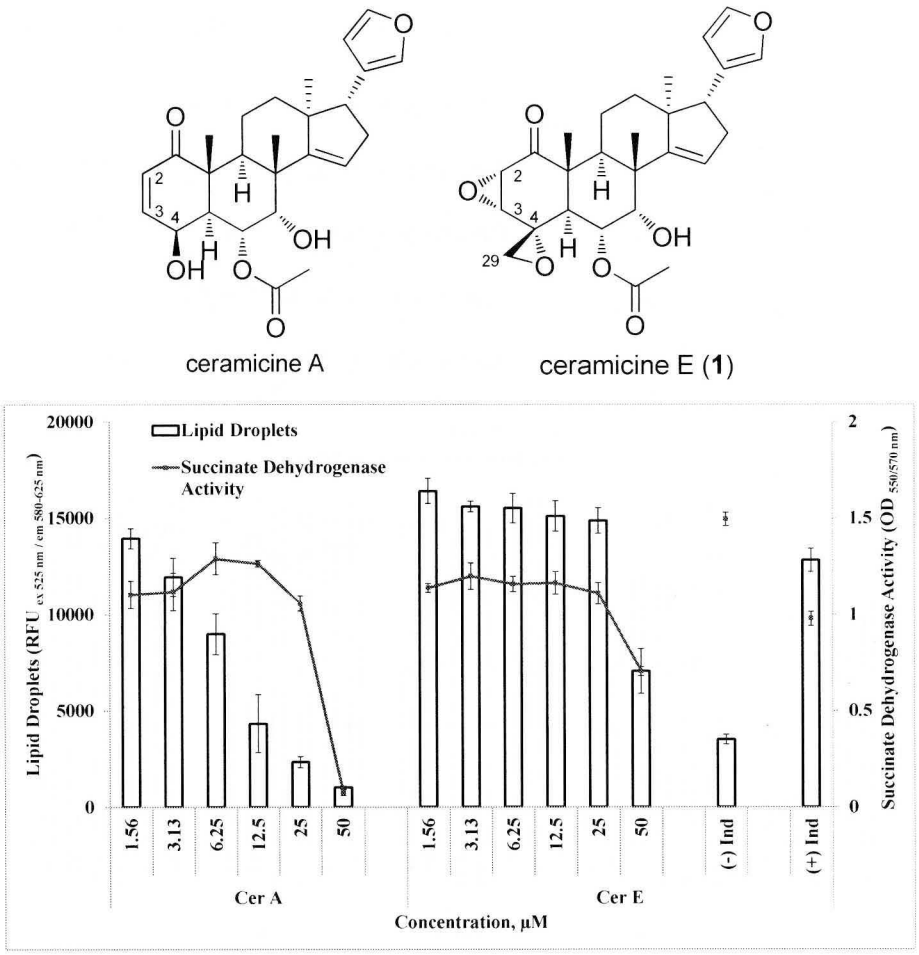

Figure IV-6. Ceramicines A and E (**1**) (top). Comparison of ceramicines A and **1** anti-lipid droplets accumulation activity (below).

In comparing ceramicine A with **2**, and **3** showed that substitution of R_1 hydroxyl at C-4 with methyl, and R_2 proton with aldehyde or methoxycarbonyl resulted in decrease of anti-LDA activity (Figure IV-7). The inversion between the C-4 hydroxyl and C-6 acetate of ceramicine A to C-4 acetate and C-6 hydroxyl of **7** resulted in loss of anti-LDA activity (Figure IV-7). While comparing ceramicine A and **8**, alterations of R_1 hydroxyl to methyl and R_2 proton at C-4 with hydroxyl at C-4; and C-6 acetate to hydroxyl also result in loss of anti-LDA activity (Figure IV-7). However more data are required to confirm the importance of C-4 and C-6 components on anti-LDA structure activity relationship.

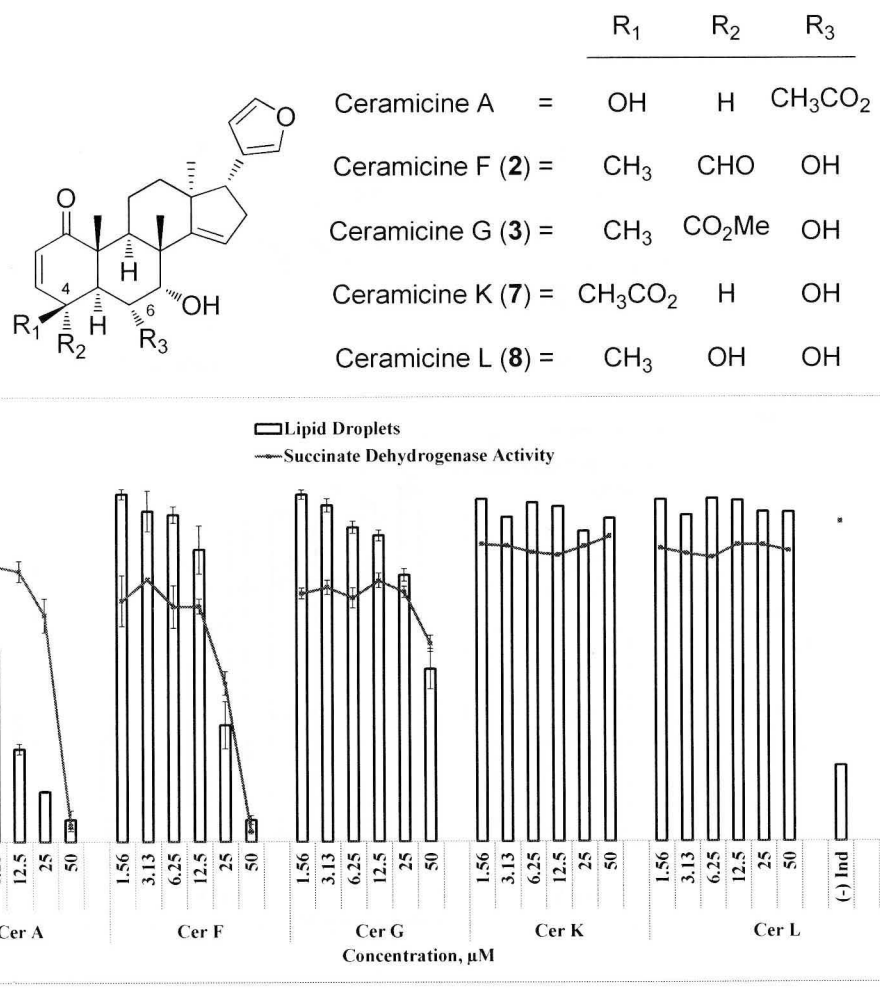

Figure IV-7. Ceramicines A, E (**1**), F (**2**), G (**3**), K (**7**), and L (**8**) (top). Comparison of ceramicines A, **1**, **2**, **3**, **7**, and **8** anti-lipid droplets accumulation activity (below).

On a final note, there is no apparent structure activity relationship correlation between ceramicine A and B as both structure showed anti-LDA activity. Results showed that, substitution pattern and stereochemistry at C-4, C-5, C-6, and C-28 are critical to anti-LDA activity. Thus further studies are thus required to compare ceramicine B which has a tetrahydrofuran ring form between ring **A** and **B** through C-4, C-5, C-6, and C-28 with ceramicine A that is without the tetrahydrofuran ring.

Summary on the preliminary structure activity relationship of ceramicines series on anti-LDA activity against mouse pre-adipocyte cell line, MC3T3-G2/PA6 cells is shown below (Figure IV-8).

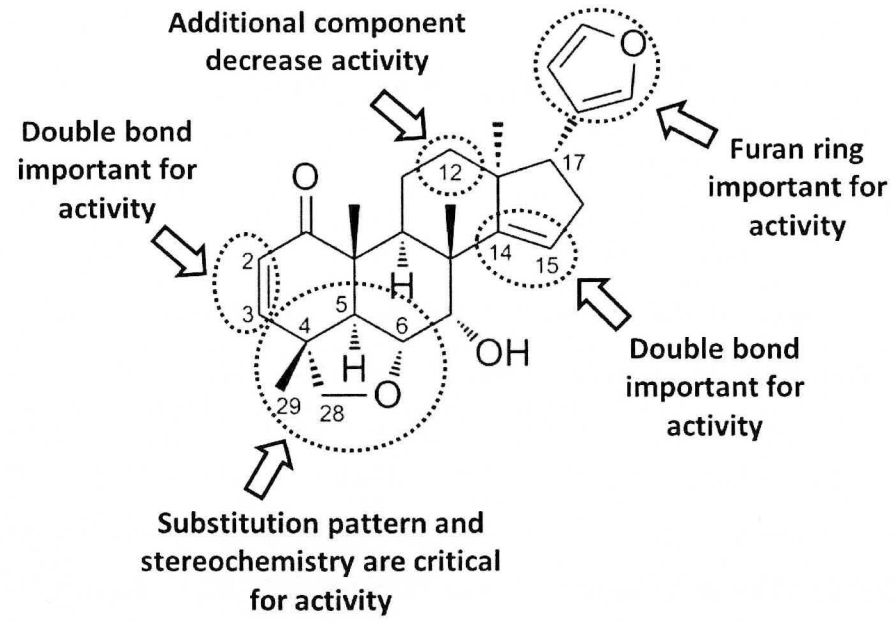

Figure IV-8. Summary of ceramicines anti-lipid droplets accumulation activity using ceramicine B as example.

Chapter V - Mechanism Studies of Ceramicine B on Anti-Lipids Droplets Accumulation Activity

V.1 Introduction

Up to date, most of the events that regulate adipogenesis are well documented. Adipocytes originate from the same pluripotent mesenchymal stem cells (MSCs) as osteoblast, chondrocytes, and myocytes but each received distinctive signals to differentiate [40]. Signals such as bone morphogenetic proteins (BMPs), transforming growth factor-β (TGF-β), activin, insulin-like growth factor 1 (IGF-1), interleukin-17 (IL-17), and fibroblast growth factor (FGF) 1 and 2 have all been reported to initiate the adipogenesis progression [41-47]. On other hand, mixture of 3-isobutyl-1-methylxanthine (IBMX), dexamethasone (DEX), and insulin (MDI induecer) have been used to stimulate adipocyte differentiation *in vitro* [48]. Upon induction into adipogenesis, C/EBPβ and C/EBPδ are initially expressed are the transcription factors of the master adipogenic gene, PPARγ and C/EBPα [49-50]. PPARγ and C/EBPα positively cross regulates each other increasing the expression of adipocyte specific genes such as glucose transporter type 4 (GLUT4), LPL, and 11-beta hydroxysteroid dehydrogenase (HSD11β1) [51-53]. Apart from C/EBPβ and C/EBPδ, a well-known key intermediate regulatory of adipogenesis are krüppel like factors (KLFs). The family members of KLFs include both the positive and negative regulatory protein is signal transduction for adipocytes differentiation [54]. Up-to-date various regulatory molecules involves in adipogenesis signaling cascade have so far been reported. All these molecules could be affected by ceramicine in eliciting anti-LDA activity. Therefore, the focus of this study was elucidation of ceramicine B properties to inhibit LDA and its mechanism of action.

V.2 Results

IV.2.1 Inhibition of Adipocyte Specific Genes Expression by Ceramicine B

Ceramicine B was identified to be most potent among ceramicines series (V-1A-D). In general, LDA in adipocytes are directly related to adipogenesis. As an initial studies into the mechanism of anti-LDA activity, mRNA expression of adipocyte specific genes were determined. Expression of adipocyte specific genes mRNA was examined at MC3T3-G2/PA6

cells at pre-differentiation and terminal differentiation state, 7 and 14 days from the start of MDI induction process, respectively. RNA were harvested from four treatment groups which were divided into vehicle and MDI with or without ceramicine B. RT-PCR results showed that, adipocyte specific genes, glucose transporter type 4 (GLUT4) or also known as SLC2A4 and lipoprotein lipase (LPL) were up-regulated during MDI induction but were down-regulated in the presence of ceramicine B (Figure V-1E). HSD11β1 were found up-regulated from day 7 with or without MDI induction. Down-regulation was also observed in HSD11β1 mRNA expression in the presence of ceramicine B (Figure V-1E).

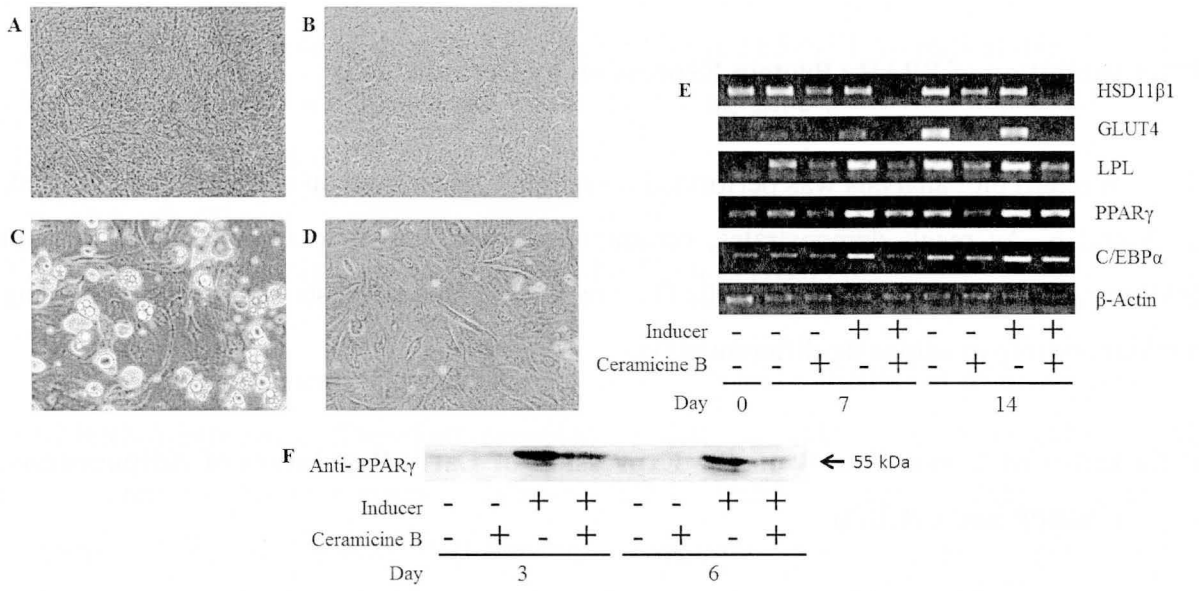

Figure V-1. A-D) Picture of MC3T3-G2/PA6 cells taken after 5 days after MDI induction. A) vehicle control, B) cells treated with ceramicine B at 12.5 μM, C) MDI induced cells D) MDI induced cells treated with ceramicine B at 12.5 μM. E) RT-PCR data of samples harvested from MC3T3-G3/PA6 cells at 7 and 14 days. Effect of ceramicine B was tested on adipocytes specific genes, GLUT4, LPL, and HSD11β1; and adipogenesis master regulating genes, PPARγ and C/EBPα. Lane 1 – vehicle control at day 0, lane 2-5 – samples harvested at day 7 in order the of vehicle control, cells treated with ceramicine B at 12.5 μM, MDI induced cells, and MDI induced cells treated with ceramicine B at 12.5 μM. Lane 5-9 - samples harvested at day 14 with similar order as above. F) Western blot analysis on total cells protein harvested from MC3T3-G2/PA6 cells at day 3 and 6. Changes in protein level of PPARγ were investigated with anti-PPARγ monoclonal antibody. Proteins were loaded in the order of vehicle control, cells treated with 12.5 μM of ceramicine B, MDI induced cells, and MDI induced cells treated with ceramicine B at 12.5 μM.

IV.2.2 Inhibition of Adipogenesis Master Regulating Genes, PPARγ and C/EBPα Expression by Ceramicine B

MDI induction was shown to up-regulate PPARγ and C/EBPα mRNA expressions (Figure V-1E – lane 4 and -8). However, both the master regulating genes PPARγ and C/EBPα mRNA were not shown to be up-regulated by ceramicine B (Figure V-1E – lane 3, -5, -7, and -9). This suggested that down-regulation of previously mentioned GLUT4, LPL and HSD11β1 mRNA expression might be caused by the down-regulation of these master regulating genes, PPARγ and C/EBPα.

IV.2.3 Inhibition of PPARγ Protein Expression by Ceramicine B

Western blot analysis was performed on samples taken from an earlier time of harvest, day 3 and 6. As result demonstrates, ceramicine B was shown to inhibit the expression PPARγ protein in MC3T3-G2/PA6 cells (Figure V-1F). This suggests ceramicine B playing an inhibitory role in adipocyte differentiation.

IV.2.4 Effect of Ceramicine B on the Expression of Early Regulators of Adipogenesis, C/EBPβ and C/EBPδ

In a typical adipocyte induction pathway, expression of PPARγ and C/EBPα were regulated by C/EBPβ and C/EBPδ. Since treatment with ceramicine B was recognized to down-regulate the master regulators, PPARγ and C/EBPα, the early regulators of adipogenesis, C/EBPβ and C/EBPδ were also studied. Both C/EBPβ and C/EBPδ mRNA expression were increased after MDI induction at 2 and 6 hours. Results showed that presence of ceramicine B did not have significant effect on the expression of both C/EBPβ and C/EBPδ mRNA (Figure V-2).

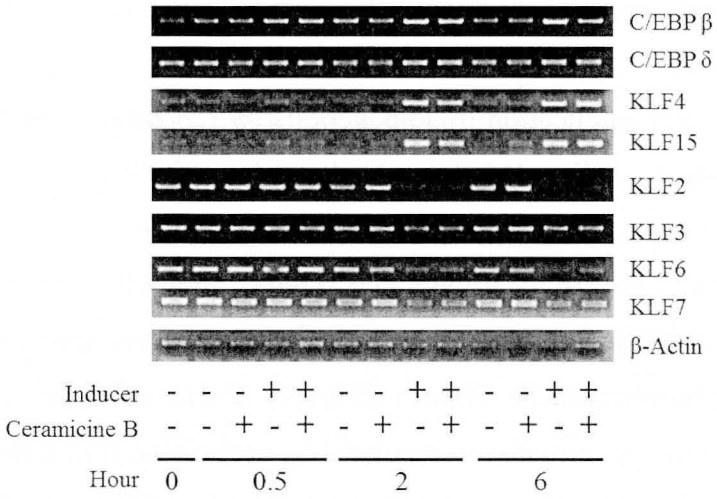

Figure V-2. RT-PCR data of samples harvested from MC3T3-G3/PA6 cells at thirty minutes, 2 and 6 hours tested on adipogenesis master regulating genes, C/EBPβ and C/EBPδ; and KLF2, -3, -4, -6, -7, and -15.

IV.2.5 Effect of Ceramicine B on Krüppel Like Factors (KLFs)

The ineffectiveness of ceramicine B on C/EBPβ and C/EBPδ led to investigation of KLFs mRNA expression. Therefore, ceramicine B effect on mRNA expression of KLFs, an important regulator of adipogenesis was assessed. It is identified that KLFs expression did not commence at 30 minutes after MDI induction. Expression positive KLFs regulator mRNA (KLF-4, -15) was observed to be up-regulated at 2 and 6 hours after MDI induction. On the other hand, expression negative KLFs regulator mRNA (KLF-2, -3, -6, and -7) was observed to be down-regulated at 2 and 6 hours after MDI induction. Studies on expression of KLFs mRNA showed that ceramicine B have no influence on both the expression of the positive KLF regulators and negative KLF regulators. Results from RT-PCR on KLFs indicated that ceramicines mechanism of anti-LDA activity was not *via* modulation of KLFs mRNA expression (Figure V-2).

IV.2.6 Effect of Ceramicine B on the Phosphorylations of Forkhead Box O1 (Foxo1)

Foxo1 have major implication in adipogenesis by repressing transcription of PPARγ mRNA. Phosphorylation of Foxo1 led to de-repression of PPARγ mRNA transcription. Phosphorylation of Foxo1 examined by western blot analysis on total protein samples harvested from MC3T3-G2/PA6 at 2 hours and 6 hours after MDI induction and treatment with ceramicine B. The outcome of protein analysis indicated an apparent reduction in the level of Thr24 phosphorylated Foxo1 (Figure V-3) although protein level of unphosphorylated Foxo1 was initially up-regulated by ceramicine B at 2 hour with or without MDI induction into adipocyte. However, at hour 6 there is no apparent difference between Foxo1 protein expression with or without induction into adipocyte.

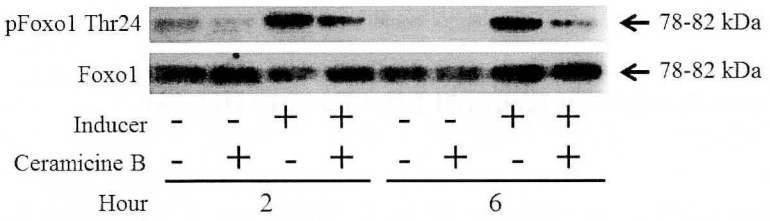

Figure V-3. Western blot analysis on total cells protein harvest from MC3T3-G2/PA6 cells at 2 and 6 hours. Phosphorylation of Foxo1 was investigated with anti-Foxo1, and anti-pFoxo1 Thr24 monoclonal antibody.

V.3 Discussions

Ceramicine B was identified to be most potent compound in inhibiting LDA in MC3T3-G2/PA6 cell lines, followed by ceramicine A while rest of the ceramicines were either weak or inactive in inhibiting LDA. It was previously reported that ceramicine B is the major component found in the *C. ceramicus* bark sample with yield up to 0.074% (w/w) [15]. This could be the main factor in anti-LDA activity of bark methanol and subsequent hexane fraction.

In this study, influence of ceramicine B on the expression of GLUT4, LPL, and HSD11β1 mRNA were investigated. GLUT4, an insulin regulated glucose transporter protein that translocation to plasma membrane facilitates the uptake of glucose into cells [55]. This protein is expressed primarily in muscle and fat tissue, making it an ideal marker for determining adipocyte differentiation. Apart from GLUT4 another lipid homeostasis related

gene was also studies, LPL. LPL is an enzyme that hydrolyzes triglycerides such as very low-density lipoproteins (VLDL), into two free fatty acids and one monoacylglycerol molecule. It is mostly distributed in adipose, heart, and skeletal muscle tissue [56]. HSD11β1 is another enzyme that is related to the metabolism that it is highly expressed in adipose tissue. This family of enzyme catalyzes the conversion of inactive cortisone to active cortisol, and vice versa [57-59]. All three GLUT4, LPL, and HSD11β1 mRNA which are mainly expressed in matured adipocyte were found to be suppressed by ceramicine B. The reduction of these three genes mRNA transcripts suggest a preliminary role of ceramicine B in inhibiting the differentiation of MC3T3-G2/PA6 cells into adipocyte.

Preliminary speculation that ceramicine B might play a role in inhibiting adipogenic differentiation leads us to further investigate the effect of ceramicine B on the two master regulating genes of adipogenesis, PPARγ and C/EBPα, respectively. Under normal circumstances, PPARγ and C/EBPα were up-regulated during MDI induction and formed positive-feedback loops that cross-regulates each other promoter. These two master regulating genes in turn induce a wide range of downstream adipogenic specific genes in developing and matured adipocytes which include aforementioned GLUT4, LPL and HSD11β1 [30-32]. Decrease in the expression of both PPARγ and C/EBPα mRNA further reinforce the preliminary speculation of ceramicine B playing a role in inhibiting adipocyte differentiation. To further support this speculation, western blot analysis was performed to determine PPARγ protein level of MC3T3-G2/PA6 cells treated with ceramicine B. Data showed down-regulation of PPARγ protein level, thus suggesting ceramicine B play a role in inhibiting adipocyte differentiation. By suppression of PPARγ role in adipocytes differentiation, ceramicine B also inhibit LDA activity.

Differentiation of MC3T3-G2/PA6 cells into adipocytes begins with MDI induction. Addition of IBMX or DEX directly influences the up-regulation C/EBPβ and C/EBPδ in a separate manner. Due to the role of C/EBPβ and C/EBPδ in regulating PPARγ and C/EBPα, mRNA expression [49-50] of these genes was also examined. However, ceramicine B was found to be non-active to the regulation of these genes. This led to the assumption that ceramicine B-induced down-regulation of PPARγ and C/EBPα mRNA expression was not via regulation of C/EBPβ and C/EBPδ.

Recent studies ascertained that KLFs regulates differentiation adipocytes activity. Consisting of both positive and negative regulators, KLFs hold an important role in both up-regulating and down-regulating many key adipogenic markers including PPARγ and C/EBPα [54]. Ineffectiveness of ceramicine B on C/EBPβ and C/EBPδ led us to investigate the

regulatory activity of KLFs on PPARγ and C/EBPα mRNA expression in MC3T3-G2/PA6. However, ceramicine B was not found to up-regulating or down-regulating KLFs mRNA expression.

Apart from the effect of IBMX and DEX, adipogenesis is also controlled by insulin signaling pathway [60]. Foxo1, also known as Foxo1A or FKHR, is an important transcriptional repressor that conveys PPARγ transcription, which was released by insulin-induced phosphorylation [61-62]. Foxo1 is regulated by the serine/theorine kinase Akt (PKB), which phosphorylates Foxo1 at three site, theorine 24, serine 256, and serine 319. Phosphorylation at these three positions, leads to the nuclear exclusion of Foxo1 and followed by ubiquination. In adipocytes, unphosphorylated Foxo1 binds to the promoter region of PPARγ, suppressing its transcription and preventing adipocyte differentiation [63].

Treatment with insulin led to phosphorylation of Foxo1, and subsequently inactivating its functions. This causes transcription of PPARγ to be released from repression and proceed to adipocytes differentiation [64]. Western blot analysis indicates that, treatment with ceramicine B resulted in decrease in Thr24 phosphorylated Foxo1 protein level but not in unphosphorylated Foxo1 (Figure V-3 – lane 7 and -8). This implies that ceramicine B might play a role in preventing the phosphorylation of Foxo1. Thus led to the speculation that transcription PPARγ mRNA was repressed and subsequently causes inhibition of adipocyte differentiation. Considering that Akt acts on phosphorylation of Foxo1 as insulin signaling pathway implies, further studies on ceramicine B effect on Akt signaling is necessary.

Chapter VI - Conclusion

Initiative on the search of drug candidates from terrestrial plants as a source of anti-obesity drug candidates leads to identification of *Chisocheton ceramicus* from Meliaceae with promising outcome. Previous studies have yielded four new limonoids, ceramicines A-D from the *C. ceramicus* bark extracts. Continuation of *C. ceramicus* bark extracts constituent in present studies have further yielded eight more new limonoids, ceramicines E-L (Figure VI-1). In addition, ceramicines were also found to possess anti-LDA activity with ceramicine B being most potent. The close relationship between LDA and obesity indicates the potential of ceramicine B as anti-obesity drug candidate.

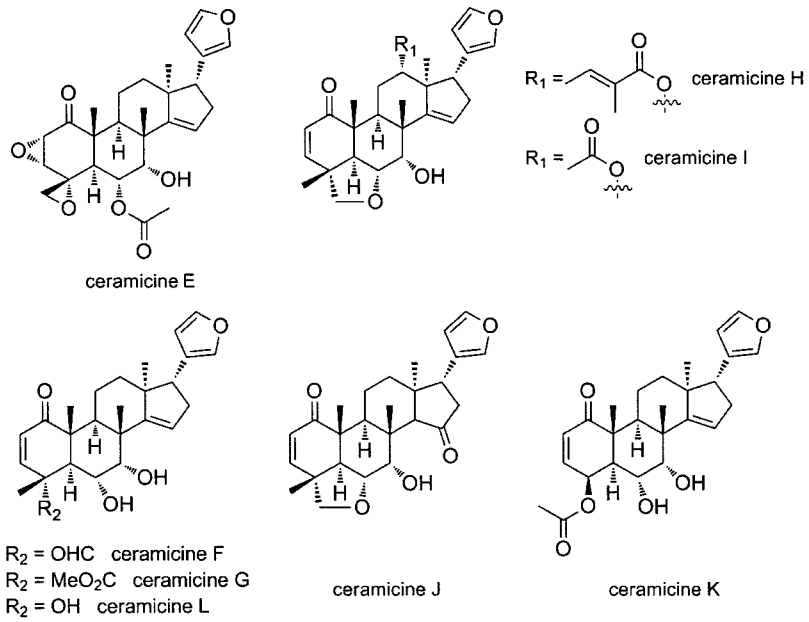

Figure VI-1. Ceramicines E (**1**) - L (**8**)

Apart from determining the anti-LDA activity ceramicines, the preliminary structural activity relationship of ceramicines was also studied. It was observed that the furan ring attached to C-17, double bond formed between C-2 and C-3, and between C-14 and C15, important for ceramicines anti-LDA activity. Whereas additional component added to C-12 will result in decrease of anti-LDA activity. Finally, it is understand that, substitution pattern and stereochemistry of C-4, C-5, C-6, and C-28 appear to be critical for elicitation of anti-LDA activity. However, further studies are required to determine the importance of the tetrahydrofuran ring form between ring **A** and **B** through C-4, C-5, C-6, and C-28.

As this studies suggested, ceramicine B might convey its anti-LDA activity through interrupting the phosphorylation of Foxo1. Thus results in continued repression of PPARγ mRNA expression which inhibition of LDA was due to suppression of adipocyte differentiation activity. However, additional studies are necessary to fully understand the mechanism of ceramicine B inhibits the phosphorylation of Foxo1. Given that Akt acts on phosphorylation of Foxo1 as insulin signaling pathway implies, further studies on ceramicine B effect on Akt signaling is necessary.

Experimental Methods

General Experimental Procedures

^{1}H and 2D NMR spectra were recorded with Bruker AV700 and JEOL ECA600. Each ceramicine's NMR sample was prepared by dissolving with $CDCl_3$ in 2.5 mm microcells (Kanto Chemicals Co., Inc., Japan) and the residual $CHCl_3$ chemical shift used as an internal standard are δ_H 7.26 and δ_C 77.0. Standard pulse sequences where used for the 2D NMR experiments. ^{1}H-^{1}H COSY, and NOESY spectra were measured with spectral widths of both dimensions of 4800Hz, and 8 scans with two dummy scans were accumulated into 1K data points for each of 256 t_1 increments. NOESY spectra in the phase sensitive mode were measured with a mixing time of 800 and 30 ms. While for the HSQC spectra in the phase sensitive mode and HMBC spectra, a total of 256 increments of 1K data points were collected. The (HMBC) spectra with Z-axis PFG, a 50 ms delay time was used for long range C-H coupling. Zero-filing to 1K for F_1 and multiplication with squared cosine-bell windows shifted in both dimensions were performed prior to 2D Fourier transformation.

Optical rotations were measured on a JASCO DIP-1000 polarimeter. UV spectra were recorded on a Shimadzu UVmini-1240 spectrophotometer and IR spectra on a JASCO Fourier transform/infrared (FT/IR)-4100 spectrophotometer. CD spectra were recorded on a JASCO J-820 polarimeter. High-resolution ESI-MS were obtained on a LTQ Orbitrap XL (Thermo Scientific, USA).

Merck silica gel 60 (40 – 63 μM) and Nacalai Tesque Cosmosil 140C_{18}-OPN were used for chromatography. Separation parameters were examined with Merck silica gel 60 F_{254} or Merck silica gel RP C-18 F_{254} TLC plates. HPLC were performed using Cadenza 5CD C18 (10 x 250 mm) and Cosmosil πNAP (10 x 250 mm).

Materials

The barks of *C. ceramicus* were collected from Pahang, Malaysia in 1996. The botanical identification was made by Mr. Teo Leong Eng, Faculty of Science, University of Malaya. Voucher specimens (Herbarium No. KL4648) are deposited in the Herbarium of Chemistry Department, University of Malaya.

Extraction and Isolation

Small Scale Extraction and Isolation

The dried ground barks of *C. ceramicus* (500 g) were extracted successively with methanol and 53 g of extract were obtained. In a small scale experiment, 7 g from the total extract was successively partitioned with hexane, ethyl acetate, *n*-butanol, and water. The hexane-soluble materials were further partitioned with a silica gel column (hexane/EtOAc, 10:0 → 1:1, and then $CHCl_3$/MeOH, 10:0 → 0:10). Fraction eluted from the silica gel column with $CHCl_3$/MeOH (7:3) was further purified using HPLC with Cadenza 5CD C_{18}, 10 x 250 mm, under gradient elution (50%-100% MeOH), flow rate 2.0 mL/min, UV: 210 nm to yield ceramicine E (**1**, 2.0 mg, 0.0004% yield), and ceramicine F (**2**, 9.5 mg, 0.0019% yield), both as colorless solid. Fraction eluted with $CHCl_3$/MeOH (1:1) was purified on HPLC with Cadenza 5CD C18, 10 x 250 mm, under gradient elution (70%-100% MeOH), flow rate 2.0 ml/min, UV: 210 nm to obtain ceramicine G (**3**, 5.6 mg, 0.0011% yield) as colorless solid. Whereas, fraction eluted with $CHCl_3$/MeOH (4:6) was purified on HPLC with Cadenza 5CD C18, 10 x 250 mm, under gradient elution (50%-100% MeOH), flow rate 2.0 mL/min, UV: 210 nm to afford ceramicine H (**4**, 0.3 mg, 0.00006% yield), and ceramicine I (**5**, 4.3 mg, 0.00086% yield). Previously identified ceramcines B and C were also isolated from hexane layer [15].

Ceramicine E (1): Colorless amorphous solid; $[\alpha]_D^{28}$ +20 (*c* 0.5, $CHCl_3$); UV (MeOH) λ_{max} 203 (ε 8640) nm; IR (KBr) ν_{max} 3437, 1718, 1506, 1389, 1372, and 1246 cm^{-1}; ^1H and ^{13}C NMR data (Table II-1); ESI-MS *m/z* 469 $(M + H)^+$; HR-ESI-TOF-MS *m/z* 469.2206 (M + H; calcd for $C_{27}H_{33}O_7$, 469.2226).

Ceramicine F (2): Colorless amorphous solid; $[\alpha]_D^{28}$ +101 (*c* 0.5, $CHCl_3$); UV (MeOH) λ_{max} 203 (ε 14592) nm; IR (KBr) ν_{max} 3437, 2980, 2920, 1724, 1679, 1448, and 1388 cm^{-1}; ^1H and ^{13}C NMR data (Table II-2); ESI-MS *m/z* 447 $(M + Na)^+$; HR-ESI-TOF-MS *m/z* 447.2120 (M + Na; calcd for $C_{26}H_{32}O_5Na$, 447.2147).

Ceramicine G (3): Colorless amorphous; $[\alpha]_D^{28}$ -39 (*c* 0.5, $CHCl_3$); UV (MeOH) λ_{max} 203 (ε 11000) nm; IR (neat) ν_{max} 3430, 2993, 1717, 1685, and 1260 cm^{-1}; ^1H and ^{13}C NMR data (Table II-2); ESI-MS *m/z* 477 $(M + Na)^+$; HR-ESI-TOF-MS *m/z* 477.2244 (M + Na; calcd for $C_{27}H_{34}O_6Na$, 477.2253).

Ceramicine H (4): Colorless amorphous solid; $[\alpha]_D^{26}$ +77 (*c* 0.15, MeOH); UV (MeOH) λ_{max} 203 (ε 29900) nm; IR (CCl_4) ν_{max} 3418, 2927, 2855, 1703, 1684, 1585, and 1260

cm^{-1}; ^{1}H and ^{13}C NMR data (Table II-3); ESI-MS *m/z* 529 $(M + Na)^+$; HR-ESI-TOF-MS *m/z* 529.2565 (M + Na; calcd for $C_{31}H_{38}O_6Na$, 529.2566).

Ceramicine I (5): Colorless amorphous solid; $[\alpha]_D^{26}$ +13 (*c* 0.3, MeOH); UV (MeOH) λ_{max} 203 (ε 14100) nm; IR (CCl_4) ν_{max} 2933, 1732, 1683, 1246, and 1030 cm^{-1}; ^{1}H and ^{13}C NMR data (Table II-3); ESI-MS *m/z* 489 $(M + Na)^+$; HR-ESI-TOF-MS *m/z* 489.2227 (M + Na; calcd for $C_{28}H_{34}O_6Na$, 489.2253).

Full Scale Extraction and Isolation

In a full scale experiment, the remaining 46 g extract was also successively partitioned with hexane, ethyl acetate, *n*-butanol, and water. The hexane-soluble materials were preliminary partitioned with a silica gel column (hexane/EtOAc, 1:0 → 0:1). Fraction eluted at hexane/EtOAc, (3:7) was identified as previously identified ceramicine B [15]. Fraction eluted from the silica gel column with hexane/EtOAc (1:9) was further purified a silica gel column (toluene/EtOAc, 6:1 → 4:1). Fraction eluted from the silica gel column with toluene/EtOAc (4:1) was finally purified using HPLC with Cosmosil πNAP, 10 x 250 mm, under isocratic elution {MeOH/H2O (78%/22%)}, flow rate 2.0 mL/min, UV: 210 nm to yield ceramicine J (**6**, 1.0 mg, 0.0002% yield as colorless amorphous solid. Fraction eluted with 100% EtOAc from the preliminary silica gel column was purified with another silica gel column with toluene/EtOAc (6:1) under isocratic condition. Eluent No.12 and No.13 was finally purified using HPLC with Cosmosil πNAP, 10 x 250 mm, under isocratic elution {MeOH/H2O (78%/22%)}, flow rate 2.0 mL/min, UV: 210 nm to yield ceramicine K (**7**, 0.6 mg, 0.00012% yield) and ceramicine L (**8**, 0.8 mg, 0.00016% yield) together with ceramicines A and C [14,15], all isolated as colorless amorphous solid.

Ceramicine J (6): Colorless amorphous solid; $[\alpha]_D^{25}$ -88 (*c* 0.5, $CHCl_3$); UV (MeOH) λ_{max} 203 (ε 13624) nm; IR (CCl_3) ν_{max} 2928, 1724, 1675, 1574 cm^{-1}; ^{1}H and ^{13}C NMR data (Table II-4); ESI-MS *m/z* 425 $(M + H)^+$; HR-ESI-MS *m/z* 425.2325 (M + H: calcd for $C_{26}H_{33}O_5$, 425.2328).

Ceramicine K (7): Colorless amorphous solid; $[\alpha]_D^{26}$ +6 (*c* 0.4, $CHCl_3$); UV (MeOH) λ_{max} 203 (ε 8764.378) nm; IR (CCl_4) ν_{max} 2927, 1747, 1691, 1653 cm^{-1}; ^{1}H and ^{13}C NMR data (Table II-5); ESI-MS *m/z* 463 $(M + Na)^+$; HR-ESI-MS *m/z* 463.2136 (M + Na: calcd for $C_{26}H_{32}O_6$, Na, 463.2097).

Ceramicine L (8): Colorless amorphous solid; $[\alpha]_D^{27}$ +14 (*c* 0.3, $CHCl_3$); UV (MeOH) λ_{max} 203 (ε 13241) nm; IR (CCl_4) ν_{max} 2926, 2854, 1689, 1653 cm^{-1}; ^1H and ^{13}C NMR data (Table II-5); ESI-MS *m/z* 435 $(M + Na)^+$; HR-ESI-MS *m/z* 435.2173 (M + Na: calcd for $C_{25}H_{32}O_5Na$, 435.2147).

Absolute Configuration

p-Br-benzoate of Ceramicine B

To a solution of ceramicine B (0.1 mg, 245 μmol) in CH_3Cl (100 μL) was added *p*-bromobenzoyl chloride with *N,N*-dimethyl-4-aminopyridine. The solution was stirred for 4 h in room temperature. Purification with column chromatography (hexane/ethyl acetate, 8:2) gave a pale yellow solid. CD (MeOH) λ_{max} 225 ($\Delta\varepsilon$ +14.52) and 246 (-9.89) nm; ^1H NMR (400 MHz, $CDCl_3$) δ 0.72 (3H, s), 1.24 (3H, s), 1.27 (3H, s), 1.34 (3H, s), 1.58 (1H, m), 1.90 (2H, m), 2.26 (2H, m), 2.50 – 2.65 (3H), 2.80 (1H, dd, 9.0, 9.0), 3.32 (1H, d, 7.2), 3.68 (1H, d, 7.2), 4.41 (1H, brd, 11.2), 5.53 (1H, brs), 5.84 (1H, brs), 5.89 (1H, brd, 9.4), 6.22 (1H, brs), 6.94 (1H, d, 9.4), 7.16 (1H, s), 7.33 (1H, brs), 7.53 (2H, d, 8.2), and 7.80 (2H, d, 8.2). ESI-MS 591 $(M + H)^+$.

X-Ray Crystallography

Measurement was made on a Rigaku RAXIS RAPID imaging plate area detector with graphite monochromated Cu-Kα radiation. Crystal data of ceramicine B: A colorless platelet crystal, orthorhombic, $C_{26}H_{32}O_4$, M = 408.54, crystal dimensions 0.14 x 0.06 x 0.02 mm, space group $P2_12_12_1$ (#9), a = 7.30805(17) Å, b = 13.4328(3) Å, c = 21.6929(15) Å, V = 2129.54 $Å^3$, Z = 4, D_{calc} = 1.274 g/cm^3. Of the 25458 reflections that were obtained, 3899 were unique (R_{int} = 0026). The structure was solved by direct methods. R1 = 0.0388 ($I>2.00\sigma(I)$). Flack parameter [39] = -0.0(2) (Fridel pairs = 1651). All calculations were performed using the CrystalStructure crystallographic software package except for refinement, which was performed using SHELXL-97. The refined fractional atomic coordinates, bond lengths, bond angles, and thermal parameters have been deposited at the Cambridge Crystallographic Data Centre (CCDC). CCDC 802102 contains the supplementary crystallographic data for this paper. These data can be obtained free of charge *via* http://www.ccdc.cam.ac.uk/deposit, or from the CCDC, 12 Union Road, Cambridge CB2 1EZ, UK (Fax: +44 1223 336 033; e-mail: deposit@ccdc.cam.ac.uk).

Anti-Lipid Droplets Accumulation Activity

Cell Culture and Induction into Adipocyte

MC3T3-G2/PA6 murine pre-adipocytes (Riken Cell Bank) were maintained in basal medium [alpha minimum essential medium (α-MEM) (WAKO) supplemented with 10% FBS (Cell Culture Bioscience)]. For the induction of adipocyte differentiation, cells were cultured for two days followed by addition of MDI inducers (0.5 mM IBMX, 25 nM DEX and 5 μg/mL insulin) and samples were added at this time point. Cells were maintained with inducer and samples for 6-days duration. Basal medium containing inducers and sample were changed during third day of treatment for maintenance purpose.

Nile Red Lipid Droplets Fluorescent Staining

Anti-LDA activity of samples was measured based on the amount of LDA after 6-days of incubation with inducers. Berberine chloride (Sigma) was used as a positive control [65]. To quantify LDA, nile red lipid droplets fluorescent staining method with slight modification was employed [66]. Cells were washed twice with PBS, and stained with nile red (1 mg/mL) for 1 hour at room temperature. Fluorescence was measured with Promega GloMax®-Multi Detection System adjusted to measure with excitation wavelength at 525 nm and emission wavelength from 580-640 nm.

Cytotoxicity

Samples cytotoxicity was also evaluated indirectly *via* MTT assay which is based on mitochondrial succinate dehydrogenase activity and confirmed *via* microscopic observation. MC3T3-G2/PA6 cells were incubated with samples under the same condition as in assessing anti-LDA activity. At the end of incubation, 15 μL of 3-(4,5-dimethylthiazol-2-yl)-2,5-diphenyltetrazolium bromide (MTT) (Sigma) at 5 mg/mL were added to each of the wells. The cultures were incubated for another 3 h before the cells supernatant are removed. After the removal of the cells supernatant, 50 μL of dimethyl sulfoxide (DMSO) was added to each well. The formed formazan crystal was dissolved by re-suspension by pipette. The optical density was measured using a microplate reader (Bio-Rad, USA) at 550 nm with reference wavelength at 700 nm.

Reverse Transcriptase-PCR

Total cellular RNA was prepared from mouse pre-adipocyte cell lines, MC3T3-G3/PA6 from various time of harvest using TRIzol® (Ambion). Reverse transcriptions were

performed using ReverTra Ace kit (TOYOBO). PCR were carried out using with PCR kit (Qiagen). Synthesized forward and reverse primer sequences are as followed – β-actin (forward – 5'-TCACCCACACTGTGCCCATCTAC-3', reverse- 5'-GAGTACTTGCGCTCAGGAGGAGC-3'), PPARγ (forward – 5'-CATGGTTGACACAGAGATGCC-3', reverse - 5'-GGTGGGACTTTCCTGCTAGTA-3'), C/EBPα (forward – 5'-CACTTGCAGTTCCAGATCGC-3', reverse - 5'-GTTTGGCTTTATCTCGGCTCT-3'), C/EBPβ (forward – 5'-CACGACTTCCTCTCCGACCTC-3', reverse – 5'-AGCTGCTCCACCTTCTTCTGC-3'), C/EBPδ (forward – 5'-ACGACGAGAGCGCCATC-3', reverse – 5'-TCGCCGTCGCCCCAGTC-3'), GLUT4 (forward – 5'-TGGTCAATACGGTCTTCACGT-3', reverse – 5'-GGACCCATAGCATCCGCAAC-3'), HSD11β1 (forward – 5'-AATCTCTGGGATAATTAACGC-3', reverse – 5'-GCTTACAGAAGTATCAGGCA-3'), LPL (forward – 5'-AATCTGGGCTATGAGATCAACA-3', reverse – 5'-TCTCTCCGGCTTTCACTCG-3'), KLF2 (forward – 5'-GGTCCCCGCAACCCGTTCCC-3', reverse – 5'-GCCGCATCCTTCCCAGTTGCAAT-3'), KLF3 (forward – 5'-CCGCCCATTAAGAAGTACTCG-3', reverse – 5'-TGTAGACCTTATTGCACCCAT-3'), KLF4 (forward – 5'-GCCCTCAAAGTTTGTGCGAAT-3', reverse – 5'-ATCGCCGGTGCCTTGACAAC-3'), KLF6 (forward – 5'-GAGGAACTTTCACCCACGAC-3', reverse – 5'-CAAAACGCCACTCACAACC-3'), KLF7 (forward – 5'-CCATCGCTGTACGTTTAACGG-3', reverse – 5'-TCTCTTCATATGGAGCGCAAG-3'), KLF15 (forward – 5'-GGCCAGAAGTTTCCCAAGAACCC-3', reverse – 5'-GTACGGCTTCACACCCGAGT-3'). All PCR products were separated by 1.5% agarose gel electrophoresis and visualized by ethidium bromide staining.

Western Blotting

Total cellular protein was prepared from MC3T3-G3/PA6 cells from various time of harvest. Total protein concentrations were quantified using BCA protein assay kit (Pierce). Twenty micrograms of total protein extract were loaded into each well of a SDS-polyacrylamide gel. Separated proteins were transferred to PVDF membrane (Amersham Hybond^{TM} – P, GE Healthcare). Primary antibody was prepared by diluting in BlockAce®. Primary antibodies used in this study are PPARγ (Santa Cruz Biotechnology), phospho-FoxO1 (Thr24)/FoxO3a (Thr32) (Cell Signaling Technology), and FoxO1 (C29H4) (Cell Signaling Techonology). Horseradish peroxidase-linked secondary antibody was used in this

study (Amersham, GE Healthcare). Fluorescence was detected using immunostar® LD kit (WAKO) and viewed with UV Transilluminator Imaging System.

References

1. Dixon, R. A., Nature, 411(6839), 843-847 (2001).
2. Keen, N. T., Plant Molecular Biology, 19, 109-122 (1992).
3. Lee, K. H., J. Nat. Prod., 67, 273-283 (2004).
4. Newman, D. J., Cragg, G. M., Snader, K. M., Nat. Prod. Rep., 17, 215-234 (200).
5. Roy, A., Saraf, S., Biol. Pharm. Bull., 29, 191-201 (2006).
6. Zhang, H., Wang, X., Chen, F., Androulakis, X. M., Wargovich, M. J., Phytotherapy Res., 21, 721-734 (2007).
7. Carpinella, M. C., Defago, M. T., Valladares, G., Palacios, S. M., J. Agric. Food Chem., 51, 360-374 (2003).
8. Bray, D. H., Warhurst, D. C., Connolly, J. D., O'Neill, M. J., Philipson, J. D. Phytotherapy Res., 4, 29-35 (1990).
9. Koul, O., Singh, G., Singh, R., Singh, J., Danielwski, W. M., Berlozecki, S., J. Biosci., 29, 409-416 (2004).
10. Thakur, R. S., Singh, S. B., Goswami, A., Curr. Res. Med. Aromat. Plants, 3, 135-140 1981.
11. Koul, O., Isman, M. B., Ketkar, C. M., Can. J. Bot., 68, 1-11 (1990).
12. Biswas, K., Chattopadhyay, I., Bajernee, R. K., Bandyopadhyay, U., Curr. Sci., 82, 1336-1345 (2002).
13. http://www.asianplant.net/Meliaceae/Chisocheton_ceramicus.htm
14. Mohamad, K., Hirasawa, Y., Lim, C. S., Awang, K., Hadi, A. H. A., Takeya, K., Morita, H., Tetrahedron Letter, 49, 4276-4278 (2008).
15. Mohamad, K., Hirasawa, Y., Litaudon, M., Awang, K., Hadi, A. H. A., Takeya, K., Ekasari, W., Widyawaruyanti, A., Zaini, N. C., Morita, H., Bioorg. Med. Chem., 17, 727-730 (2009).
16. Najmuldeen, I. A., Hadi, A. H. A., Awang, K., Mohamad, K., Ketuly, K. A., Mukhtar, H. R., Lim, C. S., Chan, G., Nafiah, M. A., Ng, S. W., Shirota, O., Hosoya, T., Nugroho, A. E., Morita, H., Journal of Natural Products, 74, 1313-1317 (2011).
17. Najmuldeen, I. A., Hadi, A. H. A., Mohamad, K., Awang, K., Ketuly, K. A., Mukhtar, H., Taha, N., Nordin, M., Litaudon, M., Gueritte, F., Nugroho, A. E., Morita, H., Heterocycles, 84, 1265-1270 (2012).
18. Haslam, D. W., James, W. P., Lancet, 366, 1197- 1209 (2005).
19. Imza, I., Martínez-Cervell, C., García-Alvarez, E. E., Sendra-Gutíierrez, J. M., González-Enríquez, J., Obes. Surg., 18, 841-846 (2008).
20. Zhi, J., Melia, A. T., Eggers, H., Joly, R., Patel, I. H., J. Clin. Pharmacol., 35, 1103-1108 (1995).
21. Weibel, E., Hadvary, P., Hochuli, E., Kupfer, E., Lengsfeld, H., J. Antibiot., 40(8), 1081–1085 (1987).
22. Torgerson, J., Hauptman, J., Boldrin, M., Sjöström, L., Diabetes Care, 27(1), 155-161 (2004).
23. Thomsen, W. J., Grottick, A. J., Menzaghi, F., Reyes-Saldana, H., Espitia, S., Yuskin, D., Whelan, K., Martin, M., Journal of Pharmacology and Experimental Therapeutics, 325(2): 577–587 (2008).
24. Shin, J. E., Han, M. J., Kim. D. H., Biol. Pharm. Bull., 26, 854-857 (2003).
25. Shin, J. E., Han, M. J., Song, M. C., Song, M. S., Baek, N. I., Kim. D. H., Biol. Pharm. Bull., 27, 138-140 (2004).
26. Xiao. J., Wang, N. L., Sun. B., Cai, G. P., Am. J. Physiol.: Cell Physiol., 299, 128-138 (2010).
27. Chen, Q., Chan, L. L. Y., Li. E. T. S., J. Nutr., 133, 1088-1093 (2003).

28. Chen, Q., Li. E. T. S., Br. J. Nutr., 93, 123-132 (2005).
29. Tan, M. J., Ye, M. J., Turner, M., Hohnen-Behrens, C., Ke, C. Q., Tang, C. P., Chen, T., Weiss, H. C., Gesing, E. R., Rowland, A., James, D. E., Ye, Y., Chem. Biol., 15, 263-273 (2008).
30. Birdsall, T. C., Kelly, G. S., Alt. Med. Rev., 2(2), 94-103 (1997).
31. Pham, T. P. T., Kwon, J., Shin, J., Biochem. Biophys. Res. Comm., 413, 376-382 (2011).
32. Rouseff, R. L., J. Agric. Food. Chem., 30(3), 504-507, (1982).
33. Ono, E., Inoue, J., Hashidume, T., Shimizu, M., Sato, R., Biochem. Biophys. Res. Comm., 410(3), 677-681, 2011.
34. Pérez-Gutiérrez, R. M., Guzman, R. M., Biol. Pharm. Bull., 35(9), 1516-1524, 2012.
35. Turner, C., Tempsta, M., Taylor, R., Zagorski, M., Termini, J., Schroeder, D., Nakanishi, K., Tetrahedron, 43, 2789-2803, (1987).
36. Baba, H., Yaoita, Y., Kikuchi, M., Helv. Chim. Acta., 90, 1028-1037 (2007).
37. Lanzotti, V., Termolino, P., Dolci, M., Curir, P., Bioorg. Med. Chem., 20, 3280-3286 (2012).
38. Subhadhirasakul, S., Takayama, H., Miyabe, Y., Aimi, N., Ponglux, D., Sakai, S., Chem. Pharm. Bull., 42, 2645-2646 (1994).
39. Flack, H. D., Acta Cryst., A39, 876-881 (1983).
40. Rodeheffer, M. S., Birsoy, K., Friedman, J. M., Cell, 135, 249-249 (2008).
41. Huang, H., Song, T. J., Li, X., Hu, L., He, Q., Liu, M., Lane, M. D., Tang, Q. Q., Proc. Natl. Acad. Sci. USA, 106, 12670-12675 (2009).
42. Zamani, N., Brown, C., Endrocr. Rev., 32, 387-403 (2010).
43. Kawai, M., Rosen, C. J., J. Biol. Chem., 111, 14-19 (2010).
44. Zúñiga, L. A., Shen, W. J., Joyce-Shaikh, B., Pyatnova, E. A., Richards, A. G., Thom, C., Andrade, S. M., Cua, D. J., Kraemer, F. B., Butcher, E. C., J. Immunol, 185, 6947-6959 (2010).
45. Widberg, C. H., Newell, F. S., Bachmann, A. W., Ramnoruth, S. N., Spelta, M. C., Whitehead, J. P., Hutley, L. J., Prins, J. B., Am. J. Physiol. Endocinol. Metab., 296, E121-E131 (2009).
46. Xiao, L., Sobue, T., Esliger, A., Kronenberg, M. S., Coffin, J. D., Doetschman, T., Hurley, M. M., Bone, 47, 360-370 (2010).
47. Zaragosi, L. E., Wdziekonski, B., Villageois, P., Keophiphath, M., Maumus, M., Tchkonia, T., Bourlier, V., Mohsen-Kanson, T., Ladoux, A., Elabd, C. et al., Diabetes, 59, 2513-2521 (2010).
48. Kawai, M., Namba, N., Mushiake, S., Etani,Y., Nishimura, R., Makishima, M., Ozono, K., J. Mol. Endocrinol., 38, 19-34 (2007).
49. Rosen, E. D., MacDougald, O. A., Nat. Rev. Mol., Cell Biol., 7, 885-896 (2006)
50. White, U. A., Stephens, J. M., Mol. Cell., Endocrinol, 318, 10-14 (2010).
51. Lefterova, M. I., Zhang, Y., Steger, D. J., Schupp, M., Schug, J., Cristancho, A., Feng, D., Zhuo, D., Stoeckert, C. J., Jr, Liu, X., S., et al, Genes, Dev., 22, 2941-2952 (2008).
52. Nielsen, R., Pedersen, T. A., Hagenbeek, D., Moulos, P., Siersbaek, R., Megens, E., Denissov, S., Borgesen, M., Francois, K. J., Mandrup, S., et al., Genes Dev., 22, 2953-2967 (2008).
53. Takahara, Y., Kobayashi, T., Takemoto, K., Adachi, T., Osaki, K., Kawahara, K., Tsujimoto, G., J. Pharmacol. Sci., 107, 1-7 (2008).
54. McConnell, B. B., Yang, V. W., Physiol. Rev., 90, 1337-1381 (2010).
55. James, D.E., Brown, R., Navarro, J., Pilch, P.F., Nature, 333 (6169), 183–5 (1988).
56. Mead, J.R., Irvine, S,A., Ramji, D.P., J. Mol. Med., 80 (12), 753–69 (2002).
57. Seckl, J.R., Walker, B.R., Endocrinology, 142 (4), 1371–1376 (2001).

58. Seckl, J.R., Front Neuroendocrinol., 18 (1), 49–99 (1997).
59. Anagnostis, P., Athyros, V.G., Tziomalos, K., Karagiannis, A., Mikhailidis, D.P., J. Clin. Endocrinol. Metab., 94 (8), 2692–2701 (2009).
60. Munekata, K., Sakamoto, K., In Vitro Cell. Dev. Biol., 45, 642-651 (2009).
61. Maiese, K., Chong, Z. Z., Shang, Y. C., Hou, J., Med. Res. Rev., 29 (3), 395-418 (2009).
62. Huang, H., Tindall, D. J., J. Cell. Sci., 2479-4287 (2007).
63. Rena, G., Guo, S., Cichy, S. C., Unterman, T. G., Cohen, P., J. Biol. Chem., 274 (24), 17179-17183 (1999).
64. Armoni, M., Harel, C., Karni. S., Chen, H., Bar-Yoseph, F., Ver., M. R., Quon, M. J., Karnieli, E., J. Biol. Chem., 281 (29), 19881-19891 (2006).
65. Pham, T. P. T., Kwon, J., Shin, J., Biochem. Biophys. Res. Comm., 413, 376-382 (2011).
66. Greenspan, P., Mayer, E. P., Fowler, S. D., *J. Cell Biol.*, 100, 965-973 (1985).

Appendix

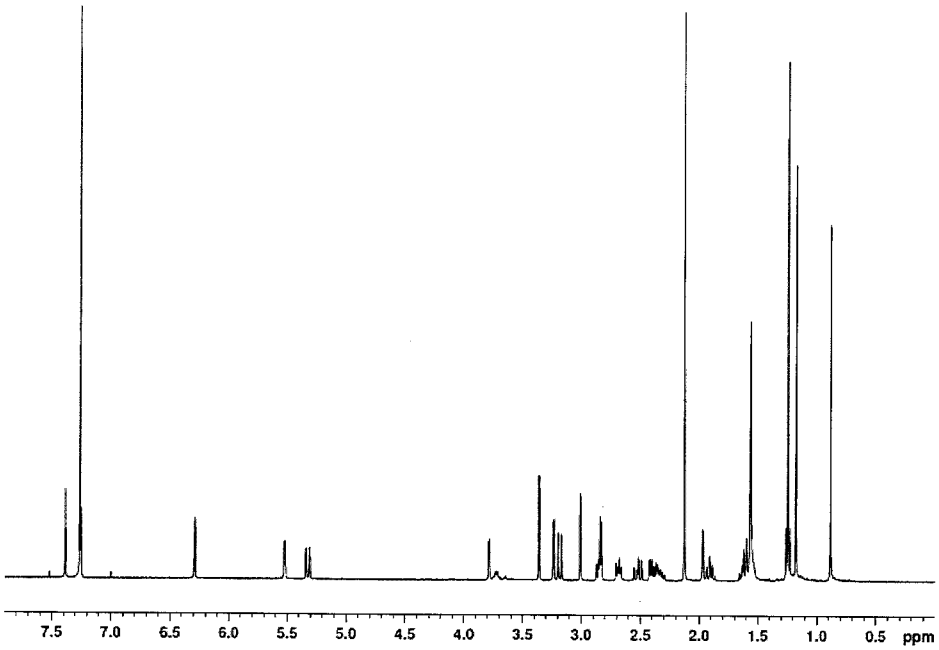

Appendix 1. ^{1}H NMR spectrum of **1** in $CDCl_3$

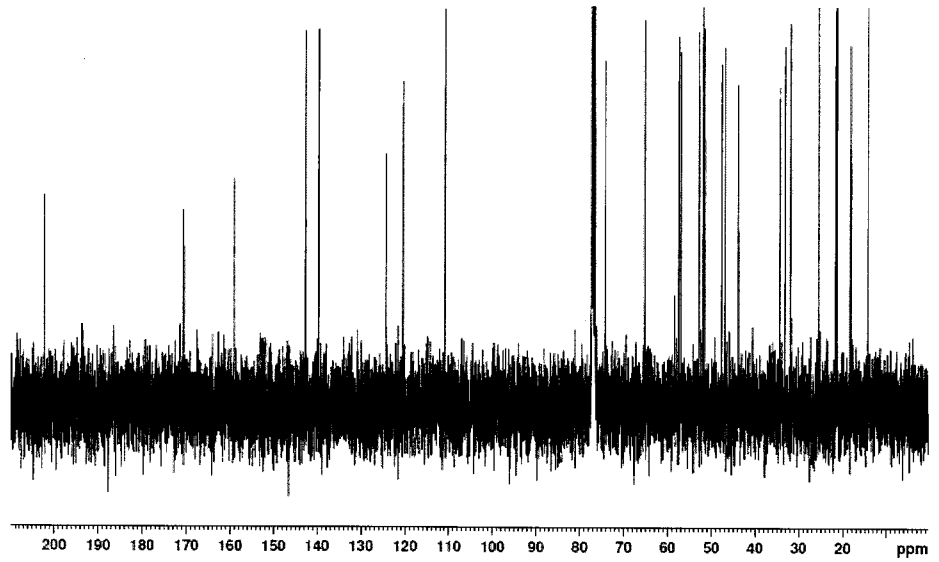

Appendix 2. ^{13}C NMR spectrum of **1** in $CDCl_3$

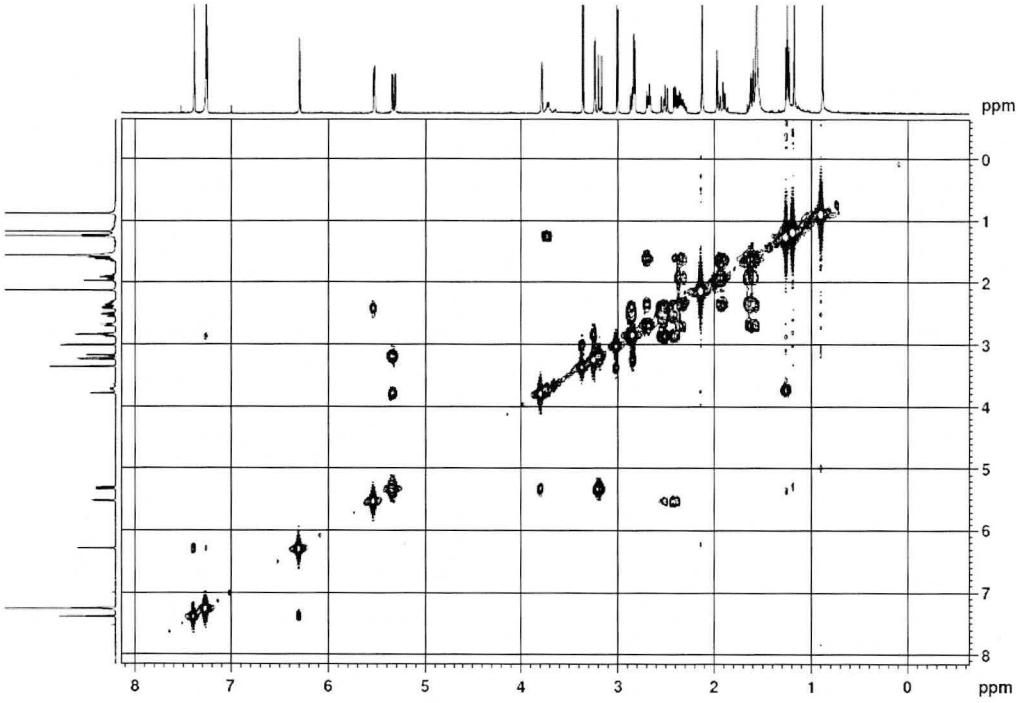

Appendix 3. ^{1}H-^{1}H COSY spectrum of **1** in $CDCl_3$

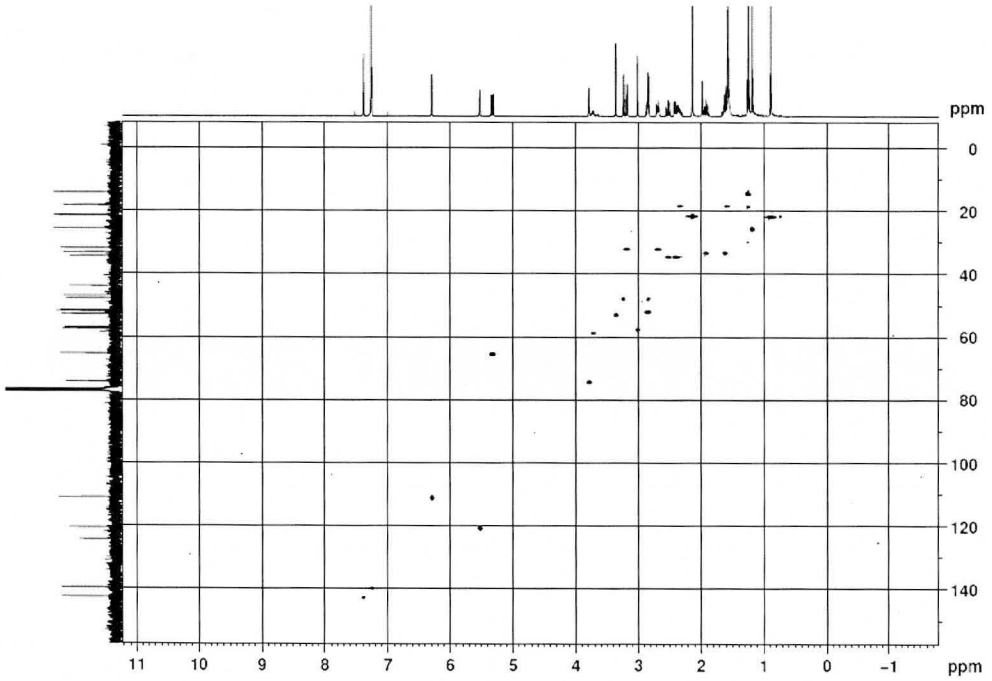

Appendix 4. HSQC spectrum of **1** in $CDCl_3$

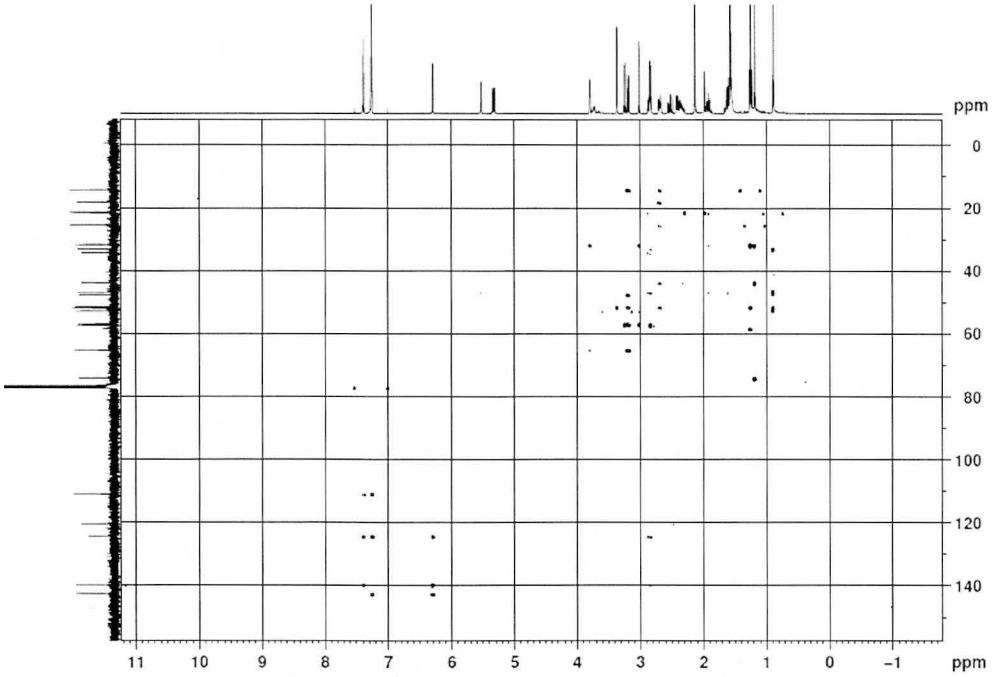

Appendix 5. HMBC spectrum of **1** in $CDCl_3$

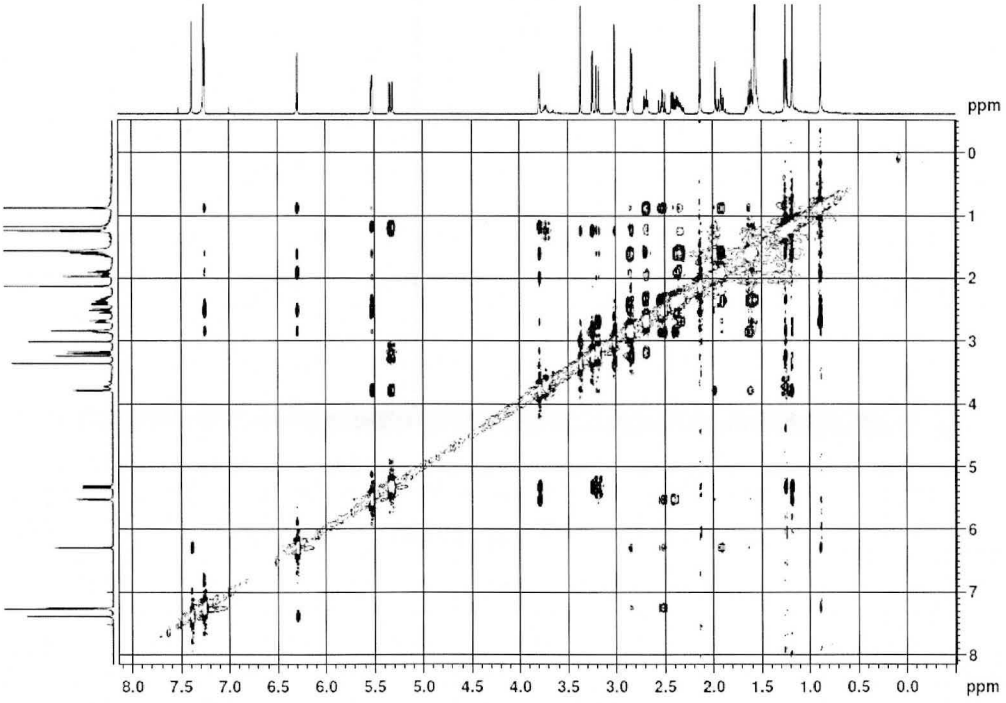

Appendix 6. NOESY spectrum of **1** in $CDCl_3$

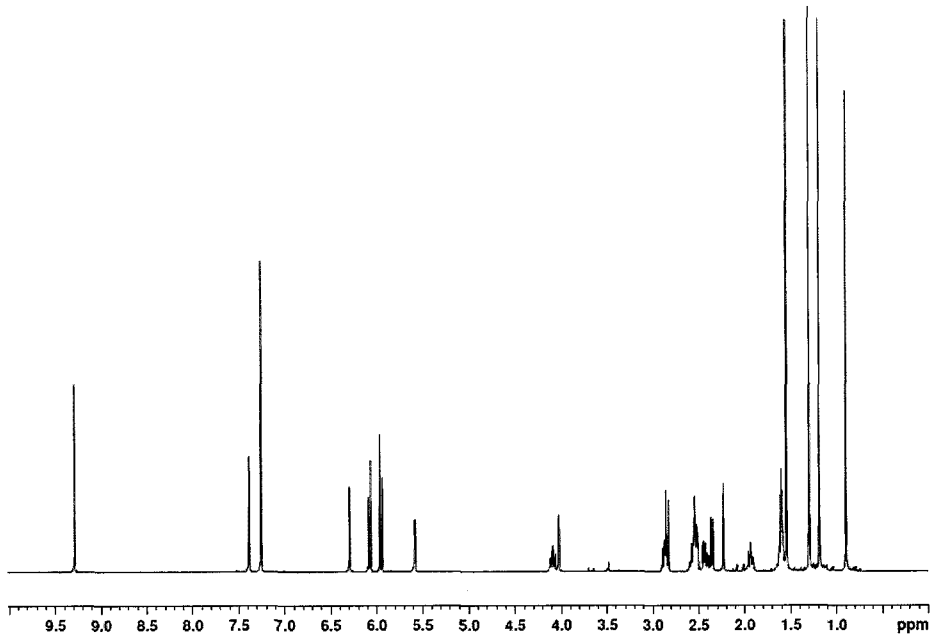

Appendix 7. ^{1}H NMR spectrum of **2** in $CDCl_3$

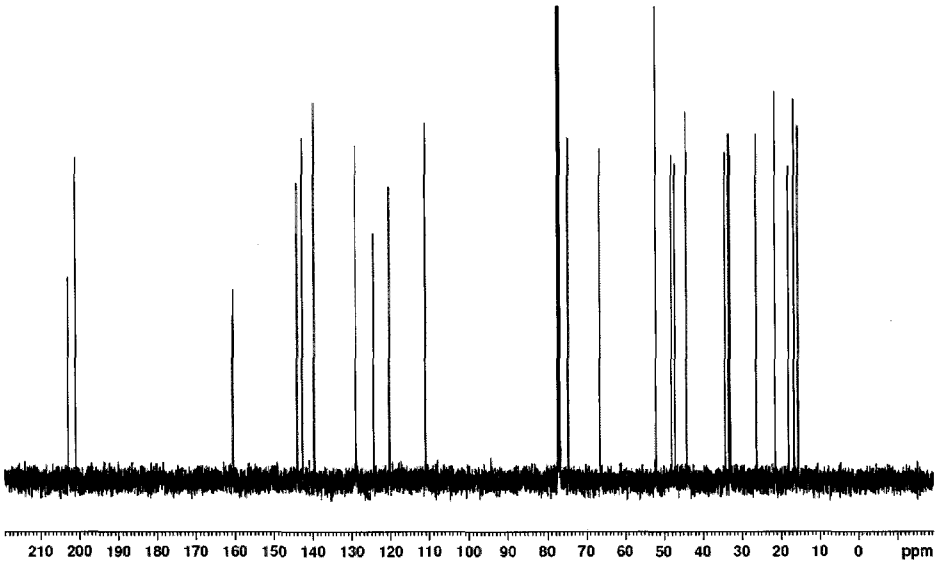

Appendix 8. ^{13}C NMR spectrum of **2** in $CDCl_3$

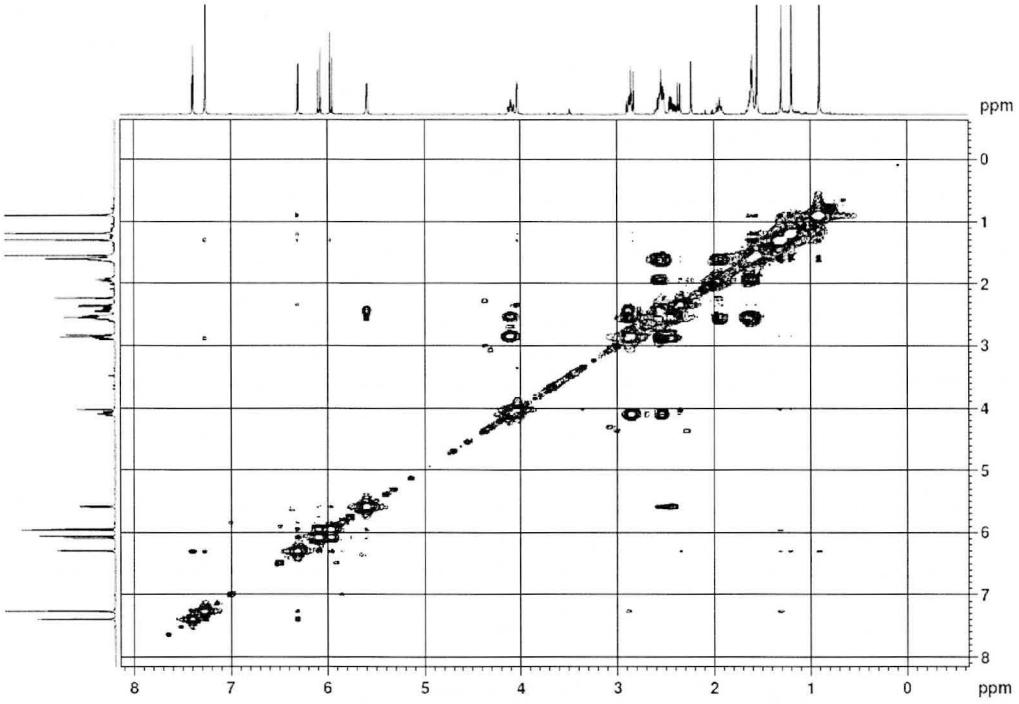

Appendix 9. ^{1}H-^{1}H COSY spectrum of **2** in $CDCl_3$

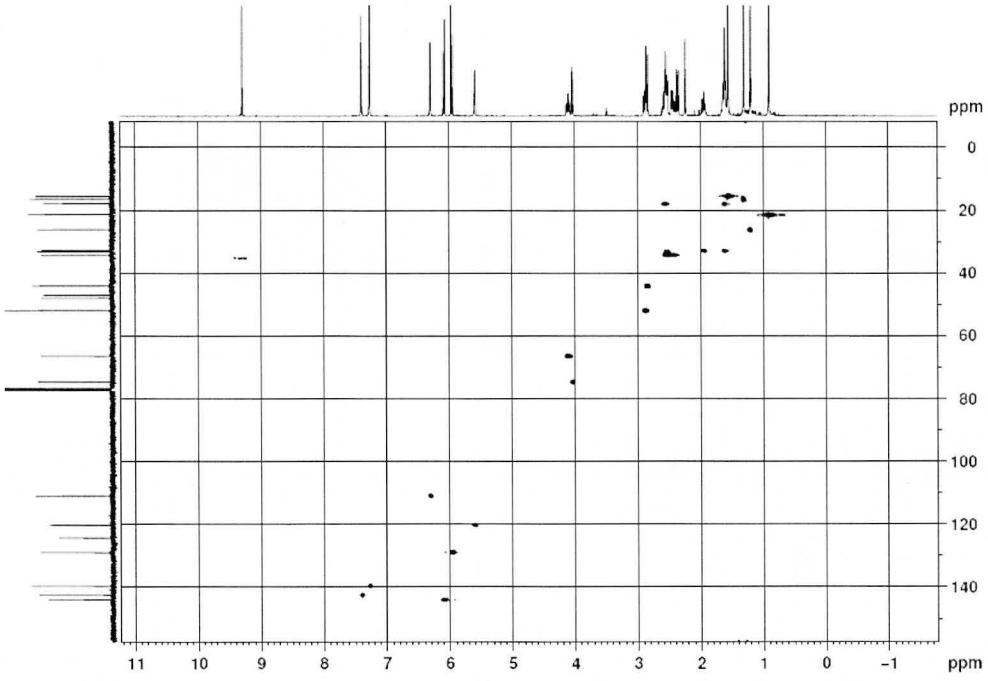

Appendix 10. HSQC spectrum of **2** in $CDCl_3$

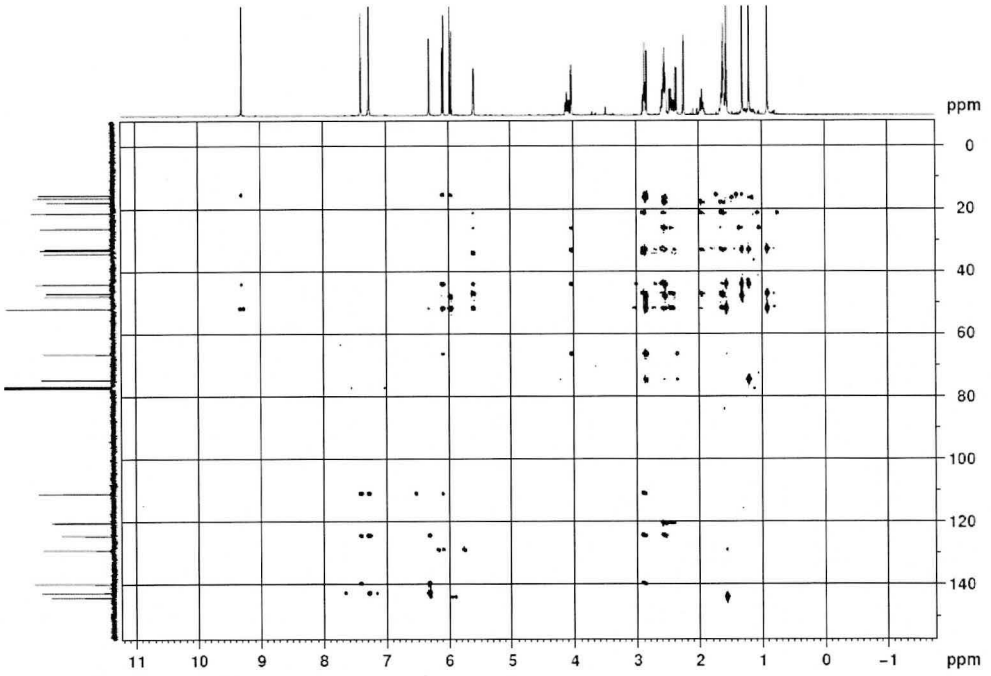

Appendix 11. HMBC spectrum of **2** in $CDCl_3$

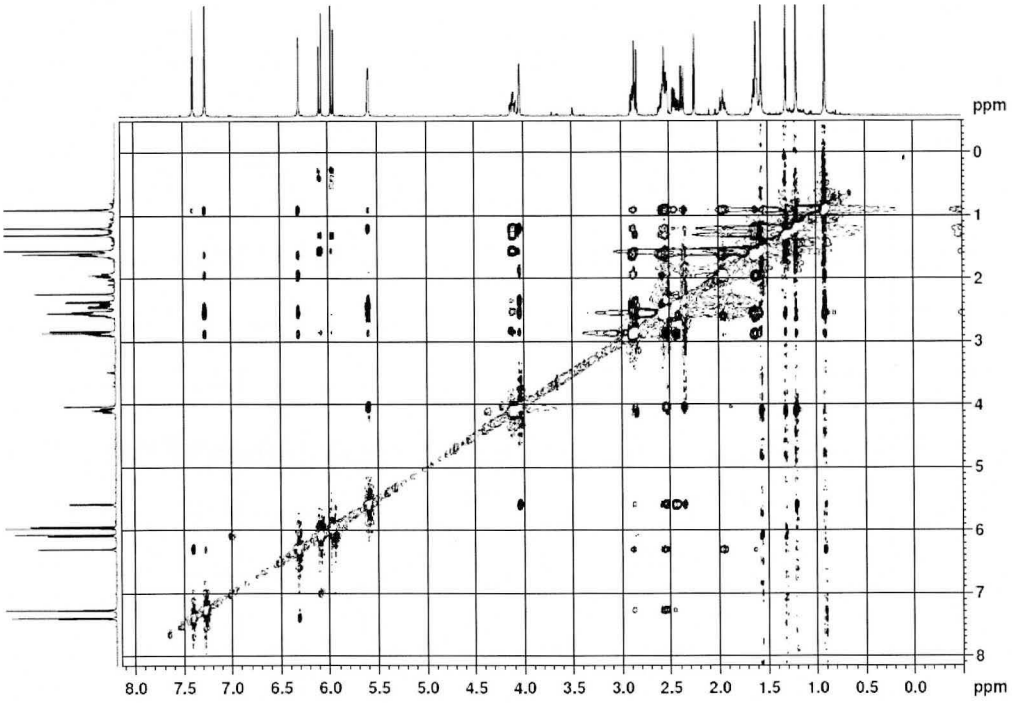

Appendix 12. NOESY spectrum of **2** in $CDCl_3$

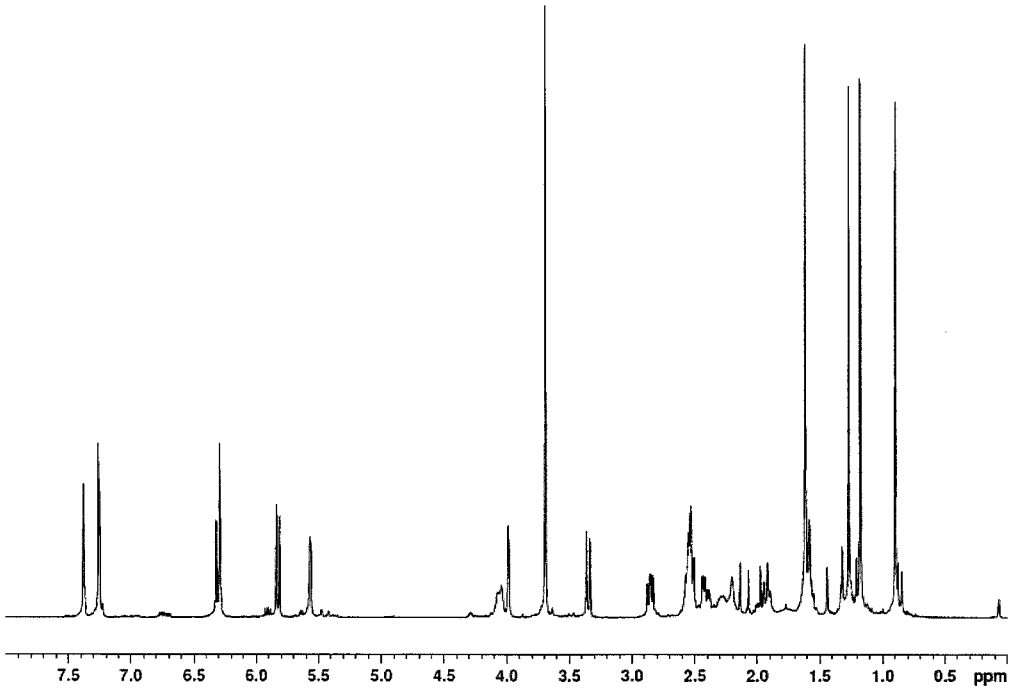

Appendix 13. ^{1}H NMR spectrum of **3** in $CDCl_3$

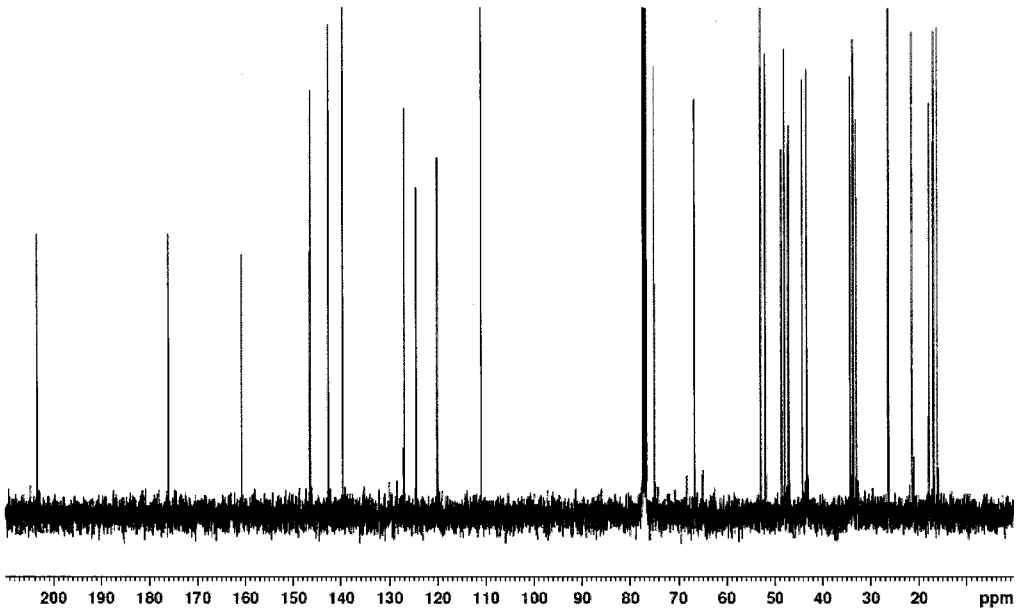

Appendix 14. ^{13}C NMR spectrum of **3** in $CDCl_3$

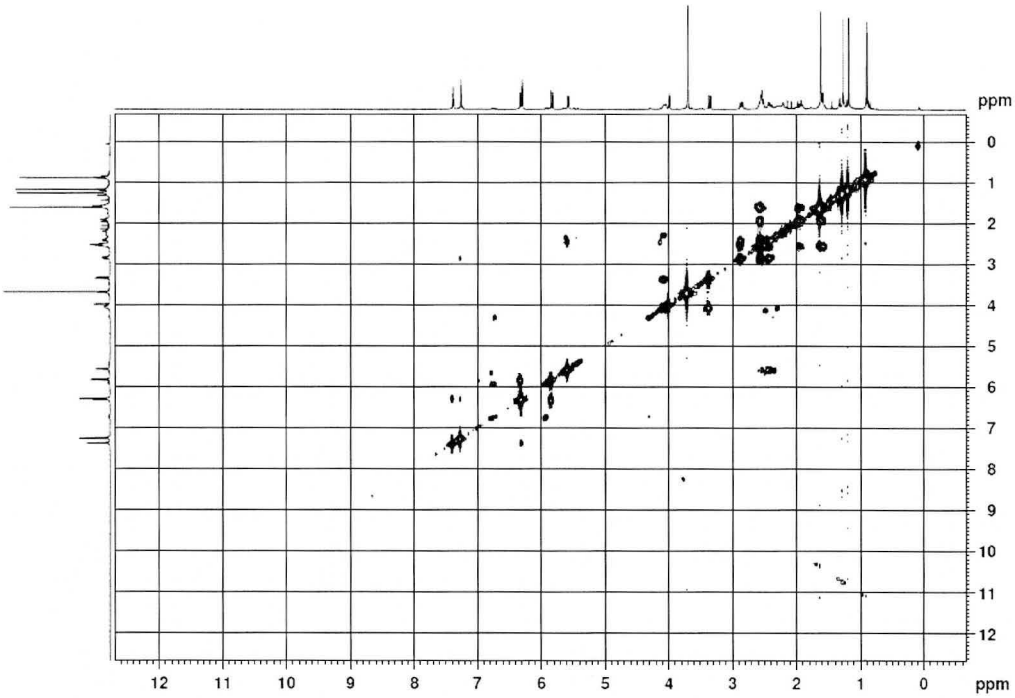

Appendix 15. ^{1}H-^{1}H COSY spectrum of **3** in $CDCl_3$

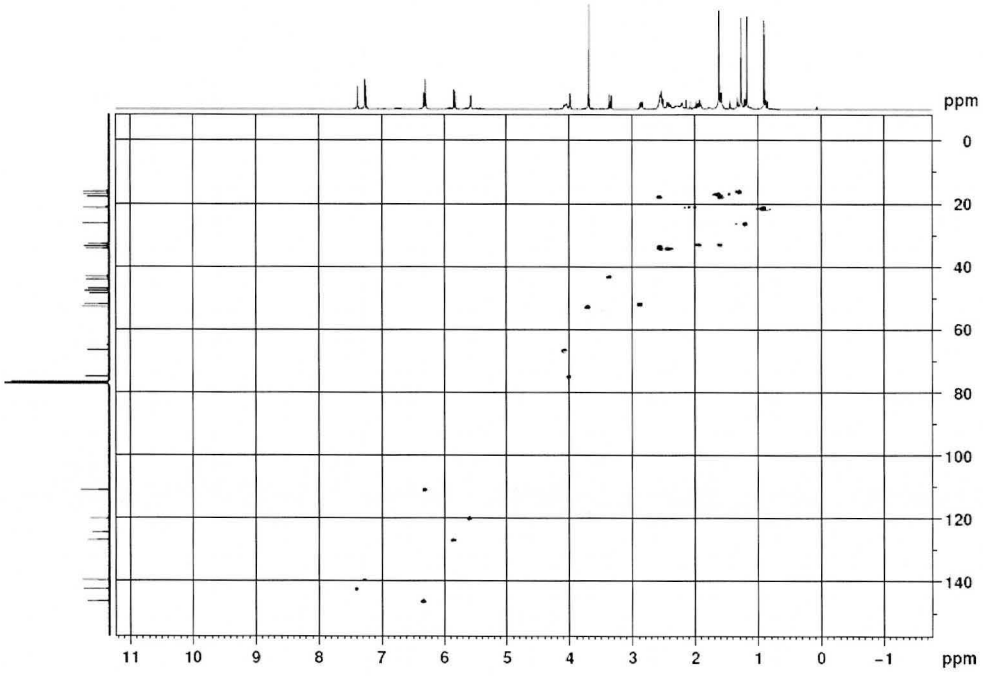

Appendix 16. HSQC spectrum of **3** in $CDCl_3$

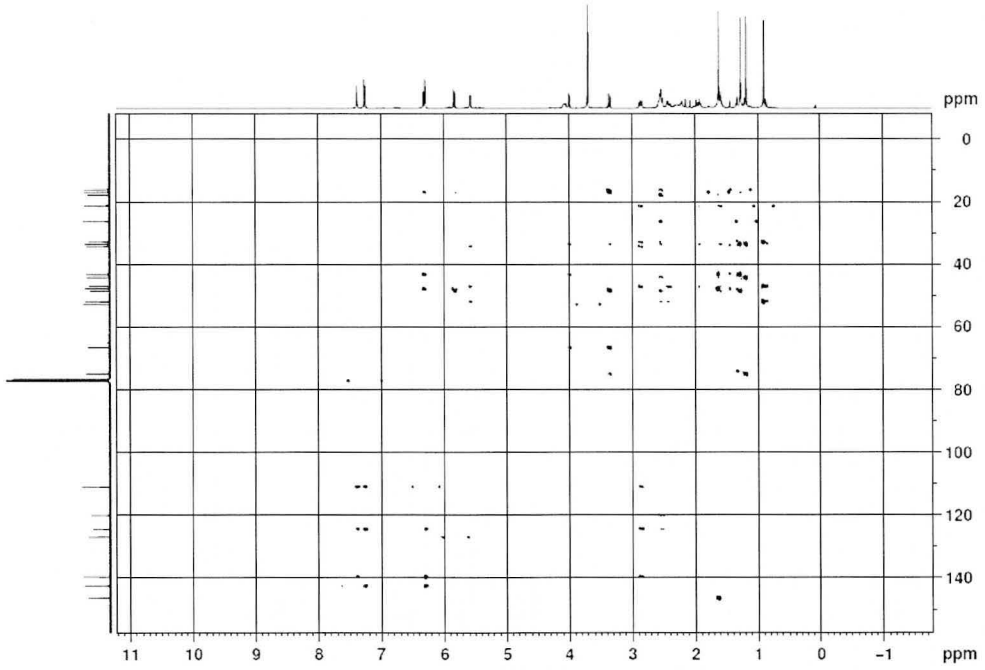

Appendix 17. HMBC spectrum of **3** in $CDCl_3$

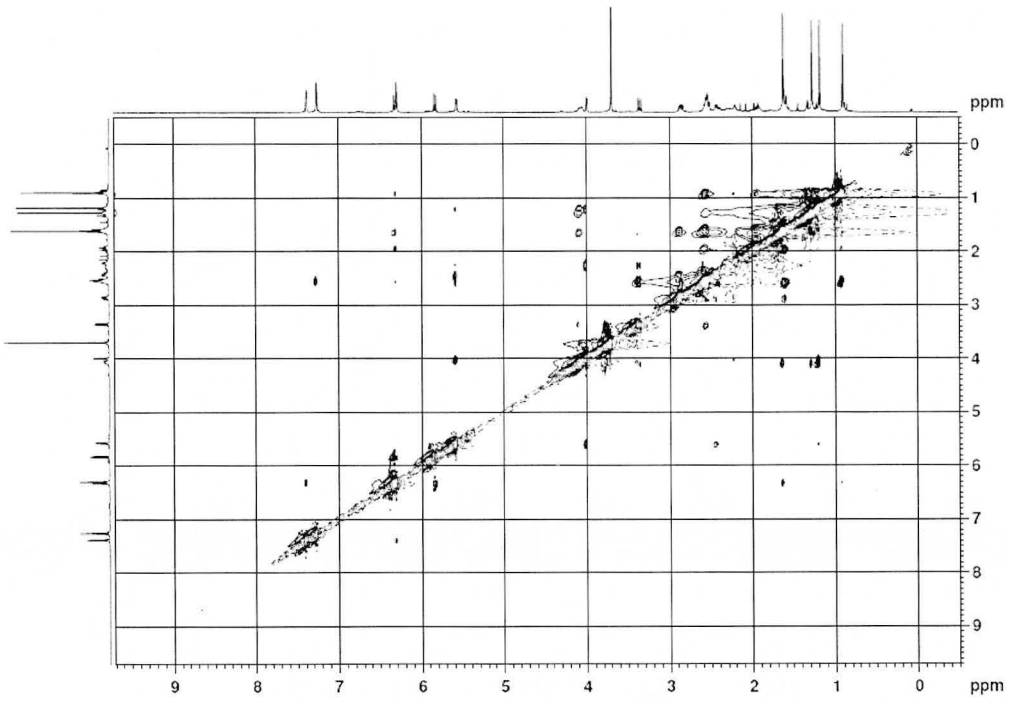

Appendix 18. NOESY spectrum of **3** in $CDCl_3$

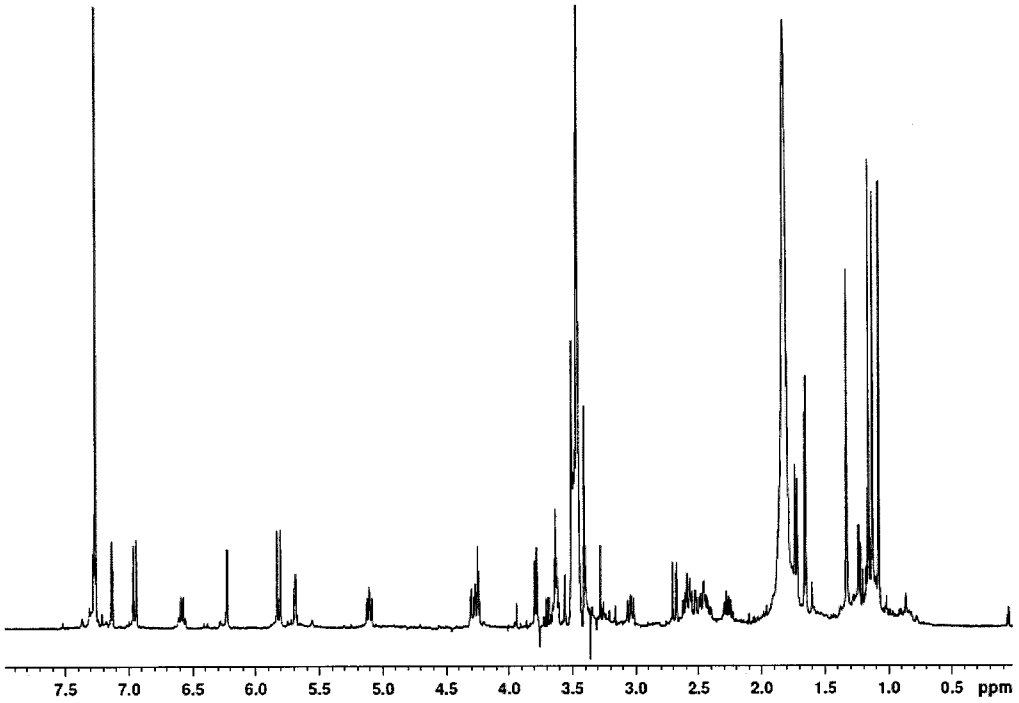

Appendix 19. ^{1}H NMR spectrum of **4** in $CDCl_3$

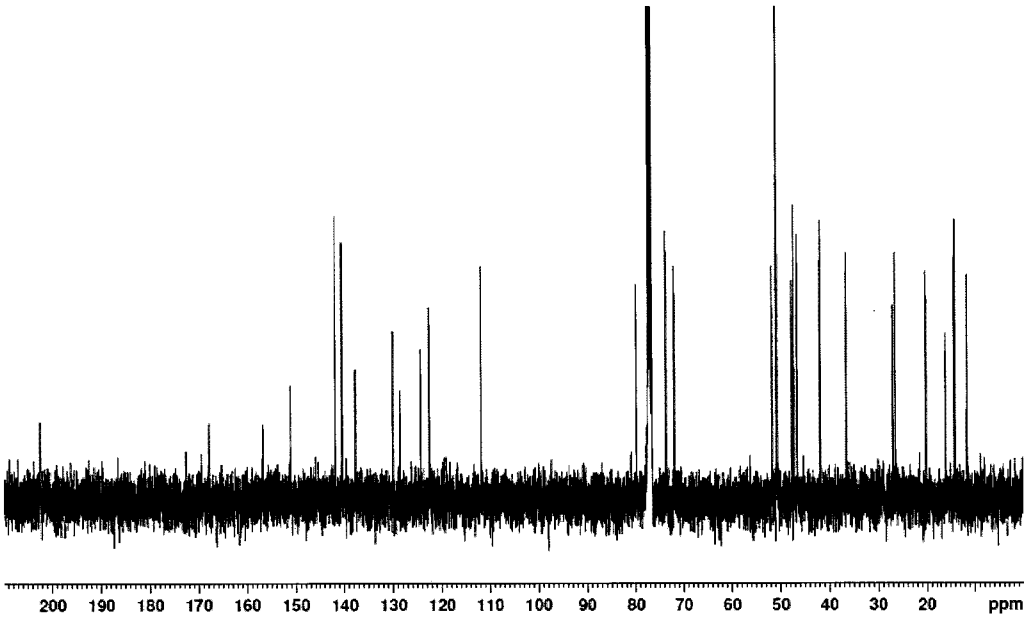

Appendix 20. ^{13}C NMR spectrum of **4** in $CDCl_3$

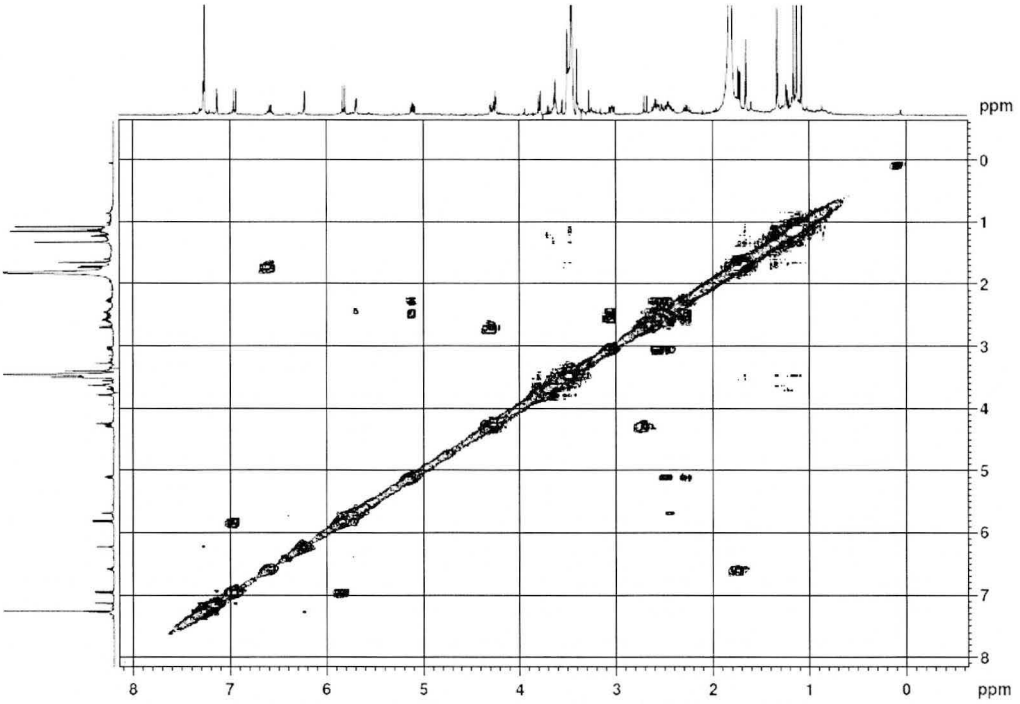

Appendix 21. ^{1}H-^{1}H COSY spectrum of **4** in $CDCl_3$

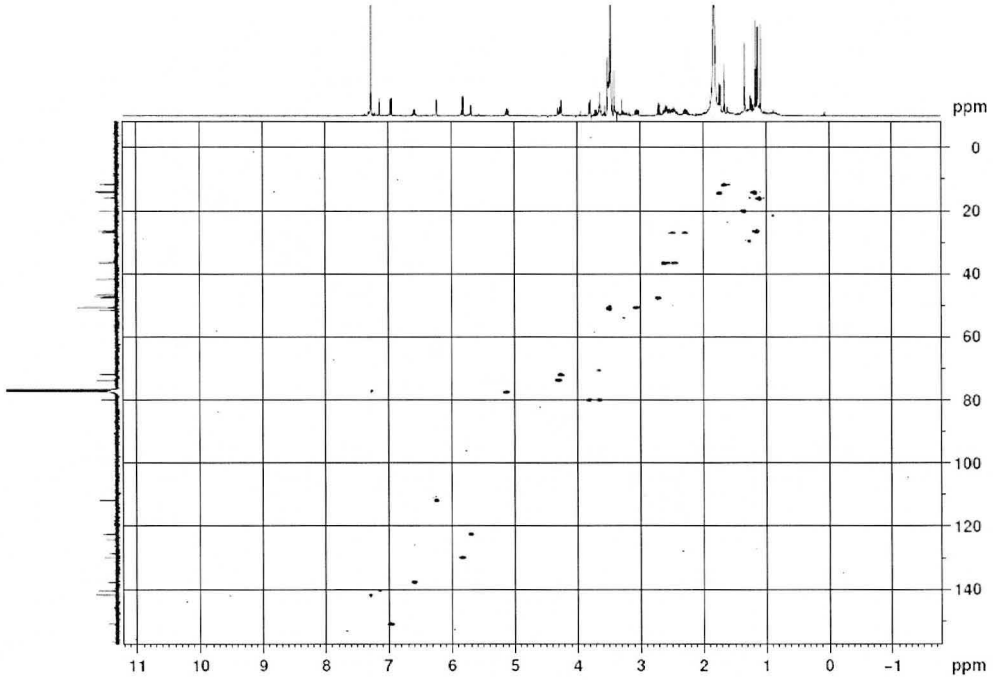

Appendix 22. HSQC spectrum of **4** in $CDCl_3$

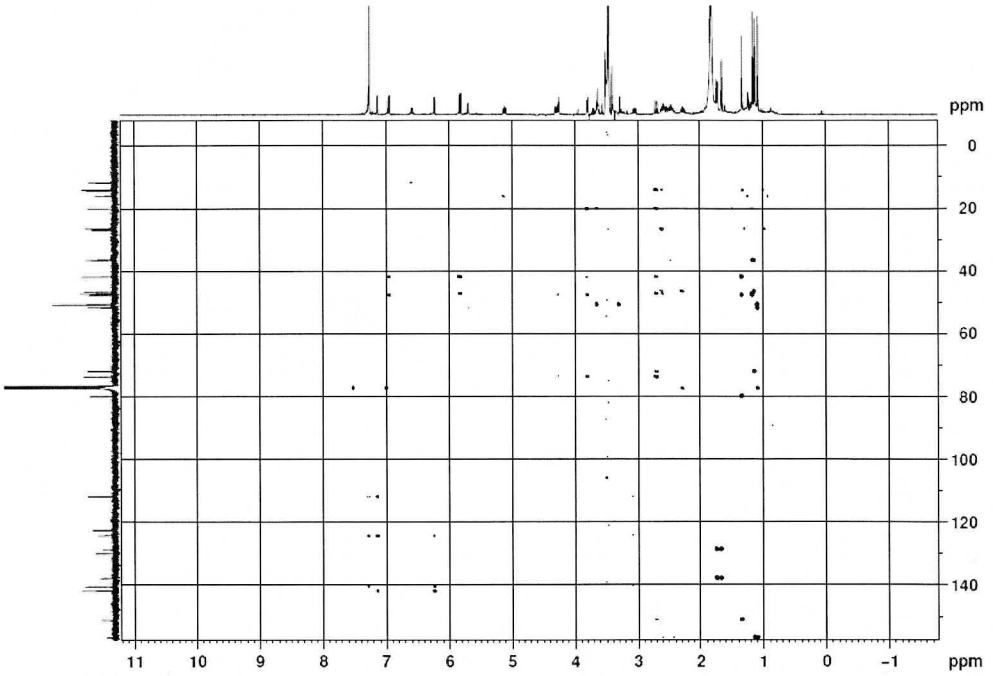

Appendix 23. HMBC spectrum of **4** in $CDCl_3$

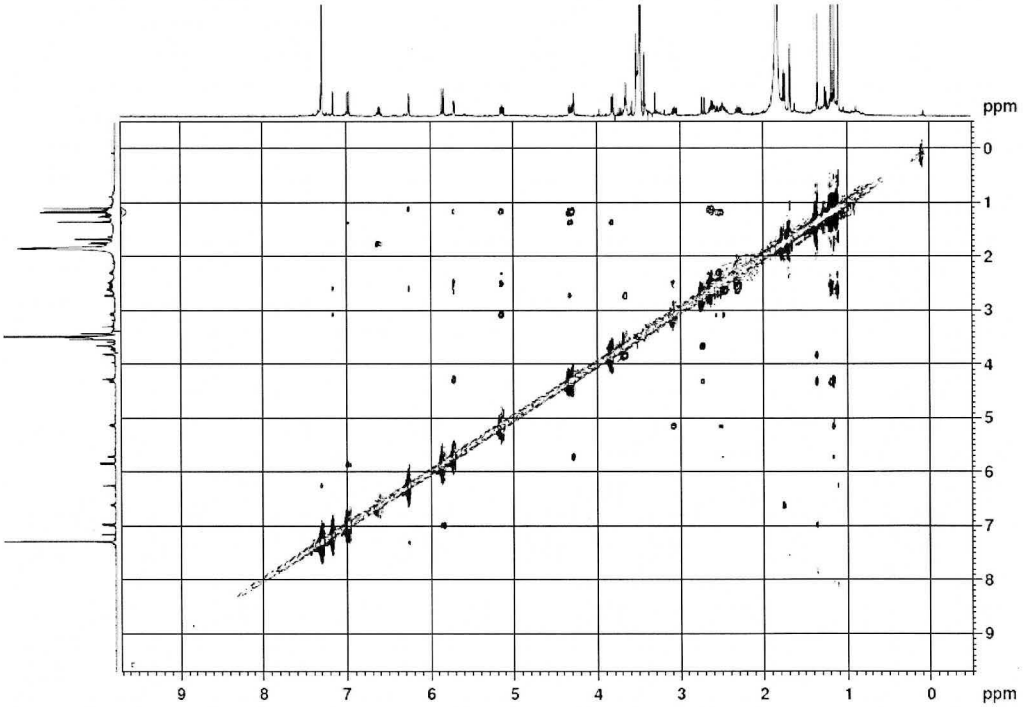

Appendix 24. NOESY spectrum of **4** in $CDCl_3$

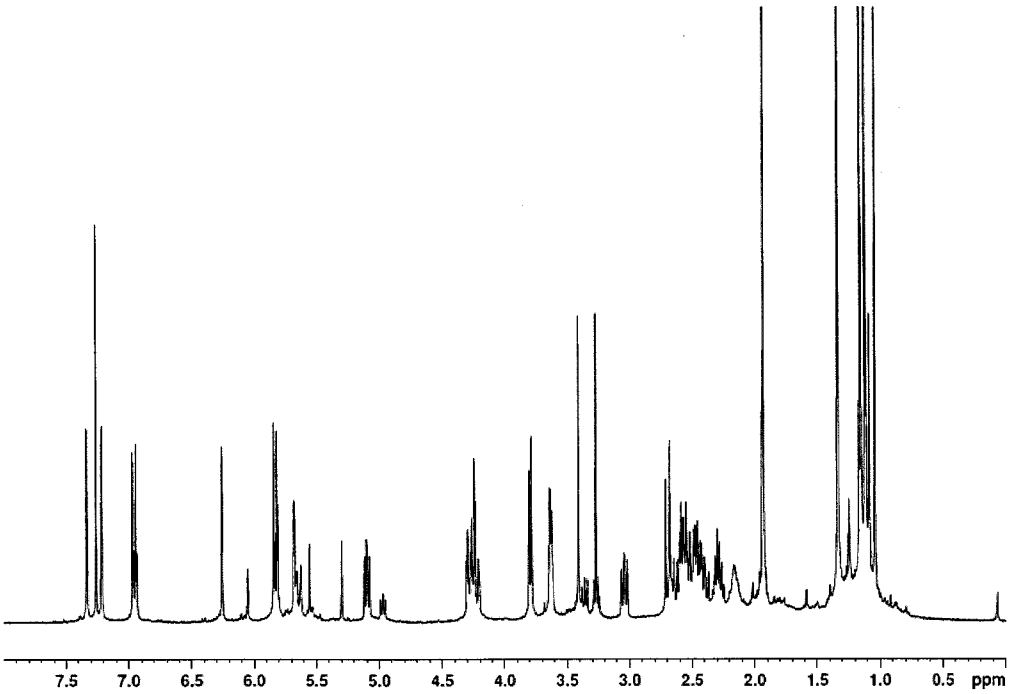

Appendix 25. ^{1}H NMR spectrum of **5** in $CDCl_3$

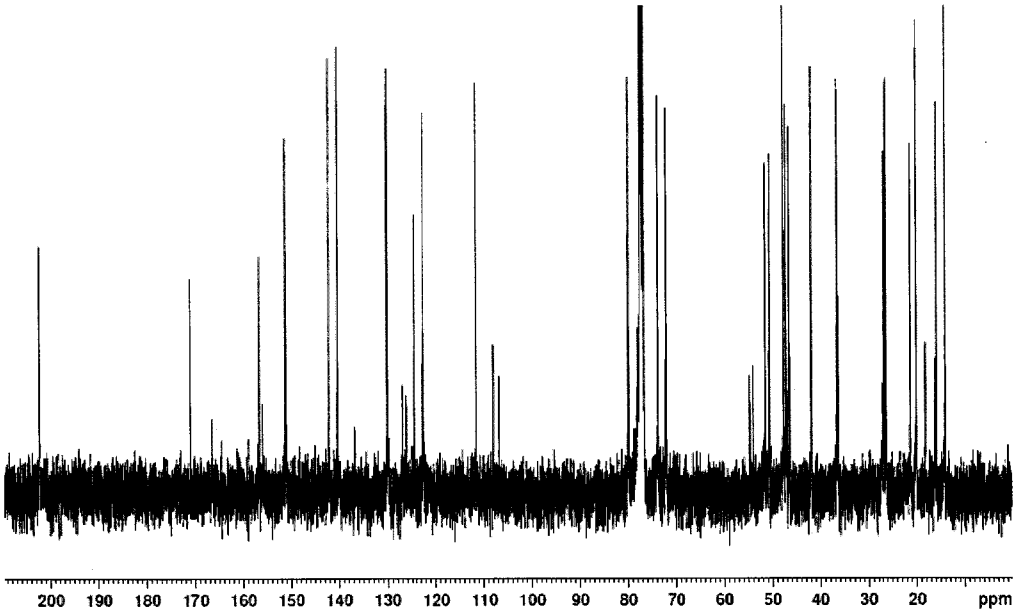

Appendix 26. ^{13}C NMR spectrum of **5** in $CDCl_3$

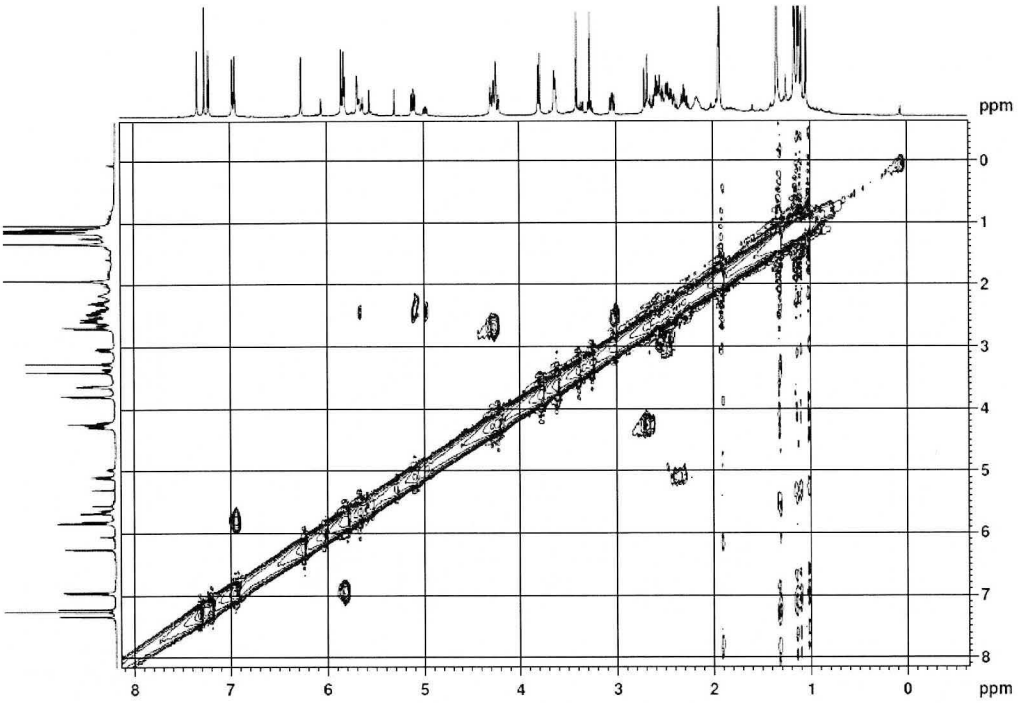

Appendix 27. ^{1}H-^{1}H COSY spectrum of **5** in $CDCl_3$

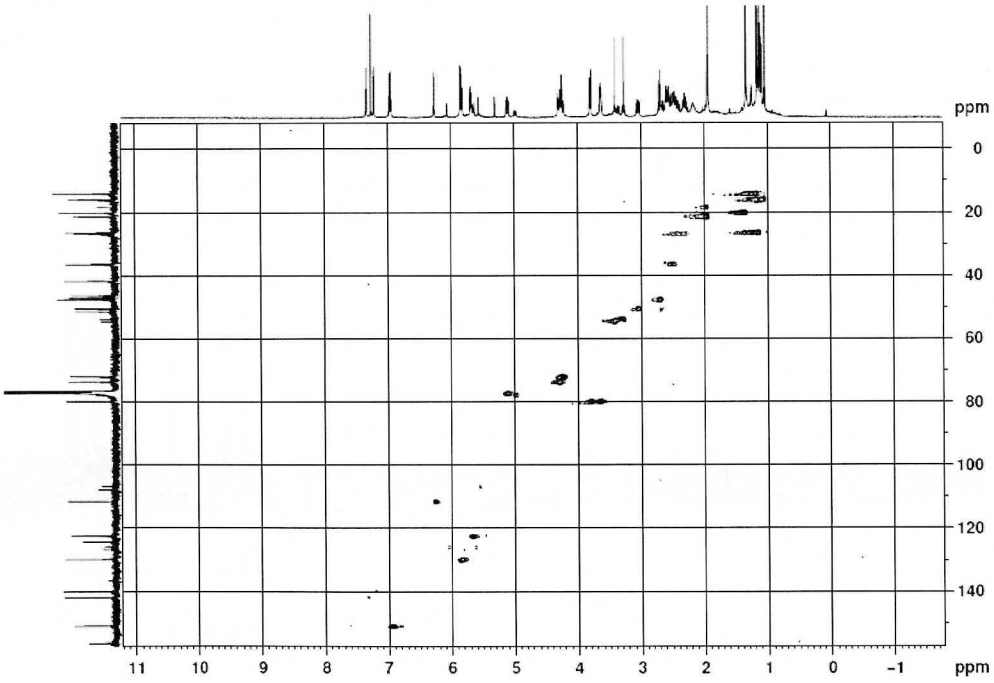

Appendix 28. HSQC spectrum of **5** in $CDCl_3$

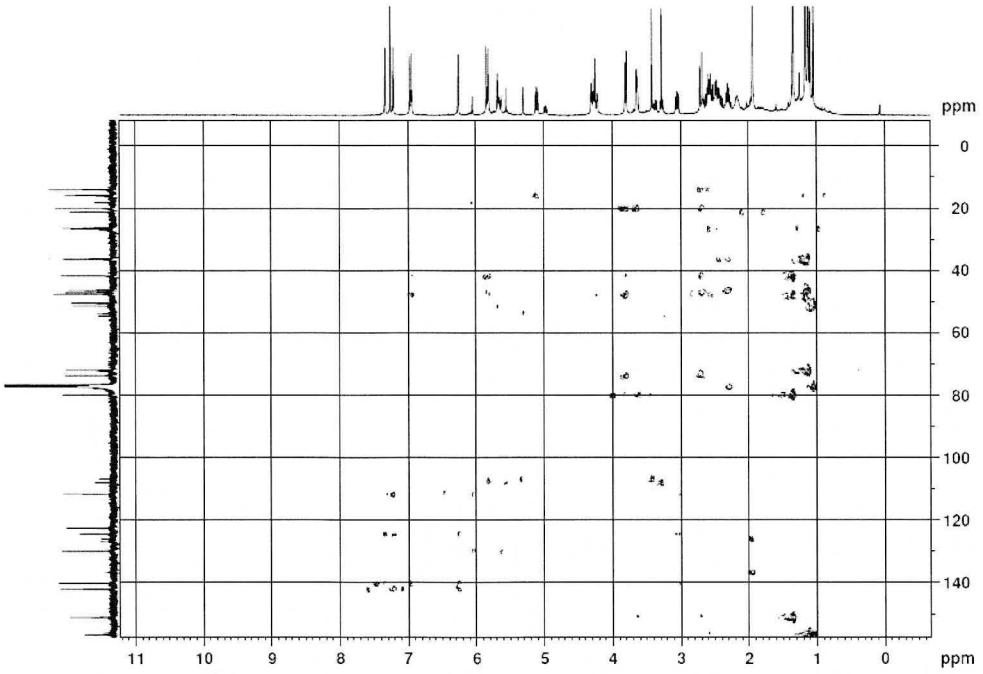

Appendix 29. HMBC spectrum of **5** in $CDCl_3$

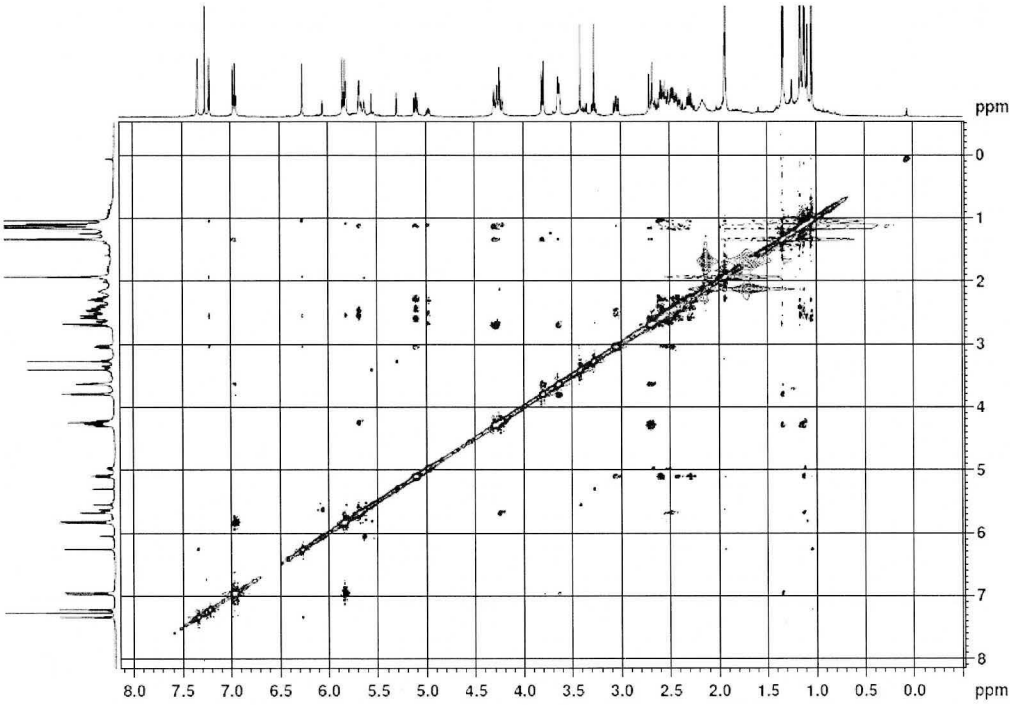

Appendix 30. NOESY spectrum of **5** in $CDCl_3$

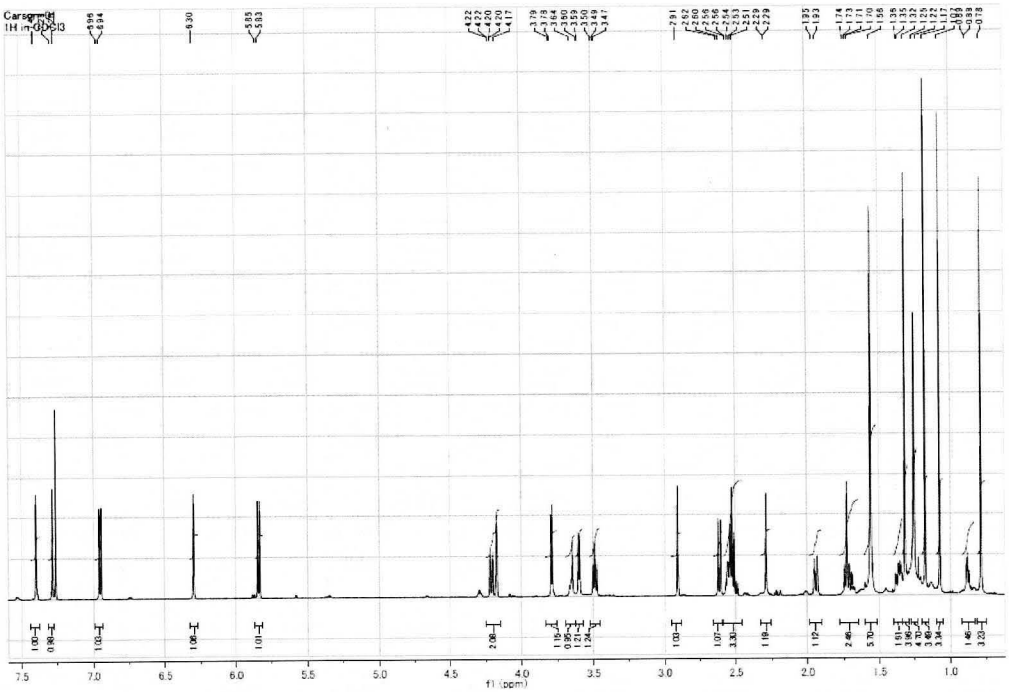

Appendix 31. ^{1}H NMR spectrum of **6** in $CDCl_3$

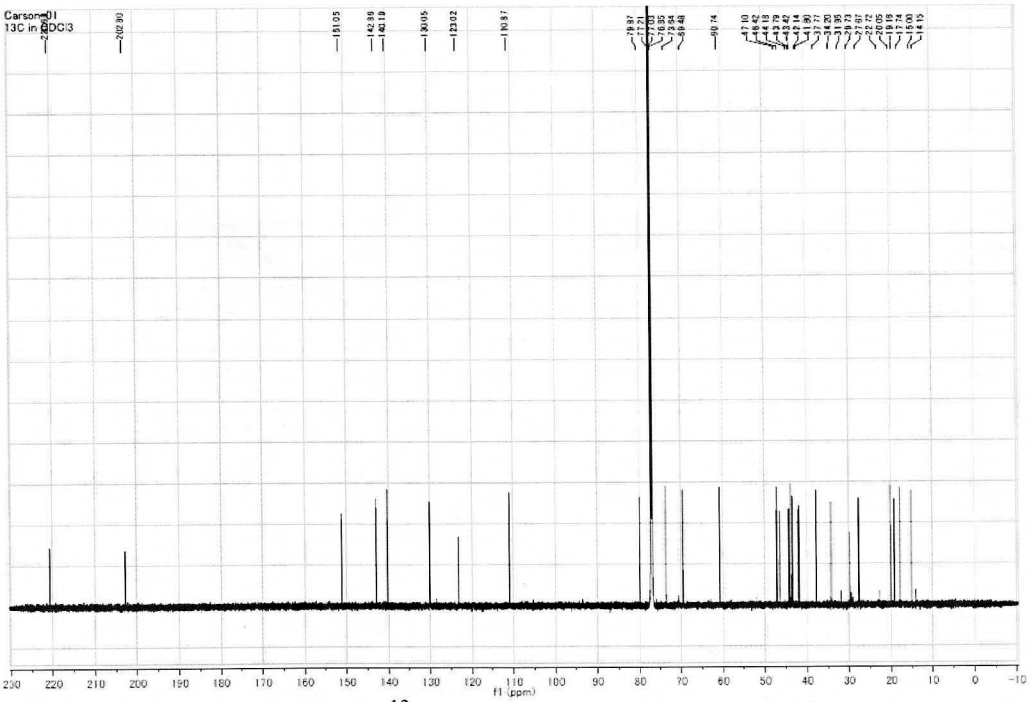

Appendix 32. ^{13}C NMR spectrum of **6** in $CDCl_3$

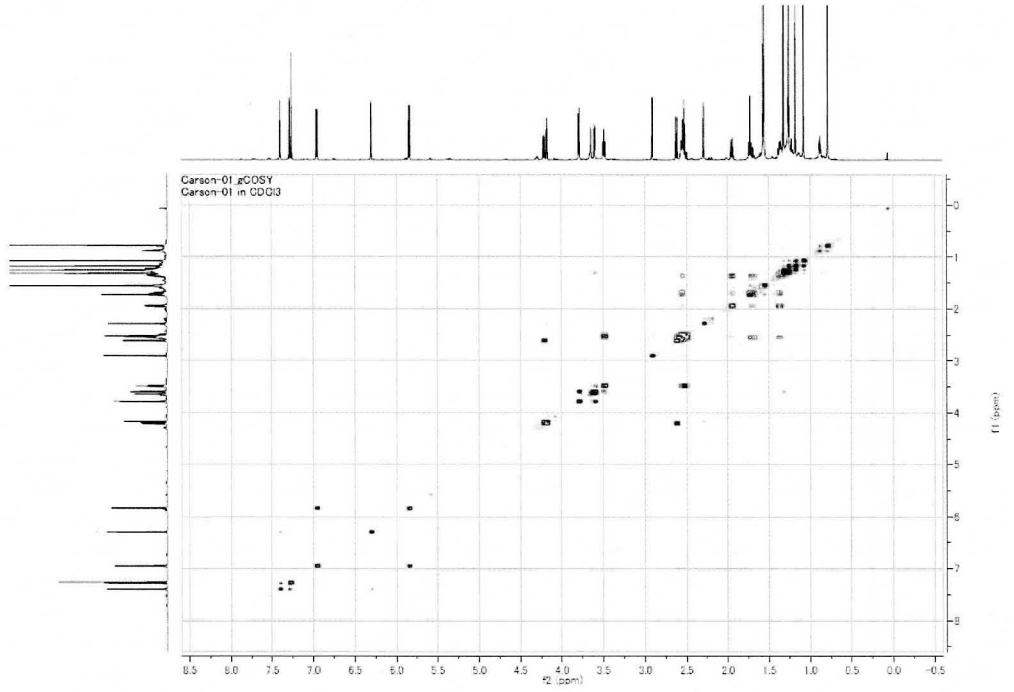

Appendix 33. ^{1}H-^{1}H COSY spectrum of **6** in $CDCl_3$

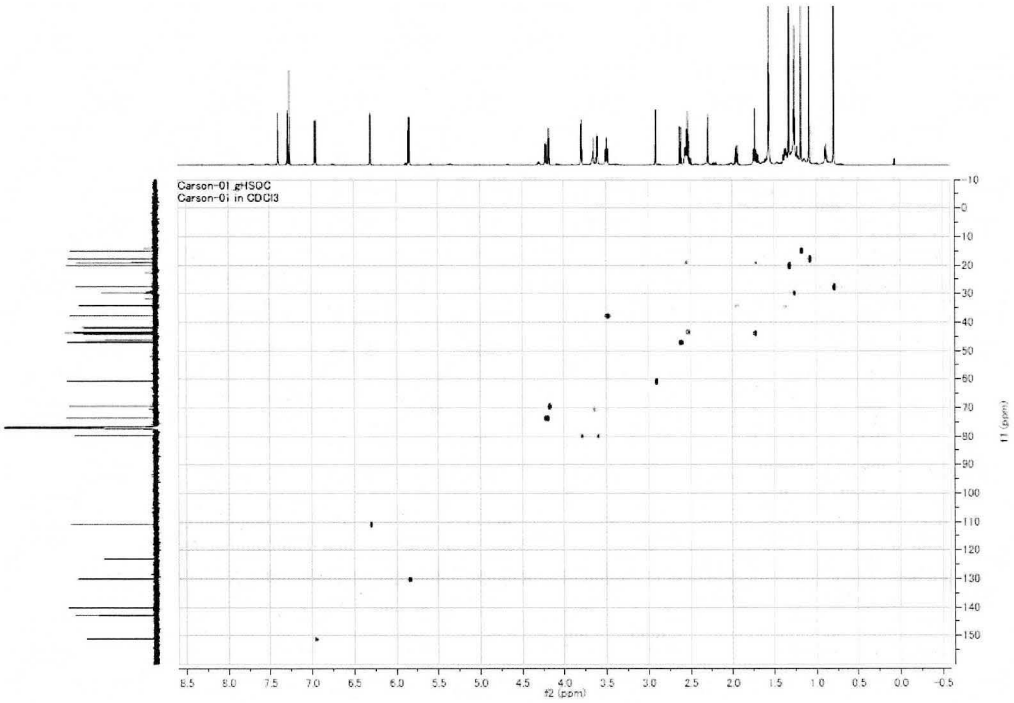

Appendix 34. HSQC spectrum of **6** in $CDCl_3$

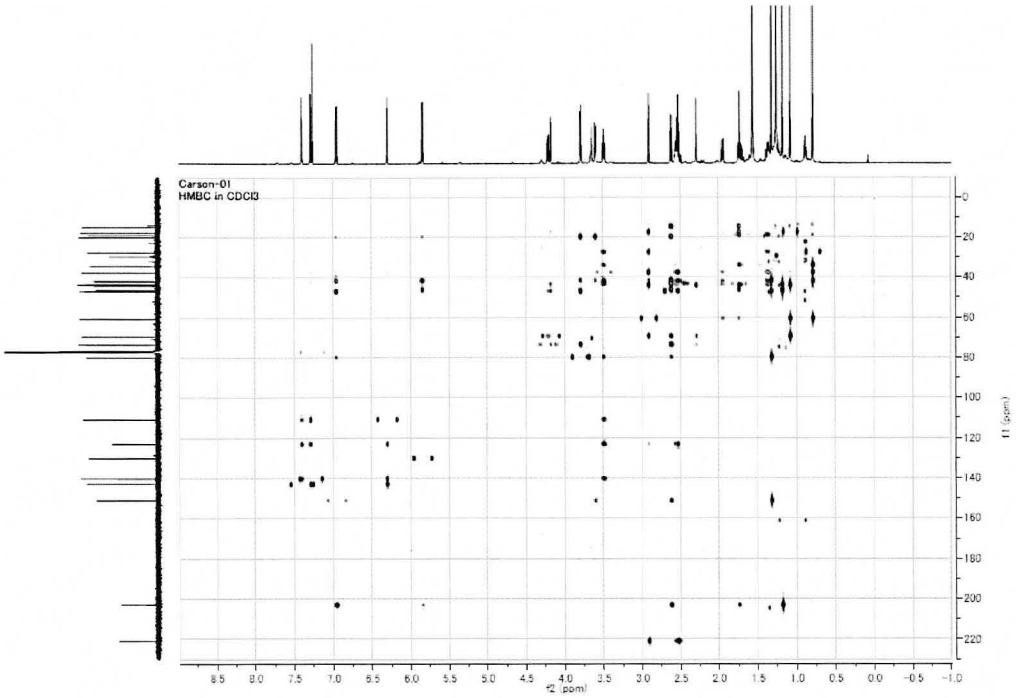

Appendix 35. HMBC spectrum of **6** in $CDCl_3$

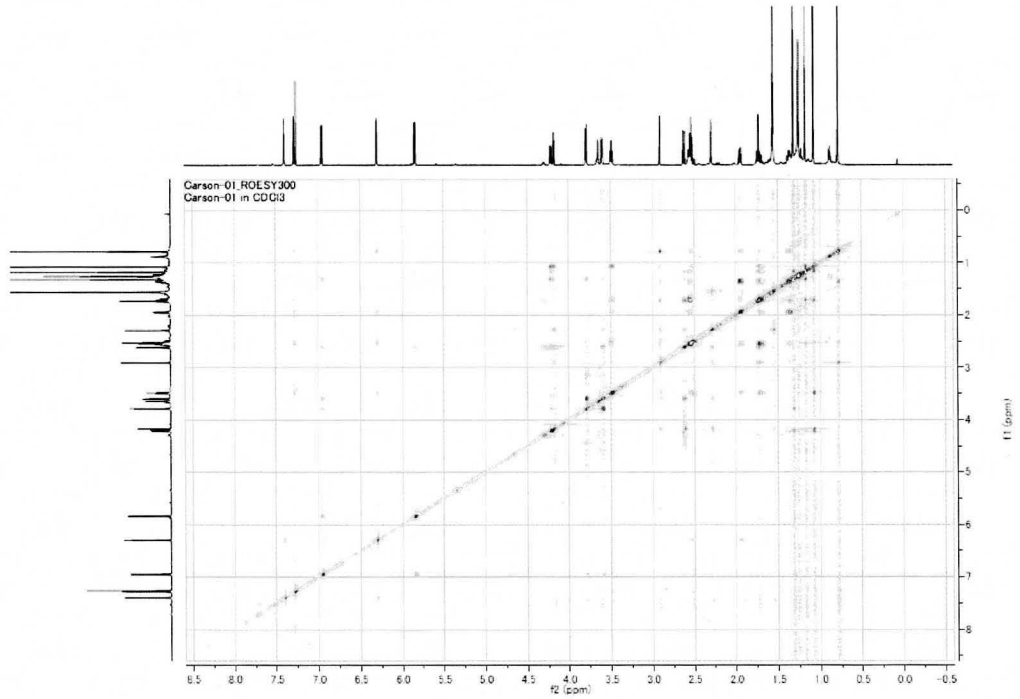

Appendix 36. ROESY spectrum of **6** in $CDCl_3$

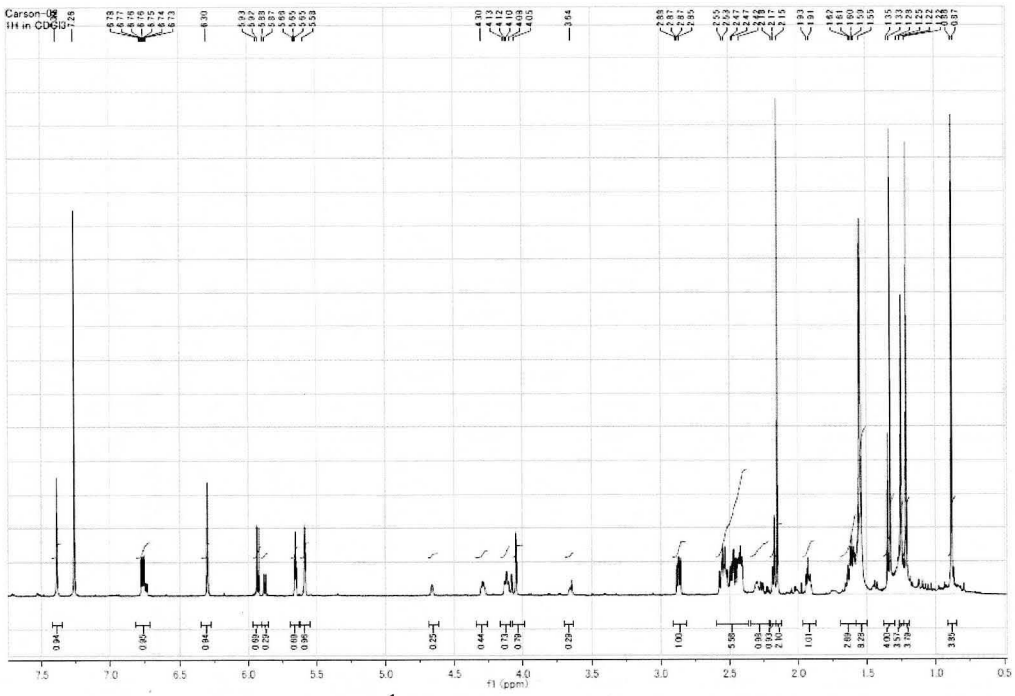

Appendix 37. ^{1}H NMR spectrum of **7** in $CDCl_3$

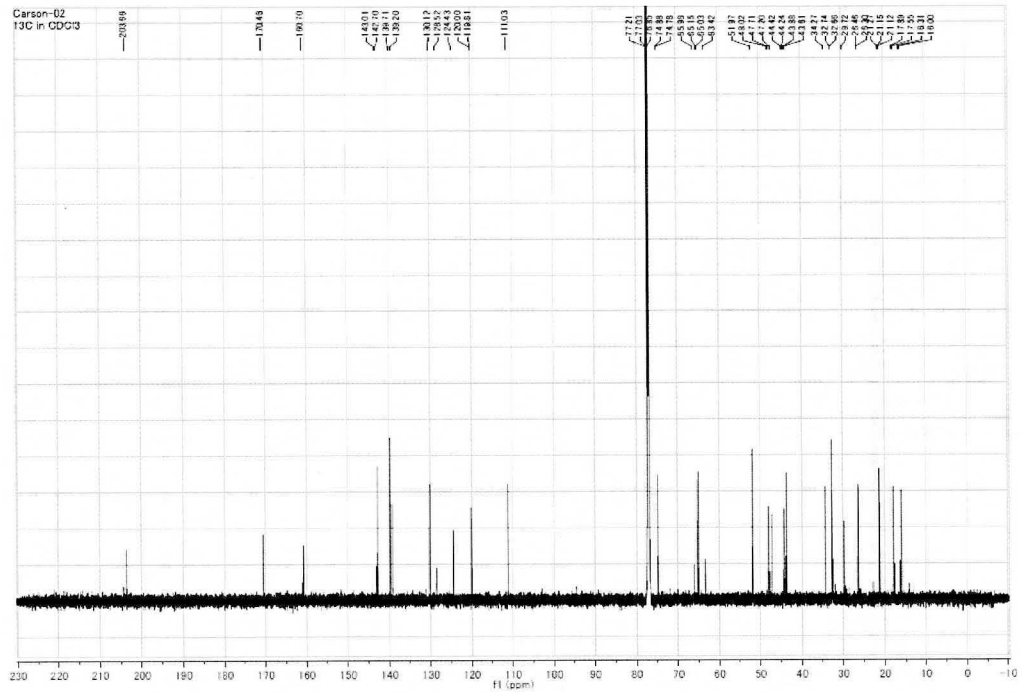

Appendix 38. ^{13}C NMR spectrum of **7** in $CDCl_3$

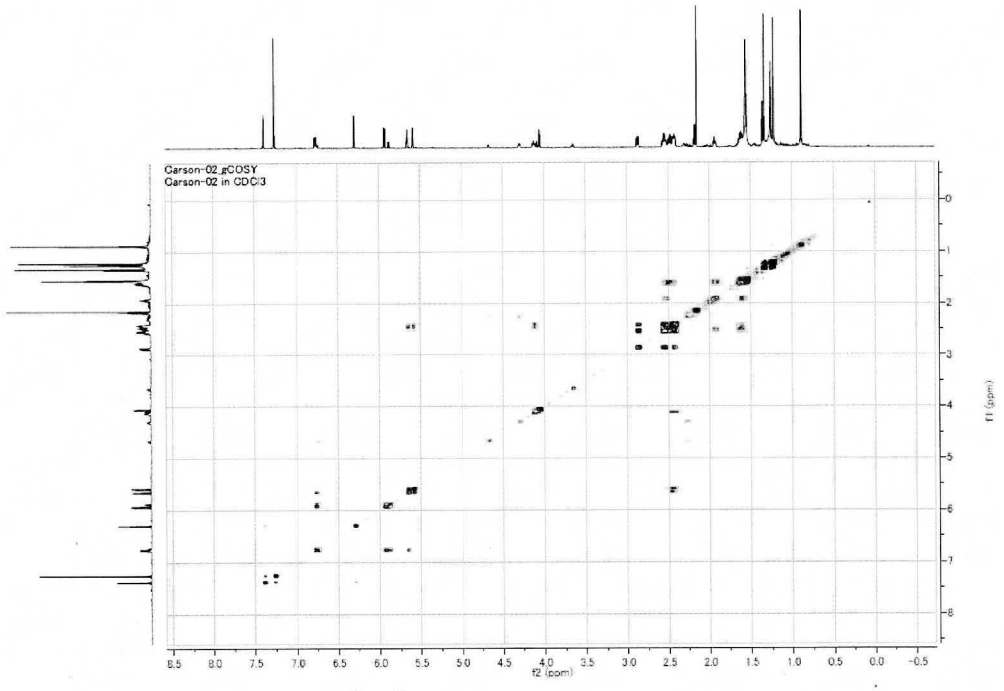

Appendix 39. ^{1}H-^{1}H COSY spectrum of **7** in $CDCl_3$

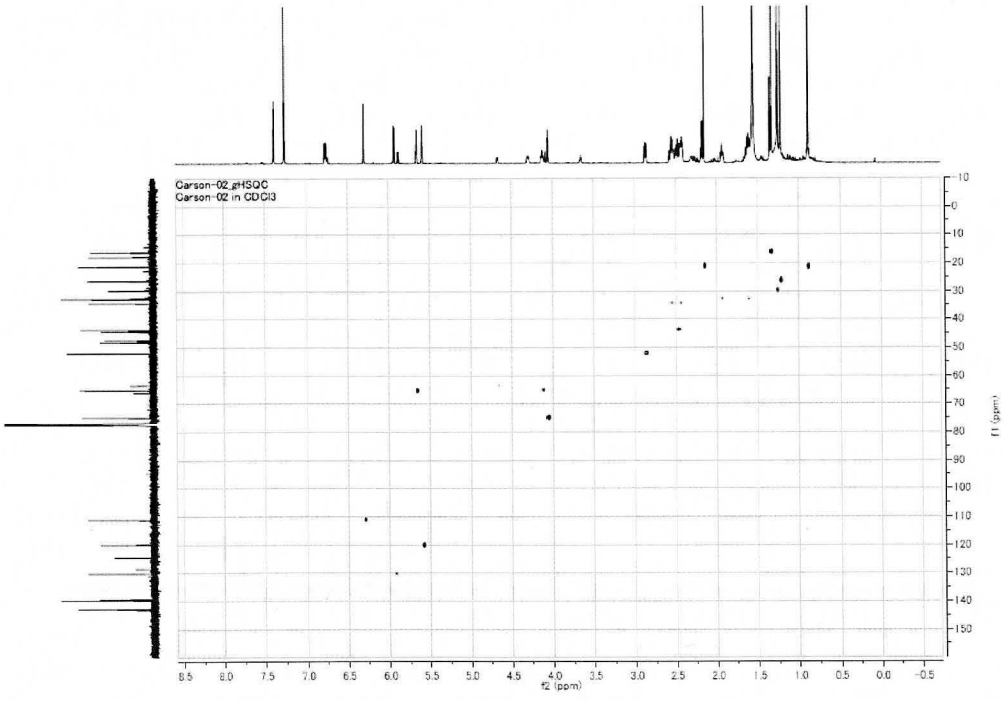

Appendix 40. HSQC spectrum of **7** in $CDCl_3$

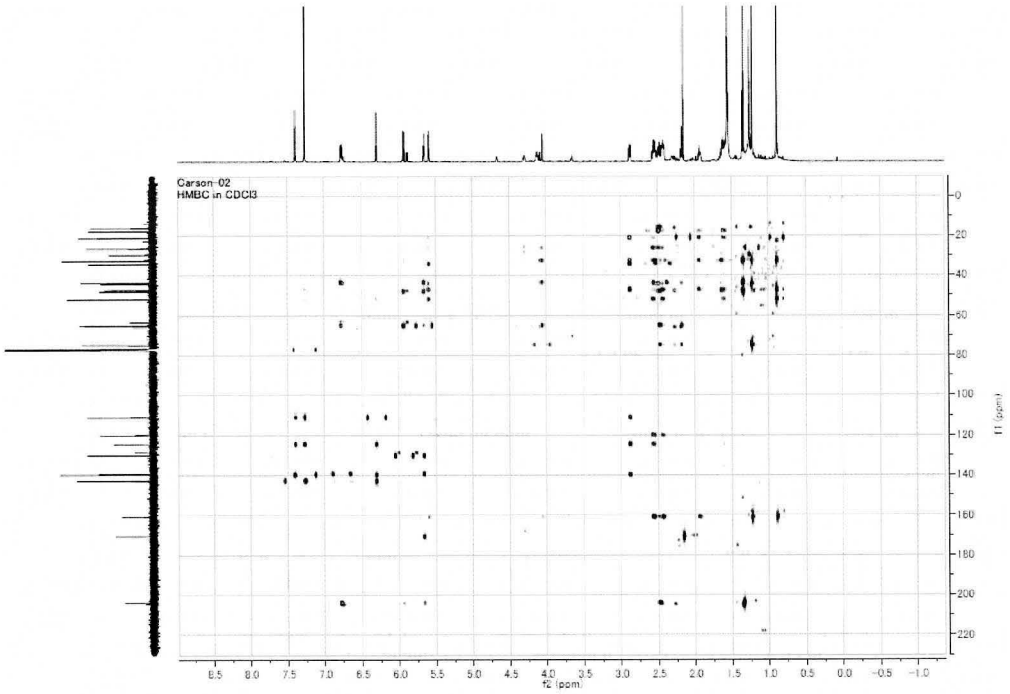

Appendix 41. HMBC spectrum of **7** in $CDCl_3$

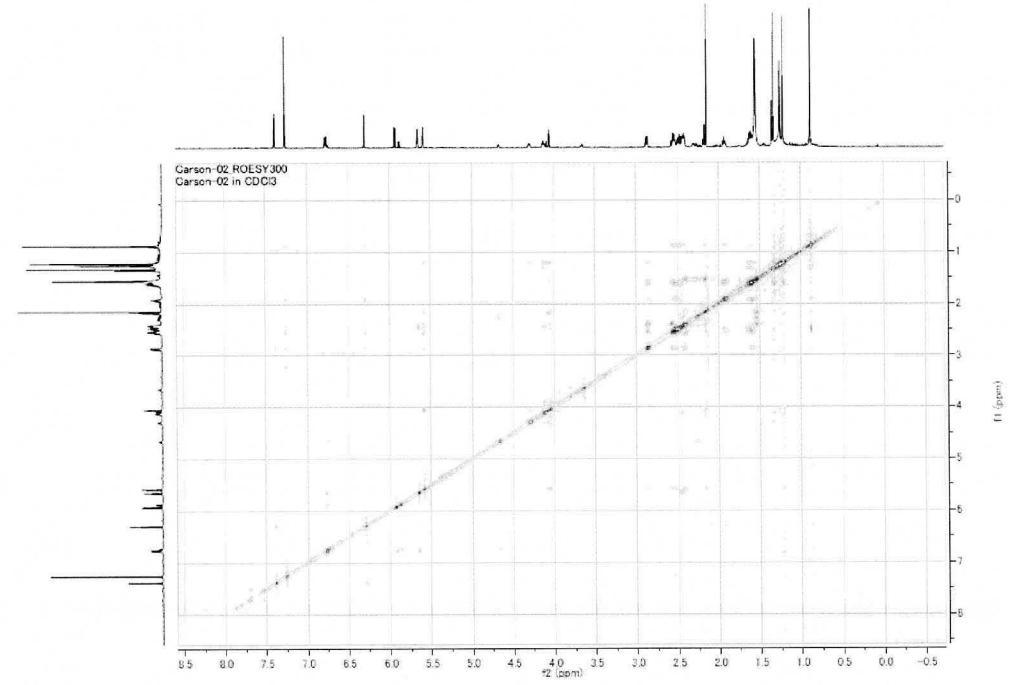

Appendix 42. ROESY spectrum of **7** in $CDCl_3$

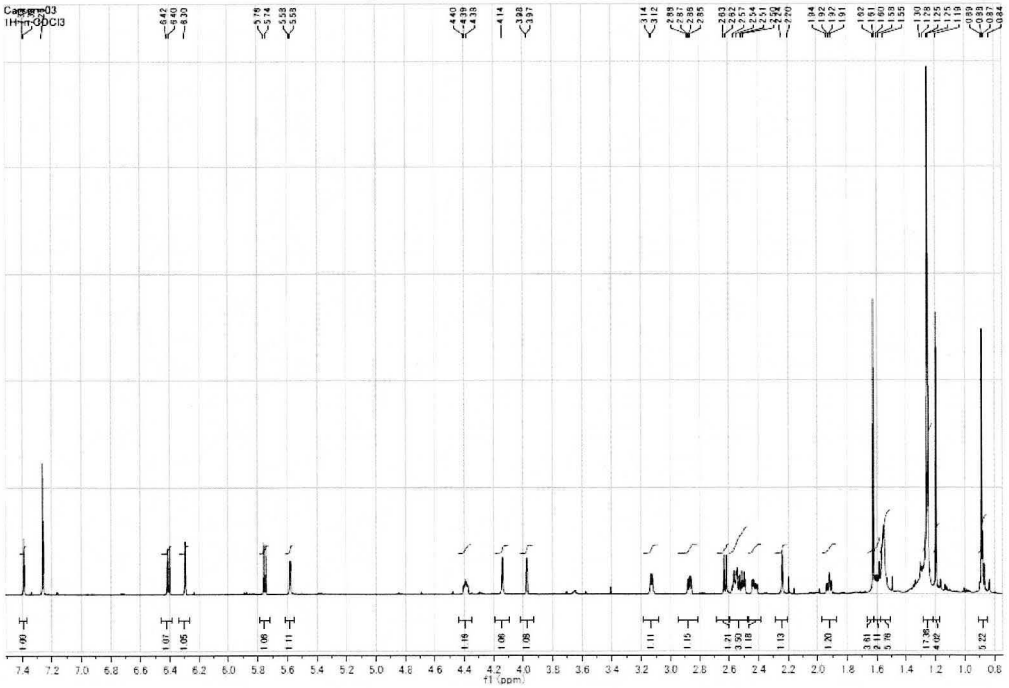

Appendix 43. ^{1}H NMR spectrum of **8** in $CDCl_3$

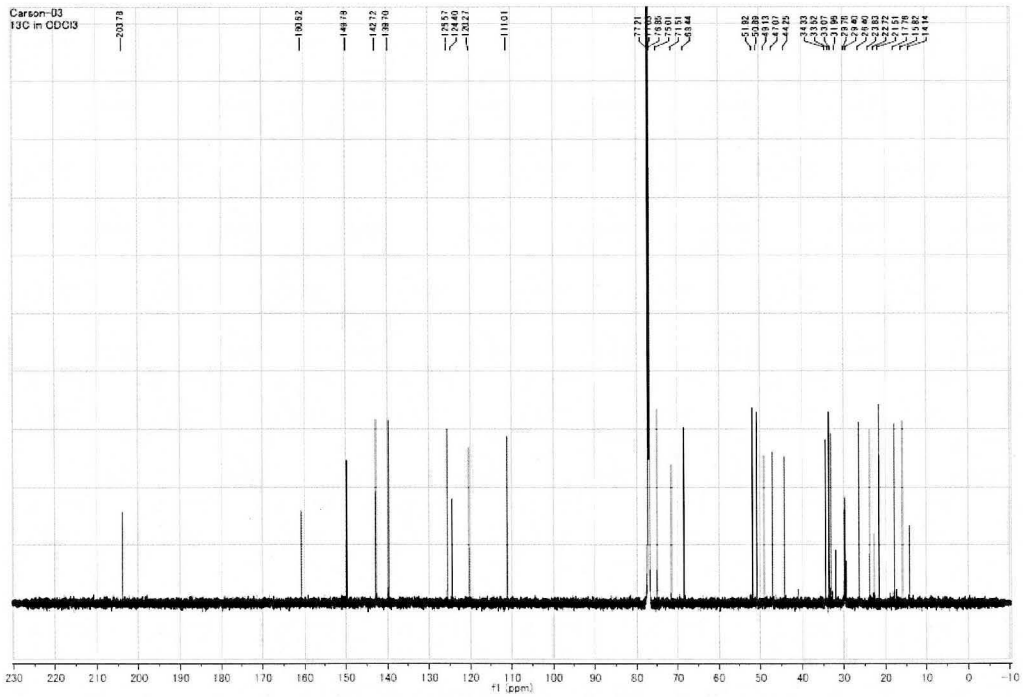

Appendix 44. ^{13}C NMR spectrum of **8** in $CDCl_3$

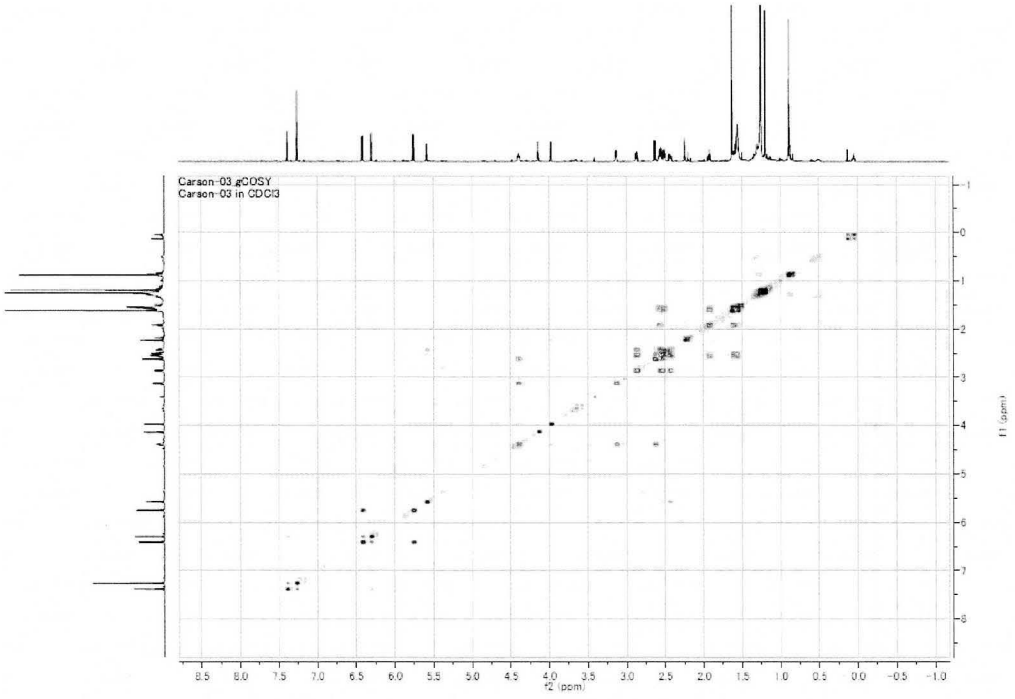

Appendix 45. ^{1}H-^{1}H COSY spectrum of **8** in $CDCl_3$

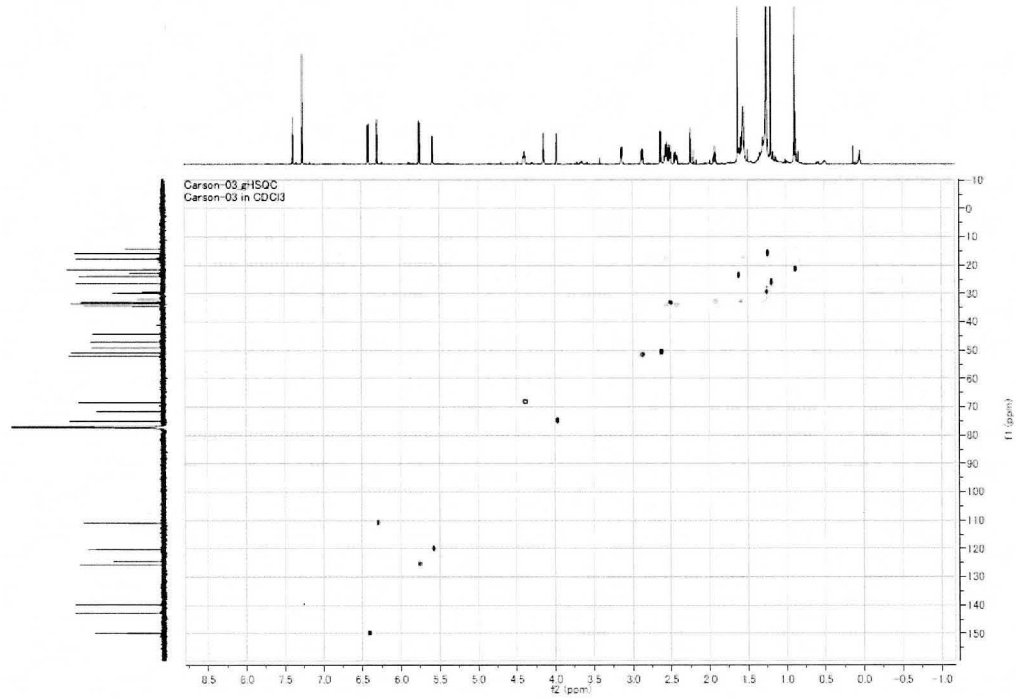

Appendix 46. HSQC spectrum of **8** in $CDCl_3$

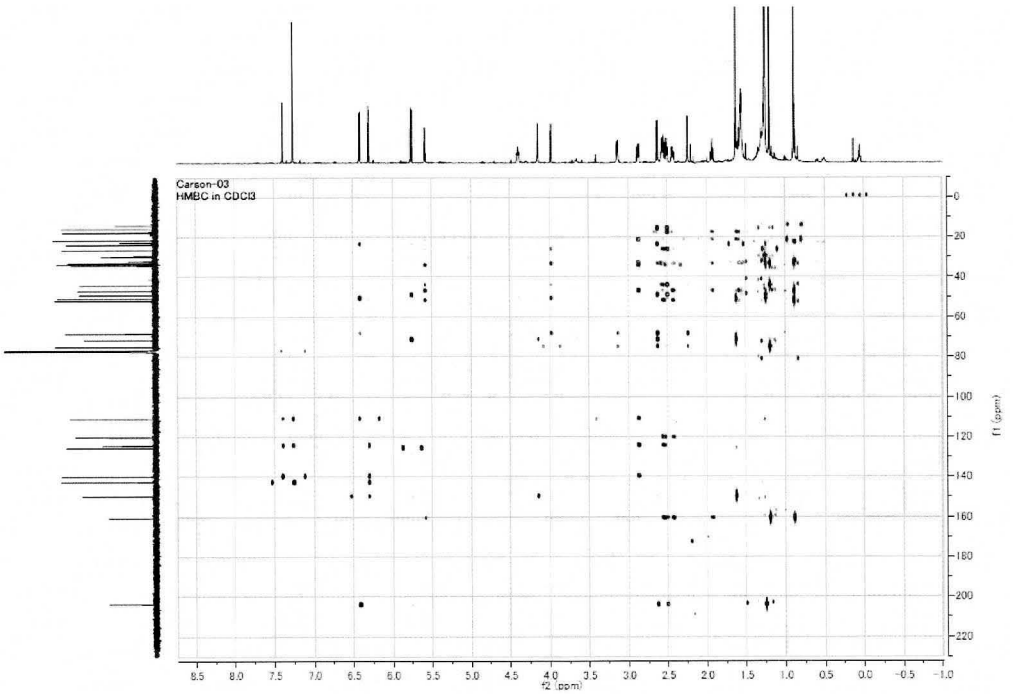

Appendix 47. HMBC spectrum of **8** in $CDCl_3$

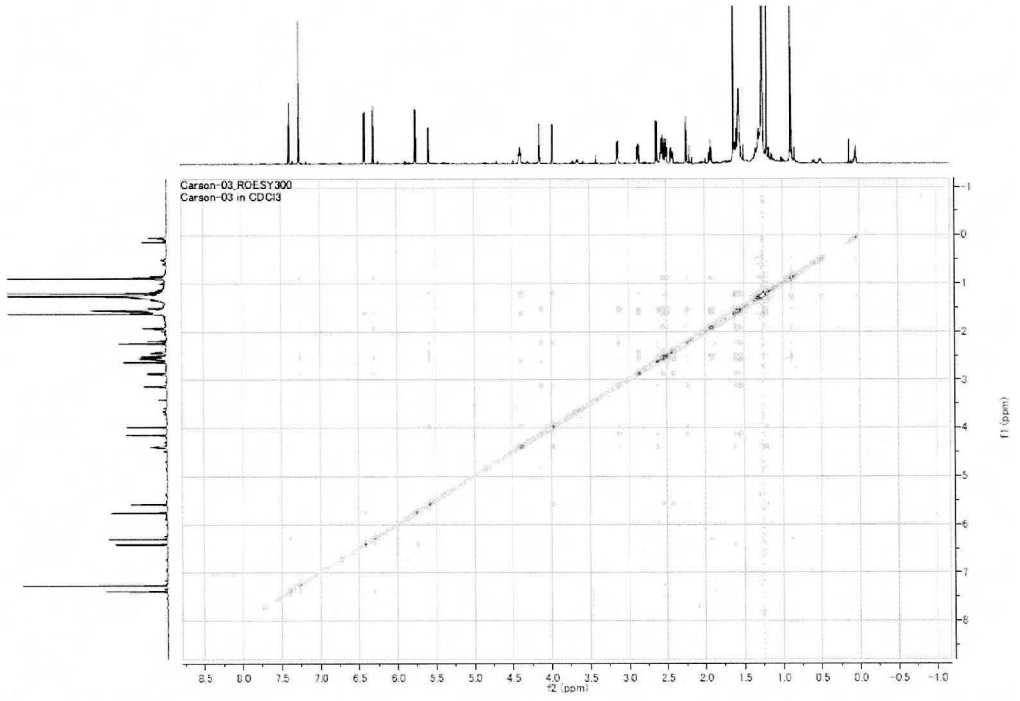

Appendix 48. ROESY spectrum of **8** in $CDCl_3$

Appendix 49. X-ray crystallography atomic coordinates of ceramicine B

Atoms	x	y	z	Atoms	x	y	z
O1	0.51452(19)	0.73127(12)	0.68024(7)	H2	0.4902	0.8956	0.6245
O2	-0.1565(2)	0.75555(10)	0.53827(6)	H3	0.2529	0.9664	0.577
O3	0.0341(2)	0.57547(10)	0.52530(6)	H5	0.16	0.7253	0.571
O4	0.5948(2)	0.10047(11)	0.64126(7)	H6	-0.1872	0.71	0.627
C1	0.3737(2)	0.76258(15)	0.65694(9)	H7	-0.1973	0.5583	0.5724
C2	0.3771(3)	0.86072(15)	0.62491(10)	H9	0.2828	0.587	0.6125
C3	0.2359(3)	0.90401(16)	0.59681(11)	H11A	0.4353	0.5664	0.7047
C4	0.0511(2)	0.85617(15)	0.59583(9)	H11B	0.2484	0.543	0.7398
C5	0.0821(2)	0.74557(13)	0.60674(8)	H12A	0.2889	0.3893	0.7235
C6	-0.0994(2)	0.69982(14)	0.59222(9)	H12B	0.4722	0.413	0.6864
C7	-0.0746(2)	0.58967(15)	0.57879(9)	H15	-0.1782	0.3762	0.5913
C8	0.0215(2)	0.53942(14)	0.63457(9)	H16A	0.0618	0.2432	0.5532
C9	0.2069(2)	0.59305(14)	0.65063(8)	H16B	-0.0515	0.2085	0.6134
C10	0.1892(2)	0.70806(15)	0.66210(8)	H17	0.1636	0.2631	0.6796
C11	0.3132(3)	0.53533(16)	0.70003(9)	H18A	0.4919	0.3663	0.5794
C12	0.3392(3)	0.42668(17)	0.68797(12)	H18B	0.4003	0.473	0.5683
C13	0.2521(2)	0.38539(14)	0.62912(9)	H18C	0.3156	0.3762	0.5361
C14	0.0641(2)	0.43081(14)	0.61966(8)	H19A	-0.0228	0.735	0.725
C15	-0.0539(3)	0.36243(16)	0.60087(11)	H19B	0.1511	0.8049	0.7367
C16	0.0306(3)	0.26024(17)	0.59632(11)	H19C	0.1561	0.6906	0.7574
C17	0.2024(2)	0.27308(14)	0.63586(9)	H21	0.4581	0.1762	0.7095
C18	0.3761(3)	0.40169(18)	0.57323(12)	H22	0.3662	0.1714	0.5272
C19	0.1112(3)	0.73734(16)	0.72623(8)	H23	0.6268	0.064	0.5503
C20	0.3544(2)	0.20067(13)	0.62410(8)	H28A	-0.1255	0.9043	0.5255
C21	0.4665(3)	0.16224(16)	0.66668(10)	H28B	0.0434	0.8398	0.4995
C22	0.4166(3)	0.15936(15)	0.56683(9)	H29A	-0.1906	0.8754	0.6449
C23	0.5592(3)	0.10071(16)	0.58000(10)	H29B	-0.0954	0.9788	0.6271
C28	-0.0467(3)	0.84578(15)	0.53344(10)	H29C	-0.0146	0.9129	0.6822
C29	-0.0736(3)	0.91075(16)	0.64162(10)	H30A	-0.0552	0.5086	0.7253
C30	-0.1145(3)	0.53819(17)	0.68916(10)	H30B	-0.2223	0.4987	0.678
H3O	0.0043	0.6174	0.4984	H30C	-0.1521	0.6065	0.6988